July 2017

The Role of Phenotypic Integration in Mammalian Tooth Function and Jaw Morphological Diversity

Andrew Conith

THE ROLE OF PHENOTYPIC INTEGRATION IN MAMMALIAN TOOTH FUNCTION AND JAW MORPHOLOGICAL DIVERSITY

A Dissertation Presented

by

ANDREW J. CONITH

Submitted to the Graduate School of the
University of Massachusetts Amherst in partial fulfillment
of the requirements for the degree of

DOCTOR OF PHILOSOPHY

May 2017

Organismic and Evolutionary Biology

THE ROLE OF PHENOTYPIC INTEGRATION IN MAMMALIAN TOOTH FUNCTION AND JAW MORPHOLOGICAL DIVERSITY

A Dissertation Presented

by

ANDREW J. CONITH

Approved as to style and content by:

_____
Elizabeth R Dumont, Chair

_____
R. Craig Albertson, Member

_____
Jason M. Kamilar, Member

_____
R. Mark Leckie, Member

_____
Jeffrey Podos
Organismic and Evolutionary Biology
Graduate Program Director

DEDICATION

To my wife, Moira Conith.

ACKNOWLEDGMENTS

I want to begin by thanking my advisor Betsy Dumont who took a chance and brought me over to the States to start my scientific career. I've learnt so much in the last five years about mammals, anatomy, science, and writing. I hope it doesn't stop there - I've got much further to go.

I want to acknowledge my thesis committee members for their advice, guidance, and comments on my thesis. The final version is much improved due to their comments and edits.

I also want to thank Penny Jaques and Maggie DeGregorio the program coordinators for directing me through the highs and lows of graduate school. Whenever I've had any questions, they've got the answer, it's made my life so much easier.

My lab-mates, old and new, have also been a great inspiring force behind the completion of my thesis. In particular, Yi-fen Lin, Brandon Hedrick, Abby Vander Linden, David Munteanu, and Dan Pulaski. Thomas Eiting and Michael Rosario also deserve a special mention for helping me complete my first publication.

I also had lots of help from UMass undergraduates. Ali Jamali, Katelyn Richards, and Jonathan Candido assisted with a great deal of data collection. I want to single out Molly Meagher for her help with the collection trips to Boston and New York City, they were great fun and I got lots of data to analyze.

The UMass Polymer Science department, especially Mike Imburgia and Al Crosby, were instrumental in developing the study on early mammal dental evolution. I want to thank them for permitting me access to their 3D printing and material testing machines.

I'm very grateful to a number of museums around the country for allowing me to come and photograph their collections. In particular Eileen Westwig at the American Museum of Natural History, Judy Chupasko at the Harvard Museum of Comparative Zoology, Bill Stanley at the Chicago Field Museum, and Esther Langan at the Smithsonian National Museum of Natural History.

I am very appreciative to my funding sources: the Graduate Program in Organismic and Evolutionary Biology, the UMass Natural History Collections, and the National Science Foundation, who allowed me to greatly expand and improve my work.

Finally, I want to thank my wife Moira for being such a supportive figure in my life and encouraging me right through to the end.

ABSTRACT

THE ROLE OF PHENOTYPIC INTEGRATION IN MAMMALIAN TOOTH FUNCTION AND JAW MORPHOLOGICAL DIVERSITY

MAY 2017

ANDREW J. CONITH, B.Sc., UNIVERSITY OF LEEDS

M.Sc., UNIVERSITY OF BRISTOL

Ph.D., UNIVERSITY OF MASSACHUSETTS AMHERST

Directed by: Professor Elizabeth R. Dumont

Here I investigate how two major components of the mammalian feeding system, teeth and jaws, are influenced by functional, environment, and developmental factors. First, I build physical models of the molars from two early mammals, *Morganucodon* and *Kuehneotherium*, and compare their ability to process a proxy food item. Early mammals were under strong selection to reduce metabolic costs, so any savings in energy during feeding would be advantageous. I tested the ability of both mammals to process a hard and soft food item with material properties similar to that of the insects they would have likely consumed. *Morganucodon* was better able to process hard food while *Kuehneotherium* was better able to process soft foods. Perhaps more importantly, *Kuehneotherium* molars inflicted significantly more damage on food items regardless of their material properties. These results suggest that changes in dental morphology in some early mammals was driven

primarily by selection for maximizing damage, and secondarily for maximizing biomechanical efficiency for a given food material property. Second, I assess the association between climatic variability and phenotypic integration (the degree of covariation among suites of traits). Taxa in climatically variable regions experience fluctuating selective pressures which may influence phenotypic integration, and by extension, disparity (morphological diversity) and the rate of morphological evolution. I extracted climatic data from range maps, and gathered landmark data from the jaws of three large families of carnivorans, Canidae, Felidae, and Mustelidae. I found that canids and felids from climatically variable regions exhibited low levels of jaw integration, low disparity, and fast rates of morphological evolution. This suggests climatic variability predicts phenotypic integration in canids and felids and may be a consequence of, or a response to, the relative magnitude of long and short-term environmental changes (e.g., glaciations, seasonality). Climate may therefore have a profound influence on the evolvability of species. Finally, I investigate how differences in the mode of placental and marsupial reproduction can influence the pattern and magnitude of phenotypic integration. Marsupial neonates are born without a fully developed oral apparatus but immediately begin suckling in the pouch. Due to suckling at such an early age, the mechanical environment in the developing jaw is vastly different to placental mammals, which exhibit simultaneous development of jaw muscles and bones that only function after they are fully developed. The marsupial mode of reproduction may therefore limit morphological evolution of the jaw in marsupials. I investigate the association among phenotypic integration, disparity, and rates of morphological

evolution using the placental Carnivora (made up of the Feliformia and Caniformia) and the marsupial Dasyuromorphia. I found dasyuromorphs exhibit fewer modules and higher integration between the angular and coronoid processes, the primary attachment sites for the jaw closing muscles. This pattern of integration may result from the overwhelming influence of muscles on the developing jaw. Carnivorans are free from this constraint and each process on the jaw can evolve independently. Despite differences in integration, dasyuromorphs and carnivorans display similar levels of disparity. Rates of morphological evolution are also similar in dasyuromorphs and caniforms, and rates are 3x slower in feliforms. Taken together, this suggests that the mode of reproduction has not affected dasyuriomroph morphological evolution and developing a carnivore-like jaw is a developmentally straightforward task given its similarity to the ancestral state. Overall, my work has demonstrated how the mammalian feeding system is influenced by phenotypic integration, the mode of reproduction, phylogeny, and the environment. Together, these factors appear to influence the disparity, rate of morphological evolution, and ultimately, the evolvability of mammalian teeth and jaws.

TABLE OF CONTENTS

Page

LIST OF TABLES

LIST OF FIGURES

CHAPTER 1

INTRODUCTION

Over the last 200 million years the diversification of the masticatory apparatus has permitted mammals to exploit a diverse range of diets and habitats. Adaptations in the dentition and jaw systems that comprise the masticatory apparatus likely came about due to high metabolic demands associated with homeothermy (Clarke and Pörtner 2010). The ability to efficiently process food is vital for a mammal to extract metabolic energy quickly for activities such as maintaining homeostasis, locomotion, and reproduction. Diet is therefore a key component to understanding how mammals became the dominant terrestrial tetrapods in the Cenozoic (Rose 2006). This has led to a number of complex adaptations involving specialized teeth and jaws. Mammalian teeth are very morphologically diverse and reflect the wide range of dietary niches that they occupy. Similarly, mammal jaw shape is also highly diverse reflecting their varied roles in feeding (Meloro et al. 2011; Prevosti et al. 2012). Diet and life history are clearly reflected in the shapes of mammal jaws, but how jaw morphological diversity was achieved and how is it is distributed over the mammal tree are two unresolved large-scale questions

However, mammals did not always occupy such a diverse range of niches during the early parts of their evolutionary history. Mesozoic mammals are often considered to be far less ecologically diverse than their extant counterparts. While it

is true that Mesozoic mammals may have been constrained in terms of body size (Slater 2013), fossil evidence suggests that they occupied many of the same niches as today (Luo 2007). Nevertheless, macroevolutionary changes to the dental and jaw architecture paved the way for the Cenozoic radiation of mammals. However, pinpointing the driving mechanisms that drove early masticatory evolution has proved difficult. This difficultly stems from the large number of biotic and abiotic factors that have shaped mammalian jaw and tooth morphology.

The mammalian jaw and dentition have undergone a complex evolutionary history. Early synapsids (the group that gave rise to mammals) possessed a jaw joint that articulated between two bones, the quadrate and the articular (Figure 1.1). Through the Mesozoic, these two bones reduce in size and become part of the middle ear. Meanwhile, two other bones, the dentary and squamosal become the primary articulation point of the lower jaw (Luo et al. 2007*b*). Similarly, the jaw musculature was also changing through the Mesozoic. The temporalis and masseter muscles that anchor the jaw to the skull invaded progressively larger areas on the skull roof through the Mesozoic. The expansion of jaw muscle area and shift in the jaw articulation point paved the way for an important mammalian trait, chewing (Kielan-Jaworowska et al. 2004). Chewing was facilitated by precise occlusion between heterodont teeth, which arose in the Late Triassic with the cynodonts (Crompton and Jenkins 1968). The incisors, canines and molars of the cynodonts represented a functional improvement over the conical, single cusp teeth of the reptiles, meaning they could more efficiently process the food they were eating.

Cynodonts were a group which included weasel-sized to dog-sized carnivores and herbivores (Benton 2005).

At the most basic level, jaws and teeth can be considered as tools for performing specific functions. The anterior tooth bearing section contacts the food, while the posterior portion bears the muscles required to drive teeth into the food. Jaws and teeth therefore represent discrete anatomical units, or modules, that can be separate targets for natural selection to act upon. These modules allow variation to accumulate in one part of the organism while another part remains unchanged. By parsing up the functional roles of anatomical structures like this, an organism can become more morphologically diverse and access a greater range of ecological niches (Hallgrímsson et al. 2009; Klingenberg 2010).

The covariation among sets of traits such as the jaws and teeth is termed "integration". Traits with high levels of integration have tight covariation, whereas traits with low levels of integration are more independent of one other. Modules are subsets of traits within an anatomical region that are more tightly correlated with one another than they are with traits in another anatomical region (i.e., covariation among traits is higher within modules than between modules). It appears that the strengths of covariation can differ among clades (e.g., Goswami 2006*a*; Goswami and Polly 2010) as a result of certain functional (i.e., mechanical advantage), developmental (marsupial suckling as an early embryo), and genetic constraints (allelic differences). Also, the organization of which traits covary together as modules on a structure can be different between populations or clades (Goswami 2006*a*), termed "pattern of integration" (Figure 1.2a).

In highly integrated structures, phenotypic evolution can be constrained and the range of morphological variation is likely reduced. In this case phenotypic evolution must proceed along a line defined by the covariation between traits, known as the line of least resistance (Goswami and Polly 2010) (Figure 1.2b). In a structure with low levels of integration traits can evolve independently of one another, increasing variation and widening the line of least resistance (Figure 1.2b). This concept of evolution occurring along 'lines of least resistance' suggests that there is a limit to the range of morphologies that a clade can evolve (Klingenberg 2010), and a number of studies have been dedicated to understanding what defines these limits in a number of taxa (Albertson et al. 2005; Goswami 2006*a*, *b*; Drake and Klingenberg 2010; Sanger et al. 2012). If regions of an organism can develop and evolve independently, then this could permit an increase in morphological diversity that may open up unique or unoccupied niches (Wagner et al. 2007), favor the evolution of extreme morphologies, and increase the rate of morphological divergence (Goswami et al. 2014). This has implications for the ability of a clade to evolve (evolvability) and more efficiently respond to constantly changing environments (Pigliucci 2008). At the most basic level, mammal jaws are comprised of two primary modules (Figure 1.1c), the corpus (the dental bearing region) and the ramus (the muscle bearing region) (Klingenberg 2009). The ability to evolve these two portions of the jaw independently may allow for a greater functional diversity. For example, the jaws of many ant-eating mammals can become highly elongated, while shrinking the ramus. Similarly, the jaws of bone-crushing mammals such as spotted hyenas shrink the dentition portion of the jaw, while expanding the

ramus. This allows for a greater mechanical advantage while simultaneously increasing surface area for muscle attachment sites. If the jaws of mammals have different patterns and strengths of covariation, then understanding how this is influenced by external or internal factors, and how it is distributed along the mammalian tree may go some way to understanding how integration can influence taxonomic and morphological diversity.

In this thesis I will use a variety of engineering, phylogenetic comparative, and anatomical methods to better understanding the driving mechanisms behind the evolution of the mammalian feeding system. The aim is to provide a better understanding of how the teeth and jaws are shaped by functional, environmental, and developmental factors. By analyzing mammalian tooth and jaw shapes I hope to address three major questions in each of my three chapters. In chapter 2 I ask, how does the transition from a simple to complex molar morphology influence the efficiency of food breakdown? In chapter 3 I ask, can climatic variability affect organisms in terms of both developmental processes (strength and pattern of phenotypic integration) and macroevolution (rates of morphological evolution and disparity)? Finally, in chapter 4 I ask, does the accelerated development of marsupial neonates influence their phenotypic integration and morphological diversity relative to placental mammals?

In chapter 2, I will begin by studying changes in tooth morphology using two late Triassic mammals that exhibit a primitive and derived positioning of their molar cusps. The literature on early dental changes is primarily based on wear patters and tooth modeling (Osborn 1907; Crompton and Hiiemäe 1969; Crompton

and Sita-Lumsden 1970; Evans and Sanson 2006). Physical testing of early mammal occlusion has yet to be attempted, and will be useful in isolating some of the variables that may be important in cusp morphology evolution. I use 3D printed tooth rows of two Triassic mammals and record the force, energy, and damage inflicted to a proxy food item. I hypothesize that the more derived and complex tooth morphology will be more efficient (reduce force and energy, while maximizing damage) compared to the primitive toot morphology.

In chapter 3 I will study the association between jaw integration and climatic variability. Understanding how climate affects the tempo and mode of morphological evolution and the role phenotypic integration plays in this, is vital to understanding why we observe uneven distributions of biodiversity among regions. I gather landmark data from the lower jaw and extracted current temperature and precipitation variability data from range maps for three carnivoran clades (Canidae, Felidae, Mustelidae). Given the close relationship between rates of morphological evolution, disparity, and phenotypic integration (Hallgrímsson et al. 2009), I expect jaw disparity to be higher and jaw integration to be lower in more climatically variable regions. Being highly integrated could be detrimental to the survival of organisms in climatically variable regions as this could limit the resources available to the organism, and make it difficult to respond to a constantly changing environment over a period of generations (Goswami et al. 2015).

In chapter 4 I will test patterns of jaw integration and morphological diversity between placental and marsupial carnivores. I compare the marsupial Dasyuromorphia and the placental Carnivora on account of their general similarity

in diet (most are carnivores although ursids and procyonids tend toward omnivorory or herbivory (Price et al. 2012)) and ancient common ancestor (~200 million years ago (Slater 2013)). Dasyuromorph neonate development is accelerated relative to carnivoran mammals because they need to reach the pouch and immediately begin suckling. Dasyuromorph jaw muscles rapidly differentiate at birth to assist in suckling, prior to complete ossification. This creates a vastly different mechanical environment for the Dasyuromorph dentary to develop in. Given the requirement for marsupial neonates to develop jaw musculature far in advance of dentary ossification, I hypothesize that dasyuromorphs will exhibit greater integration among regions of the jaw relative to carnivorans. I also hypothesize that dasyuromorphs will also exhibit reduced disparity and rates of morphological evolution as a dentary with stronger covariation means regions of the jaw will display a coordinated response to selection, thus influencing the morphology of nearby regions.

My dissertation research focuses on two parts of the mammalian feeding system, the teeth and jaws. The work in this thesis will provide a better understanding of mammal feeding system evolution over large timescales and will take advantage of the wealth of recently developed comparative methods. My work on teeth seeks to understand whether changes in the molar morphology of early mammal dentitions influence the biomechanics of food processing. My work on jaws will provide empirical data on the macroevolutionary relationship between phenotypic integration and disparity. This has implications for how clades respond

to selection (evolvability) and will provide a better understanding of the constraints acting on the feeding system as a whole.

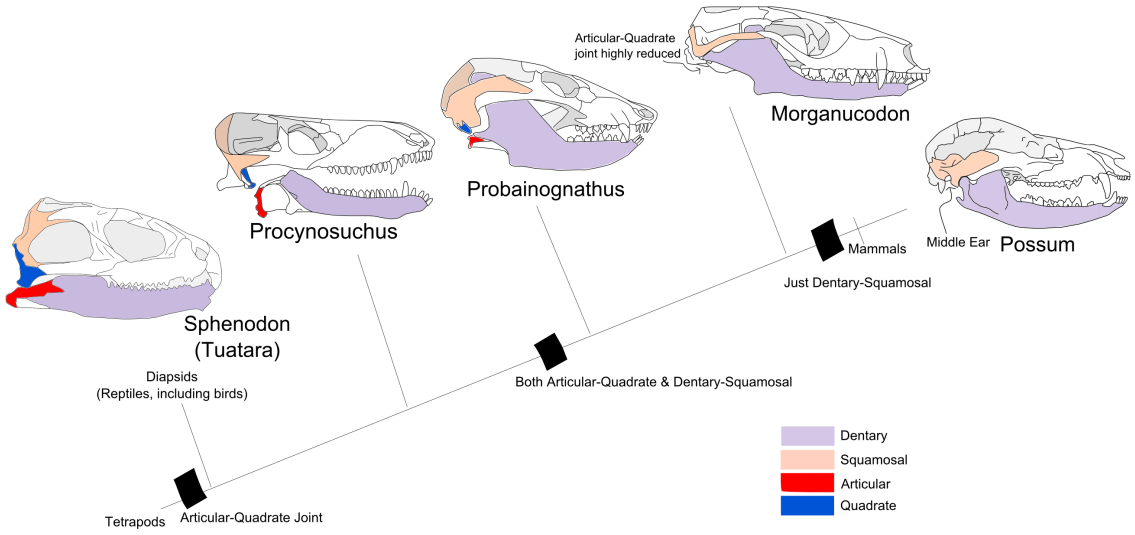

Figure 1.1: Evolution of the mammalian jaw joint and middle ear

Image from The Macro Library. Through mammalian evolution many of the jaw bones reduce in size until the dentary becomes the single jaw bone. As a result, the articular shrinks to become part of the middle ear along with the quadrate. *Thrinaxodon* and *Probainognathus* are both early cynodonts, *Morganucodon* is a derived cynodont, and the possum is a modern marsupial mammal.

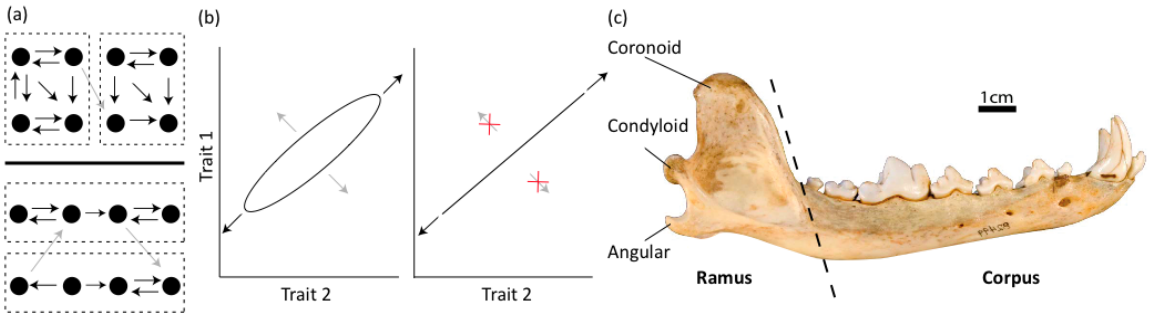

Figure 1.2: Modules, lines of least resistance and mammal jaw morphology

(a) Modular structures. Eight landmark traits arranged in a structure. Covariation (arrows) is strong within (black arrows), but weak (gray arrows) between modules (dotted lines). The pattern of modules may also differ between similar structures in different clades (top vs. bottom). (b) Lines of least resistance. Left, as trait 1 increases trait 2 also increases, but there is some variation around that increase (low integration). Right, there is a one to one relationship between trait 1 and trait 2 (high integration). (c) Mammalian jaw (coyote, *Canis latrans*). The two primary modules are either side of the dashed line and are named the ramus and corpus. Three processes for muscle attachment are located on the ramus: the coronoid, condyloid and angular.

CHAPTER 2

THE FUNCTIONAL SIGNIFICANCE OF MORPHOLOGICAL CHANGES IN THE DENTITIONS OF EARLY MAMMALS

Published as, Conith, A. J., Imburgia, M. J., Crosby, A. J., and Dumont, E. R., 2016. The functional significance of morphological changes in the dentitions of early mammals. Journal of the Royal Society Interface. 13(124): 20160713.

Introduction

The transition from a simple to complex dentition occurred multiple times during the evolution of mammals and has long been considered one of the major keys to their success (Luo et al. 2001; Kielan-Jaworowska et al. 2004; Luo 2007). Following the evolution of homeothermy early in the Mesozoic, increased metabolic demands produced strong selection for those mammals with teeth that could process food efficiently (Clarke and Pörtner 2010). As a result, the morphological diversity and complexity of teeth increased, allowing mammals to access a greater range of diets (Grossnickle and Polly 2013). During the Late Triassic and Jurassic many new tooth morphologies arose and replaced the simpler unicuspid teeth found in therocephalids (e.g., *Promoschorhynchus* (Huttenlocker et al. 2011)). These new groups included triconodonts, symmetrodonts, and docodonts, whose molars exhibited three main cusps arranged in either lines or triangles, and multituberculates, which had molars with multiple cusps arranged in parallel rows

(Figure 2.1). By the Late Cretaceous, most mammalian clades had either multituberculate molars or a new tooth morphology known as the tribosphenic molar. What these derived and very different forms had in common was the ability to cut and grind food. These molars were more functionally and morphologically complex compared to their earlier single-cusped counterparts because cutting occurred in multiple dimensions and could process a greater variety of food with heterogeneous material properties. Multituberculate molars cut and crushed food as rows of cusps on the lower molars moved past those on the upper molars (Kielan-Jaworowska et al. 2004). Lower tribosphenic molars had three primary cusps arranged in a triangle to serve as a cutting surface (the trigonid), and additional cusps that extended distally to produce a basin-like crushing surface (the talonid). The trigonid and talonid interdigitated with three-cusped upper tribosphenic molars to produce an efficient cutting and crushing complex (Davis 2011). The evolution of both types of molars with multiple, interdigitating cusps was accompanied by increased dietary and ecological diversity (Grossnickle and Polly 2013). Understanding the biomechanical consequences of the transition to these complex cusp arrangements could provide insights into the performance parameters that may have been the object of selection in driving increased molar tooth complexity and the attendant dietary diversification of mammals.

The first step in the evolution of the tribosphenic molar involved the movement of three cusps on the molar crown from a linear (triconodont) arrangement to a triangular (symmetrodont) arrangement that formed the trigonid (Mills 1971; Parrington 1978). Triconodonts and symmetrodonts form paraphyletic

groups among basal mammals, and their relationships are still poorly resolved (Averianov and Lopatin 2008; Gao et al. 2010). Qualitative studies suggest that the transition from a linear to triangular arrangement of cusps increased the number of shearing surfaces between the upper and lower teeth, perhaps facilitating food processing (Evans and Sanson 1998; Davis 2011). *Morganucodon* (a triconodont) and *Kuehneotherium* (a symmetrodont) spanned the Late Triassic – Early Jurassic and exemplify molar teeth with linear and triangular arrangements of cusps (Figure 2.2). Other differences between their molars include the sizes of small accessory cusps, the angles between the primary and accessory cusps (notch angle), the size of the cingulum (a shelf of enamel surrounding the molar crown), and the way in which the teeth wear with use (Crompton and Jenkins 1968; Mills 1971). Most studies of early mammal teeth focus on studying relationships based on tooth morphology (Luo et al. 2007*a*; Meng et al. 2011), patterns of wear on the teeth (Crompton and Jenkins 1968), and simulations of the chewing cycle (Crompton and Hiiemäe 1969; Crompton and Sita-Lumsden 1970; Evans and Sanson 2006). A single experimental study based on *Morganucodon* and *Kuehneotherium* demonstrated that the cingulum functions to dissipate stress away from the molar roots, reducing the likelihood of tooth breakage (Anderson et al. 2011). No other quantitative study has documented, how linear and triangular cusp arrangements translate into differences in feeding performance. A detailed investigation of the mechanical performance of linear and triangular cusp arrangements in processing food can offer insights into why selection favored the transition from a triconodont to symmetrodont arrangement of cusps.

Here I test the hypothesis that the transition from a triconodont to a symmetrodont molar morphology increased the efficiency of food breakdown using physical models of the upper and lower molar tooth rows based on the molars of *Morganucodon* and *Kuehneotherium*. I compare the force, displacement (as a proxy for time), and energy at two distinct phases of biting a food item: the point of first fracture (when cusps first puncture though the food item) and at the point of maximum force. First fracture indicates the point at which a tooth initiates a crack in a food item, while the point of maximum force offers a window onto how the teeth penetrate and propagate cracks through a food item. By reducing the work required to process food, energy can be invested elsewhere (foraging, reproduction, etc.). I also record the displacement at which fracture occurred and the maximum force that was attained. Assuming that displacement occurs at a steady rate, it can be considered as a proxy for time. A tooth that can fracture a food item more quickly could potentially process relatively more food in a shorter amount of time. Mesozoic mammals were likely homoeothermic and had high metabolic rates that required a great deal of food to maintain. They were under strong selection for energy efficiency (Clarke and Pörtner 2010): any reduction in force, time, or energy expended during food processing could have been beneficial.

Previous studies indicate that *Kuehneotherium* likely preyed on softer insects compared to *Morganucodon* (Mills 1971; Kielan-Jaworowska et al. 2004; Gill et al. 2014). This is evidenced by different molar wear patterns between the mammals, and a more slender jaw morphology in *Kuehneotherium* that was not as capable of withstanding high bite forces (Gill et al. 2014). To replicate this I used hard and soft

gels encased in a tough film that together exhibit material properties similar to those of the invertebrate prey that these mammals probably consumed (e.g., beetles and scorpion flies) (Vincent and Wegst 2004; Gill et al. 2014). Insects are structurally complex, requiring multiple fractures to process them completely. Both hard and soft invertebrates require a combination of cusps and crests (Figure 2.2) to initiate and propagate cracks through the entire body (Evans and Sanson 2005). Given these differences in diet I predict that the molar models of *Kuehneotherium* will process soft food items more efficiently while the molar models of *Morganucodon* will process hard food items more efficiently. Efficiency is measured as the ability of a model to reduce energy, force, and time during a bite. I also predict *Kuehneotherium* will inflict more damage to the gels given the more complex triangular arrangement of cusps on the crown. These aspects of performance make intuitive sense from the classical perspective that teeth are tools optimized for breaking apart food.

Materials and methods

Molar measurements, CAD and insect model construction

18 morphological measurements of *Morganucodon watsoni* (n=11) and *Kuehneotherium praecursoris* (n=11) were taken from isolated lower molars (Figure S1; Table S2.1). In order to identify the variables that most clearly differentiate between the two species I assessed correlations among all variables within each species (Table S2.2). I then compared each variable between *Morganucodon* and *Kuehneotherium* using *t*-tests (Table S2.3). The variables that differed most between

the two species, and were not correlated with other variables, were used as the foundation for computer aided design (CAD) models of molar teeth for each species. These key variables were: position of the accessory cusps (linear or triangular), notch angle, and height of the *b*-cusp. I used species means of these three variables to build a model for each species. Values for the remaining 15 variables in both models were based on the pooled sample from both species.

I created CAD models for each species using Creo Parametric 2.0 (PTC, inc.) and isometrically scaled them to one another by making the height of the primary cusp the same for both species (Figure S2.3; Table S2.4-S2.5). Upper and lower molars are essentially identical within species, so I used the same models for both upper and lower tooth rows. I used 3 uppers and 4 lower molars for both models. Cusp tips came to relatively sharp points in both models, which may initiate crack propagation more easily than the somewhat more blunt cusps of real teeth. I scaled up the models by a factor of ten and 3D printed them with a Dimension uPrint SE Plus printer, using an acrylonitrile butadiene styrene (ABS) plastic and a printed layer resolution of 254μm (Figure 2.3).

I constructed two proxy food items of different stiffness to mimic a hard and a soft food item with material properties based on values gathered from the literature ((Vincent and Wegst 2004), Table S2.6). I use the term 'soft' to describe food items that exhibit low stiffness, and the term 'hard' to describe food items with high stiffness (Table S2.6). Our hard food item consisted of a poly(dimethyl siloxane) [PDMS] elastomer gel (Sylgard® 184, Dow Corning, Inc.), encased in a polyethylene terephthalate (PET) film (GmbH (Hostaphan® TT, Mitsubishi

Polyester Film) (Figure S2.4a). Our soft food item consisted of a poly(methyl methyacrylate) [PMMA]-poly(n-butyl acrylate) [PnBA]-[PMMA] triblock copolymer gel (Kurarity™, Kuraray Co.), encased in a PET film (Figure S4b-S5). The ability of the gel complexes to resist compressive force during biting depends on the tensile strength of the film, the tensile stiffness of the film, and the compressive stiffness of the inner gel. The gels model the ability of an entire insect to resist compressive force. I altered the fracture properties of the food item by changing the material properties of gels and keeping PET film material properties constant. I changed the material properties of the gels as this approach is technically easier and accomplishes the same final goal: to change the material properties of the entire proxy food item. I confirmed this by testing the material properties of the hard and soft food items (Table S2.6). For further explanation of stiffness calculations and gel construction, see appendix A.

Physical testing

Lower tooth rows were affixed to the base of an Instron machine (model 5500R) and the upper tooth rows were attached to a 50N load cell via a plate that could be moved in the x-y plane. This allowed us to consistently place the upper tooth row into precise alignment with the lower tooth row, so to replicate the orthal pattern of occlusion hypothesized for *Morganucodon* and *Kuehneotherium* (Crompton and Jenkins 1968). Although the upper and lower molar models occlude during the production of the fractures they do not come into full contact, so some elements of the masticatory cycle such as shearing forces are not modeled in this study. Chewing is also not modeled in this study although, given the material

properties of insect exoskeleton, much of the processing likely occurs in the first few chewing cycles (Appelqvist 2013). Beginning with the upper and lower teeth just in contact with the upper and lower surfaces of the gel, I displaced the upper molar tooth row 8.5mm for the soft gel and 10.6mm for the hard gel at a constant rate of 0.15 mm/s (Figure S2.9). These distances ensured that the teeth punctured the gel but did not come into contact with the base-plate, which could have damaged the models and/or the load cell. I used a constant rate of displacement for all trials as changing the rate can impact fracture properties of elastic materials, such as PDMS and triblock, over the time scale of our puncture experiments (Fakhouri et al. 2015). For each species I conducted twelve trials using the soft food item and ten trials using the hard food item. There was no evidence that the force or energy decreased with additional tests, indicating that the models were not experiencing wear that affected the results (Figure S2.6).

I extracted the force, energy (work done), time at initial fracture, and point of maximum force from the force-displacement curve generated by each trial, and compared the values of these mechanical performance variables between *Morganucodon* and *Kuehneotherium* using *t*-tests (Table S2.7-S2.8).

To compare the damage inflicted on the gel by the *Morganucodon* and *Kuehneotherium* models, I photographed the hard and soft gels after trials were completed and measured the length of fractures in the film using ImageJ (Figure S8-S9) (Schneider et al. 2012). I compared the length of fractures in the cuticle film between *Morganucodon* and *Kuehneotherium* using *t*-tests (Table S2.9). All statistics were performed in R version 3.1.0 (R Core Team 2014).

Results

There were differences in the force-displacement curves for the two species (Figure 2.4, 2.5). In soft foods (Figure 2.5a-c), initial fracture was achieved at a similar time (2.5a, $P = 0.09$), with a similar force (2.5b, $P = 0.47$), and with expenditure of energy (2.5c, $P = 0.33$) by the *Morganucodon* and *Kuehneotherium* models. The mean maximum force for *Kuehneotherium* model the occurred after less time (2.5a, $P = 0.0001$), with less force generated at the maximum force point (2.5b, $P = 0.002$) and with less energy expenditure (2.5c, $P = 0.0009$) compared to the *Morganucodon* model. In sum, *Kuehneotherium* was more efficient at reducing the time, force, and energy to reach maximum force in soft foods. There was no difference between models in their ability to initiate fracture.

In experiments with the hard food items (Figure 2.5d-f), the *Morganucodon* models achieved initial fracture more quickly (2.5d, $P = 0.0008$), with lower forces (2.5e, $P = 0.0002$), and with lower expenditures of energy (2.5f, $P << 0.01$) compared to the *Kuehneotherium* models. The *Morganucodon* and *Kuehneotherium* models achieved maximum force at similar times (2.5d, $P = 0.75$), but the *Kuehneotherium* model exhibited higher forces (2.5e, $P = 0.005$) and larger expenditures of energy (2.5f, $P = 0.01$). In sum, *Morganucodon* was more efficient at reducing the force and energy to initiate fracture and reach maximum force in hard foods.

I evaluated the amount of damage the models inflicted on the proxy food items by comparing the lengths of the fractures caused by the *Morganucodon* and *Kuehneotherium* models. The fractures made by *Kuehneotherium* were significantly

longer than those caused by *Morganucodon* (soft, $P << 0.001$; hard, $P = 0.01$, Figure 2.6a), suggesting that *Kuehneotherium* could cause substantially more damage to food items than *Morganucodon*.

Discussion

Using models of molar tooth rows for two Triassic mammals, I found many biomechanical differences between the *Morganucodon* and *Kuehneotherium* models in their ability to process hard and soft food items. I found some evidence to support our hypothesis that the transition from a triconodont to a symmetrodont molar morphology increases the efficiency of food breakdown, but the results are not straightforward. The biomechanical parameters I measured distinguished between the hard and soft diets, while the damage parameter distinguished molar complexity. The triconodont, *Morganucodon*, was more efficient at consuming hard prey. Both *Morganucodon* and the symmetrodont, *Kuehneotherium,* were similarly efficient at initiating fracture in soft food items, although *Kuehneotherium* reached maximum forces more quickly and with less energy. However, *Kuehneotherium* could inflict more damage than *Morganucodon* on both hard and soft food items. The more complex molars of *Kuehneotherium* provide the ability to inflict more damage and expose more surface area for digestive enzymes, which may be a critical target of selection given the greater metabolic demands experienced by early mammals.

The *Morganucodon* model was better able to process hard food compared to *Kuehneotherium* (Figure 2.5d-f). The linear alignment of cusps alongside the blade-like occlusion of *Morganucodon* served to concentrate the forces over a smaller area

(Figure 2.6b). By concentrating the bite forces onto a small area, the molar can maximize the pressure and stress on the food for a given force (Evans and Sanson 1998, 2005). Once fracture occurs in the hard food item, I hypothesize that much of the energy is expended through propagating the crack in the film and fracturing through the thickness of the sample, rather than deforming the food item (Freeman and Lemen 2006). Due to the linear alignment of the cusps in *Morganucodon*, much of the energy was expended through propagating the crack in the film along the length of the food item. The thin, blade-like cusps of *Morganucodon* penetrated through the hard food item and propagated cracks more easily than *Kuehneotherium*. The ability of the *Morganucodon* models to more efficiently process hard food items could be beneficial for penetrating the hard insects that they are thought to specialize on (Gill et al. 2014).

The *Kuehneotherium* molar was better able to process soft food compared to *Morganucodon* (Figure 2.5a-c). Like hard food items, energy is expended in initiating cracks in soft food items, but a larger percentage of energy is expended in deforming a soft food item. Deformation of the soft food item can occur at a considerable distance away from the initial crack. There is less advantage to concentrating force in a single area when high deformation occurs, and critical stress concentrations can be achieved with a relatively larger area of contact (Evans and Sanson 1998). This may explain why *Morganucodon* and *Kuehneotherium* were equally able to initially fracture soft foods given the larger contact area of *Kuehneotherium* (Figure 2.6b). The *Kuehneotherium* model could distribute force over a larger area because the height of the *b*-cusp is equal to the *c*-cusp, therefore they contact the food item at the

same time adjoining the *a* cusp to form a triangle. *Morganucodon* has a smaller *b*-cusp, which caused the cusps to act like a series of blades in our modeling experiments. The propagation of cracks in the soft food item is more easily achieved by a cusp than a blade as the crests of a cusp act as small blades to divide material following crack initiation (Evans and Sanson 1998). The linear alignment of crests in *Morganucodon* are at a disadvantage, here and this may go some way to explaining the increased efficiency of *Kuehneotherium* in propagating cracks through the soft food. Given previous studies investigating notch angles, *Kuehneotherium*'s more acute notch angles could be more effective than obtuse angles at reducing the amount of energy required to process food (Anderson and LaBarbera 2008; Anderson 2009). Energy reduction is achieved by localizing strain to smaller areas of the food item and reducing deformation. Acute notch angles also increase the 'trapping ability' of teeth, keeping the food item stationary while the cusps are driven through it (Anderson and LaBarbera 2008). The effect of notch angle on food item fracture may be reduced in hard food items because lower deformation of the food will produce less contact between the notch angles and food item.

The triangular arrangement of cusps in *Kuehneotherium* increased the damage inflicted on both hard and soft food items given their longer shearing crests. In biological terms this translates into breaking food into more, smaller pieces in a single bite. Damage to a food item increases the surface area that contacts digestive enzymes, which allows more rapid extraction of nutrients in the digestive tract. Rapid nutrient extraction is important in meeting the high metabolic demand of homeothermy. However, *Kuehneotherium* caused more damage at the expense of

higher forces, energy and time required to process hard food items. The jaw of *Kuehneotherium* was more gracile and so could probably not produce the higher forces required to penetrate hard foods and would likely favor soft foods. This is supported by tooth microwear studies which demonstrated how the molars of *Kuehneotherium* typically exhibit smaller pits and scratches representative of a softer diet (Gill et al. 2014). In soft food items *Kuehneotherium* caused more damage for a similar amount of time, energy and force, and was also able to propagate cracks more efficiently compared to *Morganucodon*. Strait (Strait 1993) predicted that the teeth of insectivores that specialize on soft foods exhibit longer shearing surfaces as they can contact and divide more food per chewing cycle. It is likely that there are also additional advantages associated with triangular cusp arrangements (e.g. increased capture areas and food trapping ability).

Damage may be the most important parameter in this assessment of early mammal tooth morphology and function. *Morganucodon* may exhibit low forces and energy following a feeding trail, but if the food item were still intact then it would become more difficult to extract useable energy from the food item during digestion. *Kuehneotherium* caused the greatest amount of damage to both hard and soft gels. This is the only biomechanical parameter I measured where one model was superior regardless of food item stiffness. The damage inflicted to a food item may be easier for selection to act upon because it has a direct relationship to the amount of useable energy that can be extracted from the food item (Evans and Sanson 1998; Berthaume 2016; Sanson 2016). The transition to complex teeth improved the ability to inflict damage on a food item that transcends the biomechanical variables I

measured here. Complex teeth with different morphologies are often specialized for biomechanical tasks associated with the material properties of the foods that the animals eat (Evans and Sanson 2005, 2006). For example, horse teeth perform well at cutting and grinding grass while cat teeth are good at cutting and piecing meat, they are both complex dentitions with very different morphologies that are specialized for damaging food with a specific material property (Evans et al. 2007). *Kuehneotherium* is more complex than *Morganucodon* so performs better at inflicting damage on a food item, but the biomechanical variables show that *Kuehneotherium* was tuned to soft food and *Morganucodon* to hard food.

Conclusions

Here I show, by testing physical models of tooth rows, that increased tooth complexity can have a significant impact on the biomechanics of food processing. I find evidence for dietary specialization based on molar morphology; the triangular molars of *Kuehneotherium* are more suited to processing soft foods while the blade-like molars of *Morganucodon* are more suited to processing hard foods. I also highlight the importance of incorporating food item damage into studies of dental functional evolution, as this may be an important target of selection. This study provides more evidence to suggest stem mammals exhibit more morphological and functional diversity than previously thought, and specializations in the teeth of early mammals could lead to trophic diversification and niche partitioning. Changes to tooth morphology can originate in relatively simple developmental shifts that alter the position and number of cusps on the molar crown (Rodrigues et al. 2013;

Harjunmaa et al. 2014). Subsequent selection for differences in molar structure that affect food processing led to the close association between molar morphology and diet I see in modern mammals (Evans et al. 2007). Due to the intimate relationship between molar form and function and the rising metabolic costs of homeothermy, the ability to break food into small pieces was likely a significant factor in driving the trophic diversification of Mesozoic mammals and their living descendants (Luo 2007; Gill et al. 2014).

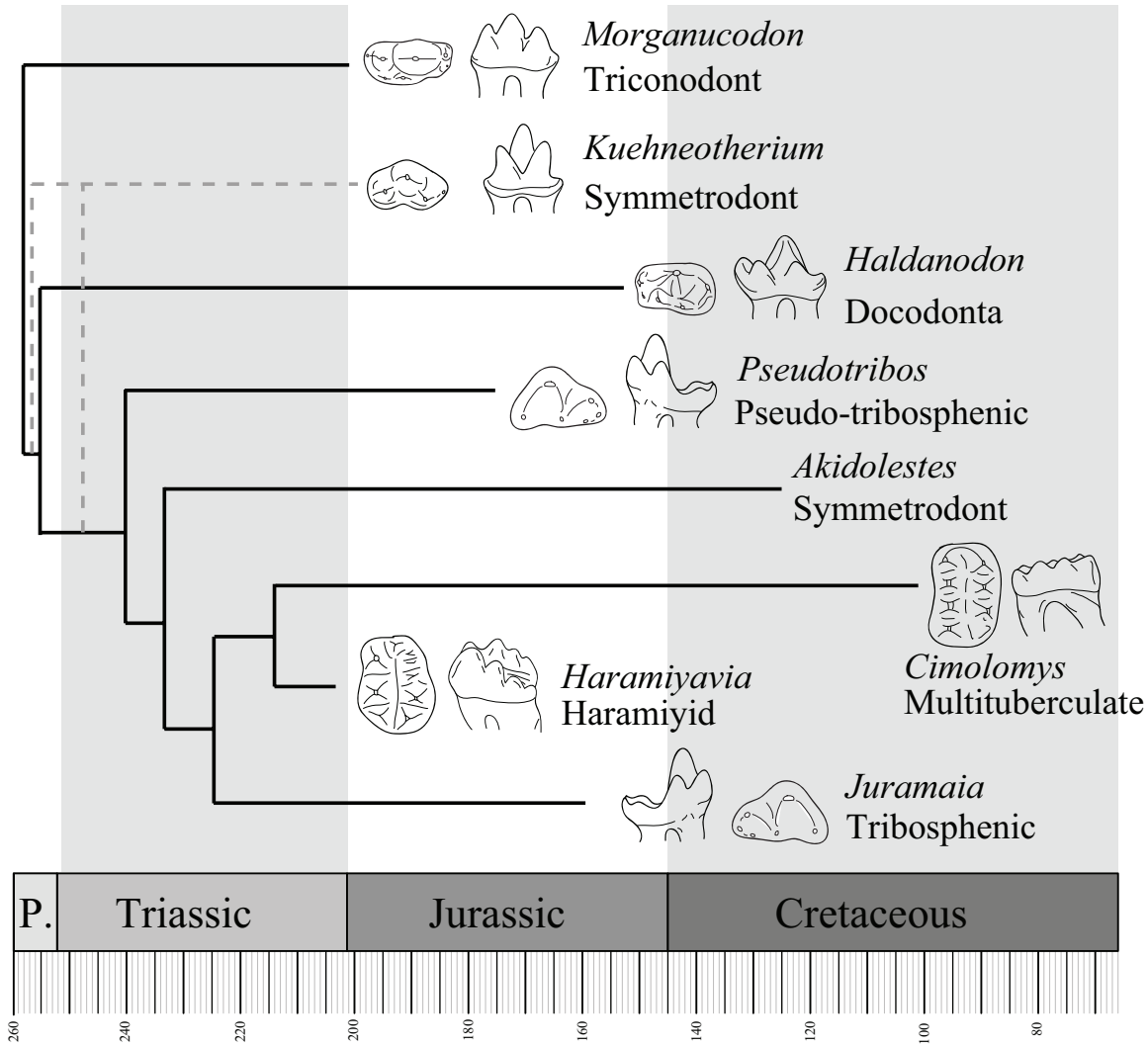

Figure 2.1: Phylogeny of select Mesozoic mammals with example lower molar morphologies.

Phylogeny based on (Luo et al. 2002; Rougier et al. 2012; Meng et al. 2015). P. is used to represent Permian. Position of *Kuehneotherium* is poorly resolved but always falls out as more derived than *Morganucodon* (grey dashed branches).

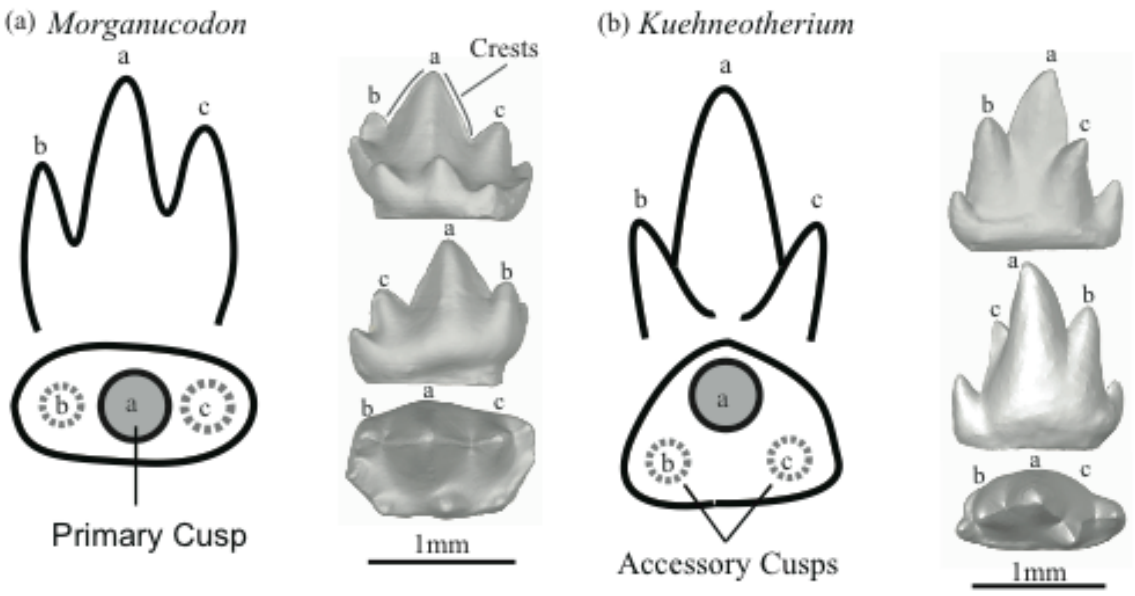

Figure 2.2: Schematic and CT images of the teeth used in this study.

Schematic drawings and computed tomography (CT) scans of *Morganucodon watsoni* (a) and *Kuehneotherium praecursoris* (b) from Late Triassic-Early Jurassic fissure fills in Glamorgan, Wales, UK. Upper scans, lingual view; middle scans, buccal view; lower scans, occlusal view. See supplementary information for scanning and specimen details.

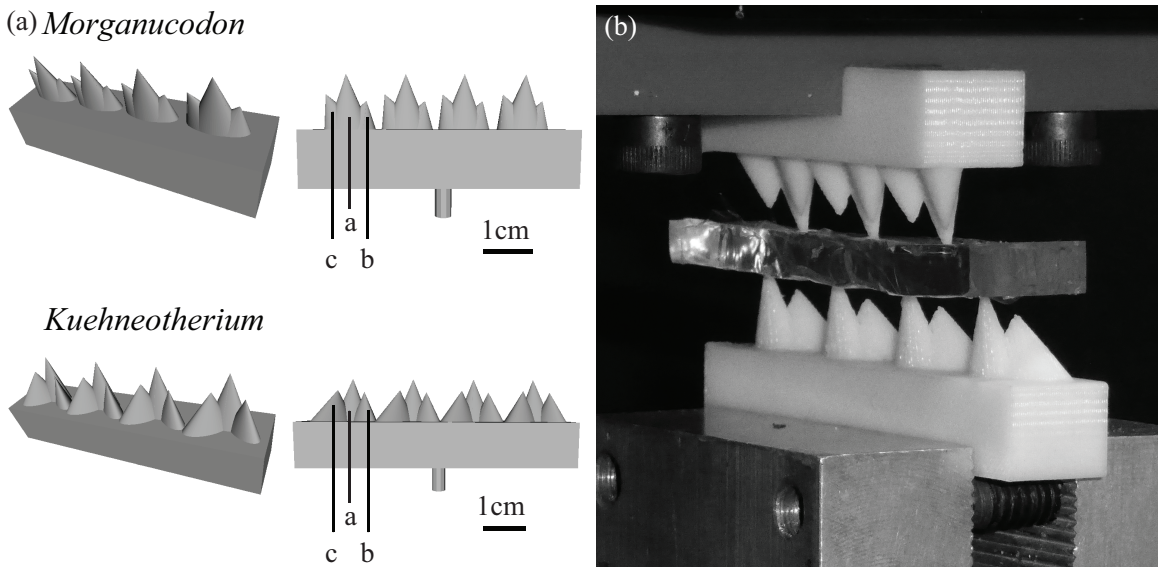

Figure 2.3: CAD models and experimental set-up.

(a) CAD models of each molar row. (b) Experimental set-up using *Kuehneotherium* and PDMS-PET proxy food item.

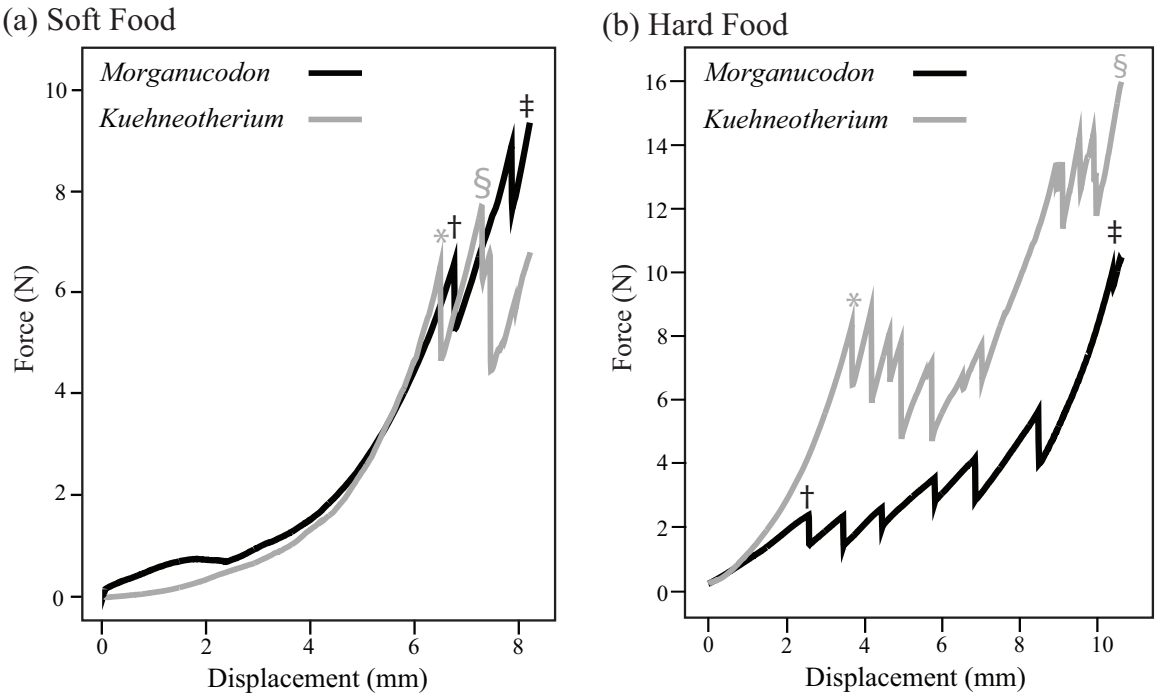

Figure 2.4: Force landscape for gel puncture trials

(a) Soft food item, (b) hard food item. * Denotes initial fracture in *Morganucodon*, † in *Kuehneotherium*. § denotes the peak of maximum force in *Morganucodon*, ‡ in *Kuehneotherium*.

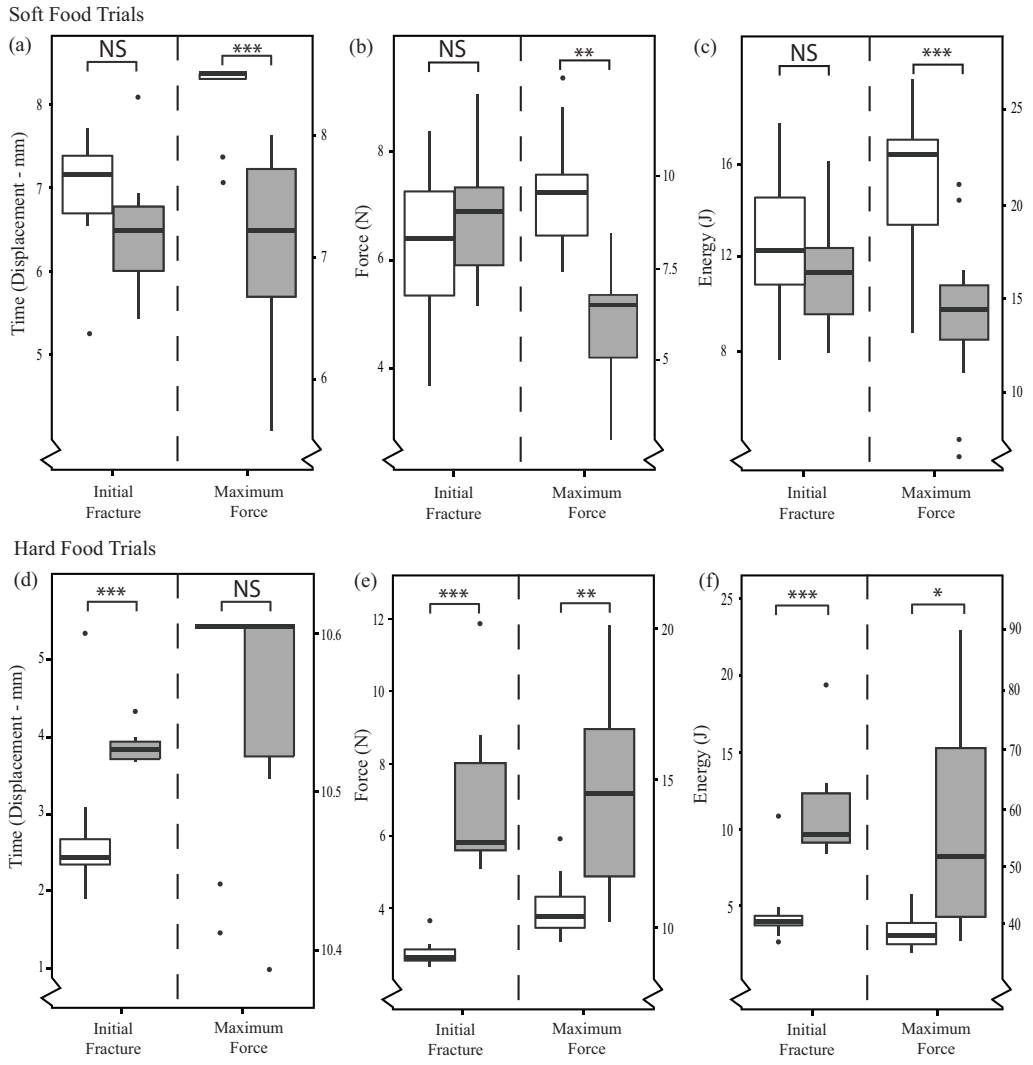

Figure 2.5: Time, force and energy boxplots for both species

Kuehneotherium, grey boxplots; *Morganucodon*, white boxplots. (a-c) Soft food items; (a) Boxplots of displacement at point of initial fracture and maximum force, (b) boxplots of force at fracture and maximum force, (c) boxplots of energy at point of initial fracture and maximum force, (d-f) Hard food items (d) boxplots of displacement at point of initial fracture and maximum force, (e) boxplots of force at fracture and maximum force, (f) boxplots of energy at point of initial fracture and maximum force. * = $P < 0.05$, ** = $P < 0.01$, *** = $P < 0.001$, NS = not significant.

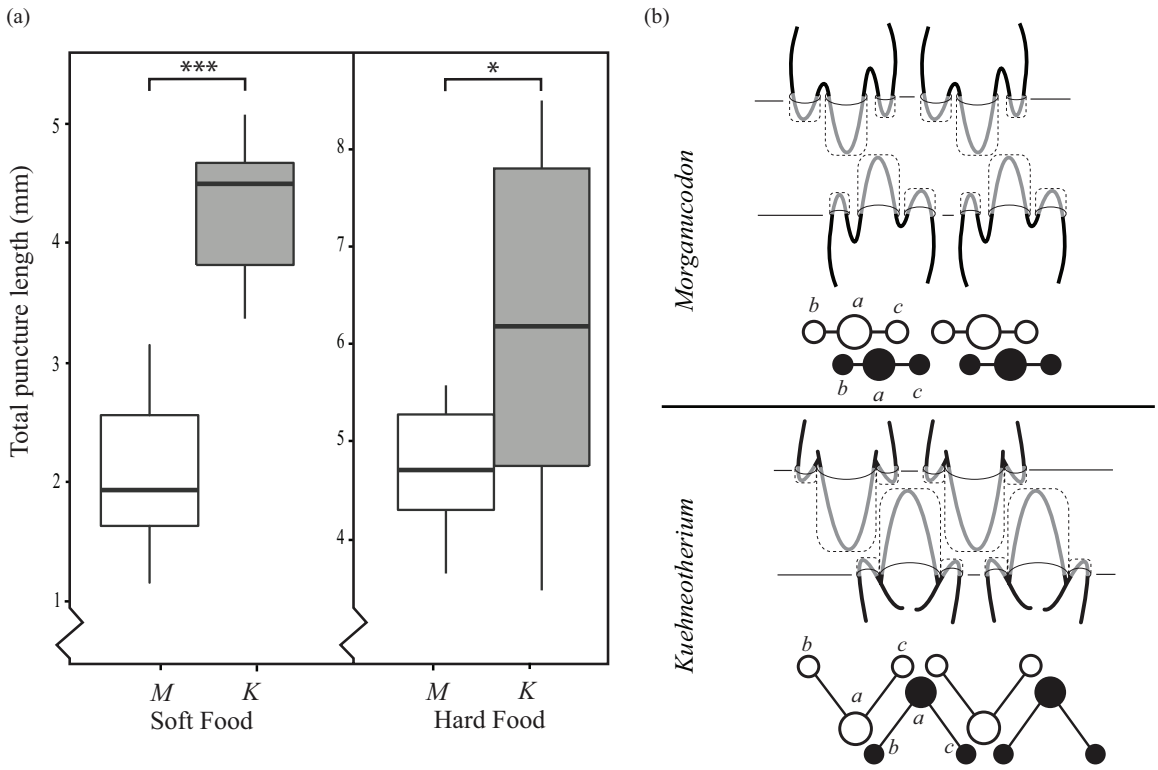

Figure 2.6: Cuticle damage

(a) Boxplot illustrating the total length of cuticle puncture for both species (M – *Morganucodon*, white; K – *Kuehneotherium*, grey), * = P < 0.05, *** = P < 0.001. (b) Schematic to illustrate where forces are being exerted on the gel at the point of maximum force (white = upper cusps; black = lower cusps). After the primary cusp a fractures the cuticle the accessory cusps come into contact to further propagate cracks through the food item. In *Morganucodon* the accessory cusps contact the cuticle sequentially, the c cusp followed by the b cusp, such that force is initially concentrated over a smaller area. In *Kuehneotherium* both accessory cusps contact the cuticle simultaneously, forming a triangle and distributing force over a wider area.

CHAPTER 3

DIFFERENCES IN PHENOTYPIC INTEGRATION, RATES OF MORPHOLOGICAL EVOLUTION, AND MORPHOLOGICAL DISPARITY ARE ASSOCIATED WITH CLIMATIC VARIABILITY IN THE CARNIVORA

Introduction

A latitudinal gradient in biodiversity is posited to arise from climatic differences between tropical and temperate regions (Mannion et al. 2014). Biodiversity reaches its peak in tropical regions and decreases towards the poles. This spatial distribution of biodiversity is driven by many factors, including speciation and extinction rates, associations between body shape and physiology, and rates of morphological evolution. High taxonomic diversity in the tropics is associated with high rates of net diversification (fast speciation rates and slow extinction rates), which are often ascribed to favorable climatic conditions, higher primary productivity, and a wider variety of niches (Weir and Schluter 2007; Botero et al. 2013; Rolland et al. 2014). It was Dobzhansky (1950) and later Fischer (1960), who first untangled the likely reasons for a latitudinal gradient in organismal biodiversity, physiology, and morphology – climatic variability. High variability in precipitation is more typical of lower latitudes while high variability in temperature is more typical of higher latitudes, and both can influence spatiotemporal patterns of diversity and migration (Cooper et al. 2011; Fraser et al. 2014). Climatically

variable regions typically contain habitats with the fewest niches, largest fluctuations in food availability, lowest primary productivity, and lowest species diversity. Dobzhansky (1950) and Fischer (1960) hypothesized that the more variable climatic conditions common in temperate and montane regions produced trophic generalists, which do not exhibit a great deal of morphological or physiological variation. In contrast, the more stable climatic conditions common in rainforests and deserts permitted the evolution of trophic specialists with a wider range of morphological and physiological characteristics (Schemske et al. 2009). Understanding how climate affects the tempo and mode of morphological evolution is vital to understanding why we observe uneven distributions of biodiversity among regions.

Here I assess the impact of climatic variability (seasonal fluctuations in temperature and precipitation) on morphological evolution, and begin by outlining two predictions. The first prediction is that climate affects morphological integration (the degree of covariation between suites of traits), and by extension, disparity (morphological diversity) (Goswami et al. 2014). Low climatic variability can lead to species with restricted environmental tolerances and limited dispersal ability (Merritt et al. 2001; Bluhm and Gradinger 2008; Mannion et al. 2014), and high integration can facilitate the evolution of trophic specialists common in these regions (Monteiro and Nogueira 2010). The second prediction is that climate affects rates of evolution by producing a broader or narrower range of niches which would enhance or reduce the rate of morphological evolution respectively (Yoder et al. 2010). The availability of ecological niches can vary greatly with climate and

depends on environmental conditions and the ability of taxa to migrate to and exploit them (Mannion et al. 2014). Understanding the role of climate in shaping phenotypic integration and rates of morphological evolution is critical to understanding current geographical variation in biodiversity and modeling the potential for phenotypic responses to climatic change.

Inter- and intraspecific differences in disparity are often associated with the level of phenotypic integration – the strength of covariation among sets of anatomical traits or landmarks (Klingenberg 2008; Goswami and Polly 2010; Goswami et al. 2014). The evolution of phenotypic integration can be mediated by selection on heritable, functionally correlated traits and genetic pleiotropy (Blows 2007). Subsets of landmarks within an anatomical region that are more tightly correlated with one another than they are with landmarks in another anatomical region are called modules (i.e., covariation among landmarks is higher within modules than between modules). Integration and modularity lie at either end of a continuum in trait covariation. On one end of the continuum one can imagine an anatomical structure that is highly integrated and all of its parts evolve in unison. At the other end of the continuum one can imagine an anatomical structure that is highly modular and all of its parts evolve independently (Klingenberg 2008). Genetic and developmental processes ultimately control the continuum of trait covariation and reflect coordination between development and function and evolution. In highly integrated structures, where covariance between modules is strong, phenotypic evolution can be constrained and the range of morphological variation is likely reduced (Drake and Klingenberg 2010; Klingenberg 2010). This

has implications for the ability of a clade to evolve (its evolvability) and respond to constantly changing or hostile environments (Pigliucci 2008; Le Rouzic et al. 2013). The phenotypic evolution of highly integrated structures must proceed along a narrow line delimited by the covariation between landmarks, known as the line of least resistance. If different anatomical modules can develop and evolve independently, then the wider range of potential morphological diversity could allow access to unique or unoccupied niches (Wagner et al. 2007) and thereby influence the rate of morphological evolution (Goswami et al. 2014).

Variation in rates of morphological evolution within and among clades may arise due to a combination of functional and ecological factors. For example, phyllostomid bats underwent increased speciation and a reduction in the rate of skull evolution as they invaded a frugivorous niche (Dumont et al. 2012). Species with skulls that had high mechanical advantage were able to pierce the tough outer flesh of hard fruits, and this favored the proliferation of species with shortened palates (Dumont et al. 2014). Alternatively, the evolution of novel feeding morphologies in reef-dwelling labrid fishes (wrasse and parrotfish) was associated with more rapid rates of morphological evolution and higher morphological disparity relative to non-reef dwelling labrids (Price et al. 2011). In each case, movement into vacant ecological niches was associated with a change in the rate of morphological evolution. A limited number of studies have identified inter- and intraspecific differences in rates of morphological evolution and disparity along climatic gradients. Rusty-nosed rat (*Oenomys*) populations collected along a climatic gradient from eastern to western central Africa exhibited intraspecific differences in

tooth size and morphology attributed to differences in diet. The *Oenomys* populations occupying wetter western African environments exhibited larger molars compared to the drier east African populations (Renaud 1999). In another example, new world monkeys with more gracile skulls, longer rostrums, and expanded teeth exhibited greater diet diversity and were found south of the Amazon, in dryer and more seasonal environments (Cáceres et al. 2014). Cáceres et al. (2014) suggested these morphological changes allowed them to deal with a broader range of foods, but in the process they became less specialized folivores (Wright et al. 2009), evidenced by smaller distance between the temporalis muscle and tooth row which served to reduce mechanical advantage. These studies suggest that differences in rates of morphological evolution are linked with ecology, diet, habitat, and, by extension climatic variability.

The mammalian order Carnivora is distributed over a wide geographical area and provides a good test case to investigate the relationships among climatic variability and integration, and climatic variability and rates of morphological evolution. I studied the lower jaws of carnivorans because it is a single bone involved in multiple, ecologically relevant tasks, including feeding and communication. I examined the interaction between climate and the continuum of trait covariation using two different methods to gain insight into how climatic variability influences morphological evolution at different levels of anatomical organization. I started by examining the relationship between the magnitude of integration across the entire jaw and climatic variability. This test estimates each species' contribution to the magnitude of jaw integration relative to the whole clade

and regresses that value against the species' mean value of temperature or precipitation variability (determined from the centroid of its geographic range). I investigated the pattern of integration within the jaw by assessing the degree of covariation between two *a priori* functional modules, the posterior, muscle bearing region and the anterior, tooth bearing region. For each of these analyses I divided our sample into a low and high climatic variability group and determined the rates of jaw morphological evolution and jaw disparity in each group. I restricted our sampling to three carnivoran clades that span regions with high and low climatic variability: Canidae (dogs, foxes, and their allies), Felidae (cats), and Mustelidae (weasels, badgers, and otters). Each of these clades has roughly equal taxonomic diversity in regions with low and high climatic variability, a narrow range of diets, a global distribution, and species that inhabit more and less climatically variable regions are interspersed throughout the phylogeny.

Given the close association between climate and biotic interactions I hypothesize that climatic variability can affect organisms in terms of both developmental processes (magnitude and pattern of phenotypic integration) and macroevolution (rates of morphological evolution and disparity) (Figure 3.1). In particular, I expect to observe faster rates of morphological evolution in taxa from more climatically variable regions, as these conditions can produce rapidly changing selective pressures (Schemske et al. 2009; Botero et al. 2013; Rabosky et al. 2013). Simulation studies reveal that populations encountering a rapidly changing environment evolve faster (Kashtan et al. 2007, 2009), and empirical evidence points to faster rates of speciation and evolution in mammalian body size within

climatically variable regions (Diniz-Filho et al. 2009; Cooper and Purvis 2010). Given the close relationship between rates of morphological evolution, disparity, and phenotypic integration (Hallgrímsson et al. 2009), I expect disparity among jaws to be higher and integration within jaws to be lower in more climatically variable regions. Being highly integrated could be detrimental to the survival of organisms in climatically variable regions as this could limit the resources available to the organism, and make it difficult to respond to a constantly changing environment over a period of generations (Goswami et al. 2015). High phenotypic integration working across a clade could also reduce the potential for morphological diversification over macroevolutionary time (Goswami and Polly 2010). Support for these predictions would suggest that climatic variability influences rates of morphological evolution, disparity, and phenotypic integration in carnivorans.

Materials and Methods

Specimen collection

I obtained jaw morphology data for 80% mustelid, 91% canid, and 83% felid species. The species examined represent all of the major ecological and morphological diversity in their respective clades (Table S3.1). I photographed a total of 322 individuals in lateral view with a scale bar using a digital camera affixed to a stand above the specimen. I imaged 124 males and 105 females, 94 individuals lacked gender information. The complete dataset totaled 322 individuals representing 97 canids, 90 felids, and 135 mustelids (Table S3.1).

Landmark analysis

I selected 14 landmarks from across the jaw to fully encompass the shape of the ramus and corpus (Figure 3.2). Acquisition of landmarks was performed using the *tps* software suite (Rohlf 2004). For those species with multiple individuals I used the average landmark coordinate positions to represent species in subsequent analyses. Following placement of landmarks, general least squares Procrustes superimposition was used to remove the effects of size, translation, and rotation differences among imaged jaws (Rohlf 1998). I performed a Procrustes ANOVA on the centroid size and shape data and found a significant effect of allometry on shape ($r^2 = 0.091$, $F = 32.13$; $P = 0.002$). To minimize the potential effects of allometry, I performed a regression of shape on geometric centroid size using the geomorph package (v3.0.1) in *R* to generate a landmark data set based on residuals (Adams and Otárola-Castillo 2013). I then performed a principal components (PC) analysis on these data to quantify variation in shape. From this analysis I exported four primary PC scores that represented over 70% of the total shape variation (mustelids 71.43%, felids 72.63%, and canids 75.53%). I plotted scores on the first two PCs to provide a visual representation of the range of morphological variation among jaws.

Phylogenetic and climatic data

I used a time-calibrated species-level supertree of the Carnivora to perform all phylogenetic comparative analyses (Nyakatura and Bininda-Emonds 2012). From this larger tree, I extracted separate trees for the mustelids, canids, and felids. Taxa present in the tree but lacking morphometric data were removed using the Ape package in *R* (Paradis 2012).

I downloaded Carnivoran range maps from the IUCN Red List website for all species in our tree (iucnredlist.org/technical-documents/spatial-data) and randomly sampled 12 latitude-longitude points within each species' shape file and extracted climatic data at each coordinate. I extracted species specific climatic data for current conditions using the WorldClim v1.4 database (worldclim.org). To gather information on temperature and precipitation variability I sampled data for annual temperature range (bio7) and annual precipitation seasonality (bio15) from each layer at 2.5 minute resolution (~5km^2). Annual temperature range was calculated as maximum temperature of warmest month minus the minimum temperature of the coldest month. Precipitation seasonality was taken as the coefficient of variation of annual precipitation. I extracted climatic data for all species and calculated a mean for each species. I used the *R* packages raster (v2.5.2), PBSmapping (v2.67.6) and sp (v1.2.1) to extract all climatic data.

For analyses of disparity, rates of morphological evolution, and the pattern of integration I divided the taxa in each clade into groups based on their residence in regions that experience either low or high climatic variation. For our first grouping I divided our taxa into two equal groups for each clade by ranking our taxa by temperature variability and placing half in the low variability category and half in the high variability category. For our second grouping I repeated the step above but ranked taxa in each clade by precipitation variability before placing half into the low variability category and half into the high variability category.

Phylogenetic Comparative Methods

Analysis of species level integration

I calculated integration among species using a recently developed statistical method that uses a jackknife resampling approach of PC scores to obtain inter-species variation in integration for each species (Hu et al. 2014). For each carnivoran family I calculated the variance of scaled eigenvalues (the percent variance accounted for by each PC axis) and then removed a single species and recalculated the variance of the scaled eigenvalues. The difference between the scaled eigenvalues (full dataset minus dataset missing one species) represents the contribution of the missing species to integration. If the difference between scaled eigenvalues resulted in a negative score then that species reduced the level of integration in the sample. A positive score indicated that the species served to increase integration within the sample.

I used phylogenetic generalized least squares (PGLS) regressions to examine the relationship between integration and climatic variability among species within each clade because they generate slope and intercept estimates that account for the correlation between variables that can be attributed to phylogeny (Symonds and Blomberg 2014). To account for phylogenetic structure, I first extracted the expected covariance under a Brownian motion (BM) model from our tree using the *corBrownian* function in ape (Paradis et al. 2004). I then used the *gls* function in the nlme (v3.1.120) package to perform the PGLS analysis.

Pattern of integration

I tested the pattern of integration in the jaw by assessing the degree of covariation between two well-established modules (Klingenberg et al. 2003; Meloro et al. 2011), the corpus (the anterior tooth-bearing region) and the ramus (the posterior muscle-bearing region) (Adams and Felice 2014). This method accounts for phylogeny using the evolutionary covariation matrix from the PGLS analyses to quantify the degree of covariation between sets of landmarks. I computed the pattern of jaw integration for taxa in regions with low and high climate variability separately for each clade. For each climatic variability grouping I partitioned landmarks into a 'corpus' block and a 'ramus' block' and determined the level of covariation between them. I compared the observed covariation value to a null distribution of values created by randomly permuting species' character data onto the tips of the phylogeny 1000 times. Significance indicates that the two portions of the jaw covary together (i.e., they are integrated). See Adams and Felice (2014) for full details of the method.

Procrustes disparity

I used Procrustes variance to compare disparity between low and high variability regions for each carnivore family (Adams and Otárola-Castillo 2013). The test measures the range of all observations around the mean shape for each family. Procrustes variance is the mean squared Procrustes distance of each specimen from the mean shape of the given clade, and can be calculated as the sum of the diagonal elements of the covariance matrix of that clade (e.g., Zelditch et al. 2012). I evaluated significance in disparity between low and high climatic variability groupings by

comparing the observed test statistic (taken as the group Procrustes variances) to a random permutation generated by shuffling each species contained in the shape matrix relative to the climatic variability grouping assignment (low or high). I used the *morphol.disparity* function in the *R* geomorph package to conduct the Procrustes variance analysis (Adams and Otárola-Castillo 2013).

Rates of morphological evolution

Within each clade I compared the rates of morphological evolution between taxa in regions of low and high climate variability using the Procrustes-fitted jaw shape data. I used a method that calculates a phylogenetically corrected rate based on a species distance approach (Adams 2014). The ratio of the maximum to minimum evolutionary rate is used as a test statistic, and differences between groups are determined by comparing observed data to simulated tip data under a BM model that uses a single rate for all species. I use the *compare.evol.rates* function in the *R* Geomorph package to perform rate comparisons (Adams and Otárola-Castillo 2013).

Phylogenetic MANOVA

I used a pMANOVA to test for differences in PC scores (e.g., jaw shape) between taxa from low and high variability regions. The MANOVA test statistic was calculated based on the scores from the first 4 PC axes and compared to a null distribution of PC scores. The null distribution was generated via 1000 simulations of new dependent variables determined from a single rate matrix on the phylogenetic tree. The pMANOVA was conducted using the Geiger (v2.0.3) package with the *aov.phylo* function (Harmon et al. 2008).

Results

Morphospaces

In each clade, taxa grouped by temperature variability and precipitation variability overlap in the morphospace defined by PC1 and PC2 (Figure 3.3; Table S3.1 and S3.2). The first PC axis in canids represents diversification across an elongated to shorted mandibular body (34.26% of variation). The position of the masseteric fossa defines the second PC and ranges from a shortened, posterior position to an elongated, anterior position (22.48% of variation). PC1 in felids reflects an elongated to shorted mandibular body and a ventral to dorsal shift in the angular process (34.74% of variation). PC2 is defined by a shortened to elongated ramus (20.60% of variation). PC1 (28.69% of variation) in mustelids describes variation in ramus width (short to long) and coronoid position (anterior to posterior). PC2 (17.75% of variation) represents a flat to curved mandibular body alongside a dorsal to ventral transition of the angular process. Climatic variability had a minor effect on the location of species in morphospace. Only mustelids in the temperature variability grouping exhibited differences in morphology (pMANOVA, $F=4.99$, $P=0.023$) driven by badgers and sea otters which are located in unique regions of morphospace.

Magnitude and pattern of integration

In canids and felids climatic variability is a significant predictor of phenotypic integration. More specifically, integration in canids is predicted by temperate variability, while integration in felids is predicted by an interaction

between temperature and precipitation variability. In canids, as temperature variability increases, the level of integration decreases (Table 3.1; Figure 3.4a). In felids, as temperature and precipitation variability increases, integration decreases (Table 3.1; Figure 3.4b).

I found no evidence for a ramus-corpus pattern of integration in the carnivoran jaw. Across all three clades, taxa from regions with low and high climate variability are significantly integrated, indicating that the ramus and corpus regions of the jaw covary together (Table 3.2).

Procrustes disparity

Canids and mustelids exhibit differences in morphological disparity between regions with low and high temperature variation (Table 3.2). In both clades, taxa in low temperature variability regions exhibit higher disparity. There are no significant differences in morphological disparity when grouping clades by precipitation variability, and there are no differences in morphological disparity between climatic grouping in felids.

Rates of morphological evolution

Rates of morphological evolution are consistently higher in taxa from lower temperature and precipitation variability regions (Table 3.2). Canids and mustelids exhibit significant differences in evolutionary rates when grouped by temperature variability. Felids and mustelids exhibit significant differences in their rates when grouped by precipitation variability.

Discussion

I found an association between the level of jaw integration and climatic variability in canids and felids (Figure 3.4, Table 3.1). In canids, as temperature variability increases, jaw integration decreases. In felids, increased temperature and precipitation variability is associated with decreased jaw integration. This suggests climatic variability predicts phenotypic integration in canids and felids and may be a consequence of, or a response to, the relative magnitude of long and short-term environmental changes (e.g., glaciations, seasonality). Larger annual climatic oscillations can produce greater environmental stochasticity and, in turn, produce changes in home range, niche size, and greater variation in food availability (Botero et al. 2013; Hua and Wiens 2013; Mannion et al. 2014). Low levels of phenotypic integration may allow canids and felids in more variable environments to be more evolvable (generate adaptive phenotypic variation) and more responsive to these annual environmental perturbations (Pigliucci 2008). I also found that the ramus and corpus modules of the jaw covaried together across all clades and climatic variability assignments. I therefore must revise our initial hypotheses set out in Figure 3.1, as I find low support of a pattern of integration between the ramus and corpus, regardless of climatic variability.

Rates of morphological evolution and disparity were consistently greater in regions with low climatic variability. I find a coupling between rates of morphological evolution and disparity. Rates and disparity are typically coupled when taxa undergo morphological divergence and invade new regions of morphospace (Sidlauskas 2008). Canids grouped by temperature variability

exhibited faster rates of jaw evolution and higher disparity in low variability regions. Felids grouped by precipitation variability also exhibited faster rates of jaw evolution in low variability regions. Mustelids in low variability regions exhibited faster rates of jaw evolution when grouped by precipitation variability, and exhibited both faster rates of jaw evolution and higher disparity when grouped by temperature variability. These results do not support our initial hypotheses set out in Figure 3.1, and suggest more stable climatic conditions could result in more niches and in turn could promote faster rates of morphological evolution, greater diet diversity, and greater trophic specialization (Pianka 1966; Schemske et al. 2009; Fine 2015). Trophic generalists typically occupy the most climatically variable regions (Cooper et al. 2011). Generalists may undergo longer periods of stasis as there is little pressure to undergo morphological change: they can occupy niches with little change in morphology (Renaud et al. 2005). Despite this, I found minimal evidence for differences in morphology between low and high climatic variability taxa (excluding temperature grouped mustelids). Members of the badger family (*Arctonyx* and *Melogale*) and the sea otter (*Enhydra*) primarily drove this difference in mustelids (Figure 3.3c).

The coupling (or decoupling) of integration and morphological disparity has garnered much interest in recent years. Integration can influence disparity by permitting morphological change in certain directions while constraining it in others (i.e., a line of least resistance). If the pattern of integration and the direction of selection are aligned, then morphological disparity can increase and more extreme morphologies can evolve (Goswami et al. 2014, 2015). One recent empirical

example using Antarctic icefish demonstrated that the group exhibited both high integration and high disparity, and this association likely facilitated the invasion of a novel pelagic foraging niche (Hu et al. 2016). I report a similar pattern here in canids and mustelids whereby high integration is associated with high disparity, possibility as a consequence of, or response to, residing in regions of low climatic variability.

Phenotypic integration and rates of morphological evolution are also theoretically positively correlated (Klingenberg 2008; Hallgrímsson et al. 2009), although empirical evidence is limited (but see Claverie and Patek 2013) and some simulation data suggest no relationship (Goswami et al. 2014). One factor that typically influences the rate of morphological evolution is the rate of speciation. High variability in temperature is thought to increase speciation rates in both birds and mammals (Weir and Schluter 2007; Botero et al. 2013), although they may be accompanied by high extinction rates. In carnivorans, rates of net diversification (speciation minus extinction) are equivalent between temperate and tropical regions (Rolland et al. 2014). The rate of diversification is typically linked to the rate of morphological evolution under the theories of punctuated equilibrium and adaptive radiation (Gould and Eldredge 1977; Schluter 2000; Ricklefs 2004; Rabosky et al. 2013). Given these theories I would expect few differences in rates, yet I find fast rates of morphological evolution (and high integration) in more climatically stable regions indicating that processes other than speciation have influenced the rate of jaw shape evolution. Our results, along with those of previous studies, suggest that the link between climatic variability, integration, and rates of

evolution is highly context dependent and may rely on the environment, the anatomical structure being studied, and the strength of integration within that structure.

Levels of integration are influenced by many extrinsic and intrinsic factors such as diet, biomechanical function, and genetic-developmental regulation (Klingenberg 2014). Taxa that experience similar ecological conditions are likely to exhibit similar patterns of phenotypic integration. For example, *Anolis* species occupying similar environments exhibited similar trait means and levels of integration regardless of phylogenetic relatedness (Kolbe et al. 2011). Similarly, the piscivorous black basses (*Micropterus*) all exhibit the streamlined body shape indicative of pursuit predators and is associated with high levels of phenotypic integration and low levels of morphological disparity across the genus (Smith et al. 2015). It is therefore not surprising that closely related carnivore species exhibit differences in the level of integration when they experience different ecological conditions. Given that taxa within low or high climatically variable regions are not phylogentically clustered provides additional evidence for the disassociation between covariation structure and phylogeny (Marroig and Cheverud 2001; Kolbe et al. 2011).

Temperature and precipitation variation may explain differences in integration among taxa, at least in canids and felids. It appears that those organisms in regions with greater climatic variability exhibit lower levels of integration (Figure 3.4). Previous studies have demonstrated that diet can influence integration between within and between species (e.g., Anderson et al. 2014; Albertson et al.

2005; Monteiro and Nogueira 2010; Hu et al. 2014). In particular, I propose that the association between integration and climate in canids and felids may be driven by seasonality in diet breadth and composition. For more temperate members experiencing greater climatic variability, seasonal variation in prey type fluctuates between cold and warm seasons, while tropical members can experience fluctuations during the wet and dry seasons. The result of beneficial jaw remodeling occurring from one season to the next over many generations may result in selection to maintain this plasticity. With selection acting in multiple directions between seasons, low levels of integration should facilitate this increased potential for variability over macroevolutionary scales (Pigliucci 2008). This conforms to the idea that evolvability is typically higher in fluctuating environments such as those found in temperate regions (Le Rouzic et al. 2013).

Many of the taxa I examined here seasonally fluctuate their diets in response to spatial and temporal fluctuations in food availability. Canids exhibit the broadest diet of all the taxa I examined here (see the panTHERIA database '6-1_DietBreadth' entry (Jones et al. 2009), canids average = 3.78), and can readily shift their diets in response to changing environmental conditions (e.g., *Canis lupus* (Milakovic and Parker 2011); *Canis latrans* (Dowd and Gese 2012); *Cuon alpinus* (Thinley et al. 2011); *Chrysocyon brachyurus* (Jácomo et al. 2004)). Likewise, felids experience seasonal fluctuations in prey availability, breadth, and size due to climatic cycles. This is reported in various *Lynx* species (Roth et al. 2007), *Felis silvestris* (Herbst and Mills 2010), *Puma concolor* (Iriarte et al. 1990), *Leopardus geoffroyi* (Canepuccia et al. 2007) and *Panthera onca* (Scognamillo et al. 2003). Although there was no

association between integration and climatic variability in mustelids, the literature points to some members that show seasonal variation in diet breadth and composition. Honey Badgers, (Begg et al. 2003; Zhou et al. 2014) hog badgers (Begg et al. 2003; Zhou et al. 2014), martens (Lanszki et al. 1999), otters (Gorgadze 2013), and weasels (Goszczynski 1999; Martinoli et al. 2001) all exhibit seasonal shifts in diet. Mustelids represent an interesting example of a clade that does not share an association between integration and climatic variability, while rates of morphological evolution and disparity are associated with climatic variability. I are aware of numerous clades exhibiting differences in rates of morphological evolution or disparity associated with climatic variability, likely as a result of diet and environment (e.g., capuchin monkeys (Cáceres et al. 2014), South-American canids (Bubadué et al. 2016), ovenbirds (Derryberry et al. 2011)), but differences in integration have not been explicitly documented until now. It is possible that the relationship between integration and climatic variability in some clades is not always complementary, and could depend on a variety of different abiotic and biotic factors.

In general, differences in integration appear to be associated with the degree of climatic variability. Low variation in temperature and precipitation is typical in Europe, while other regions such as Mongolia and eastern Russia can experience high variation (Figure 3.5a). Low variation in temperature and precipitation is typical of rainforest biomes such as the Congo or Amazon, while the Sahara and Sahel regions in Africa can experience high temperature and precipitation variation respectively (Figure 3.5b). However, I are yet to fully understand the ecological or

evolutionary contexts that govern differences in the strength of integration. By investigating jaw integration in other clades of mammals that exhibit a similar global distribution (e.g., cricetid rodents, bovid ungulates) I can better understand if the pattern I observed here is consistent. Similarly, by using other well-studied structures such as the skull or shoulder girdle to investigate integration I will gain a better understanding of how these structures respond to a climatic gradient. Finally, another open question is how do clades respond to climatic instability when there are fewer geographical constraints to movement (e.g., bats, birds) – does phenotypic integration typically increase or decrease in these circumstances?

Conclusions

Among vertebrates, differences in regional biodiversity are a product of variation in species richness, taxonomic diversification rates, and rates of evolution in body size and shape (Mannion et al. 2014). Here I study the relationship between climatic variability and disparity, phenotypic integration, and rates of morphological evolution using the jaws of the mammalian carnivores (O. Carnivora). I find evidence for differences in the level of integration between carnivorans residing in climatically variable and stable habitats. More specifically, I demonstrate that species from climatically stable habitats exhibit higher levels of integration. Species in these same stable habitats also exhibited greater morphological disparity and faster rates of morphological evolution. The lower levels of integration associated with high climatic variability could be either a consequence of or a response to the continued seasonal variation in food availability over macroevolutionary time scales, which favors dietary breadth. In contrast to canids and felids, integration of

the mustelids jaw did not vary with climatic variability. Phenotypic integration operates on microevolutionary scales, but it has an impact on macroevolutionary patterns, including the differences in disparity and rates of morphological evolution that I observe here. I hope this furthers the discussion on the relationship between phenotypic integration and morphological rates and the external factors that influence them. In particular, the ecological, phylogenetic, and genetic contexts in which I can predict high levels of integration to evolve remains an open question.

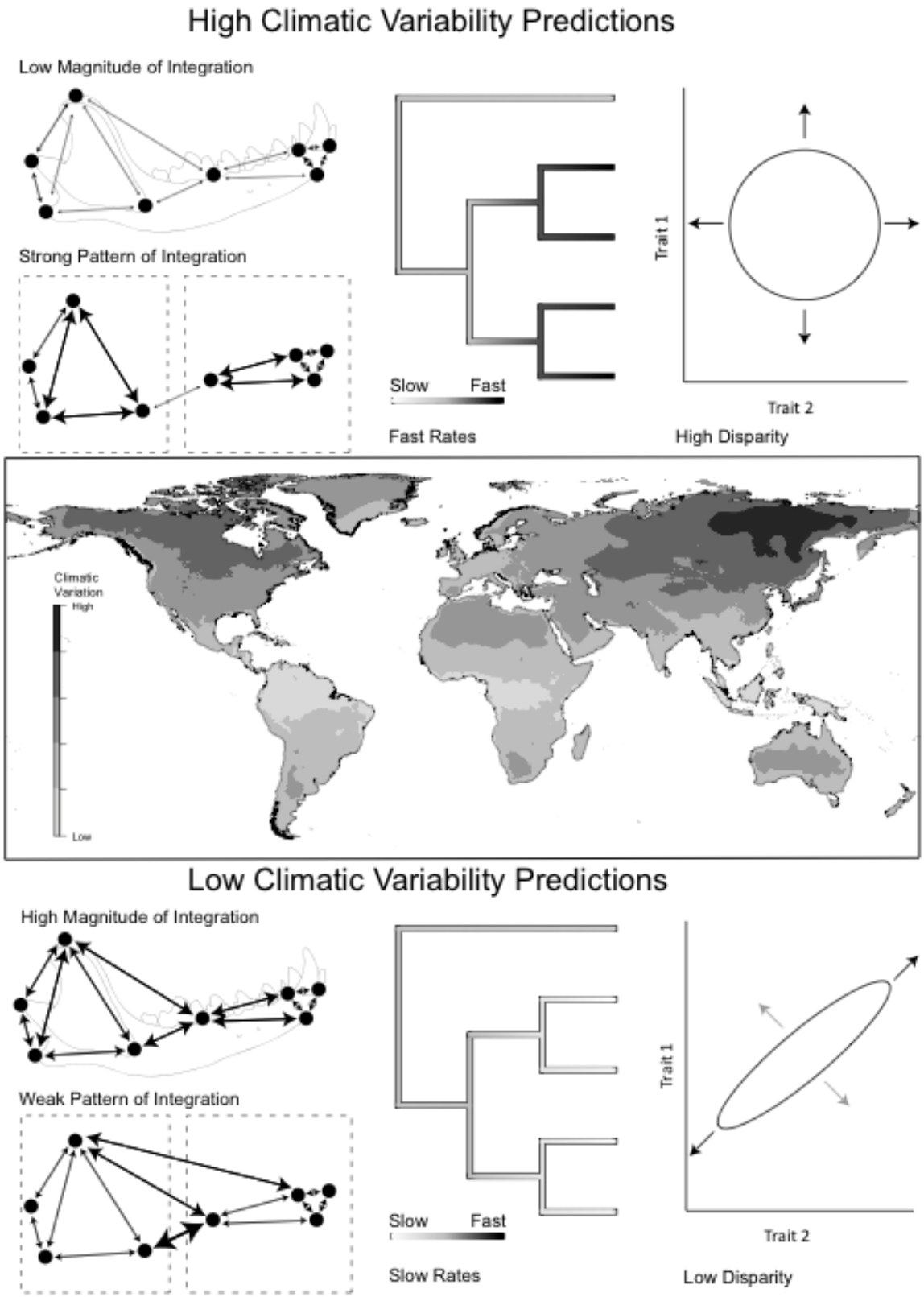
High Climatic Variability Predictions
Low Magnitude of Integration
Strong Pattern of Integration
Slow
Fast
Fast Rates
Trait 1
Trait 2
High Disparity
Climatic Variation
High
Low
Low Climatic Variability Predictions
High Magnitude of Integration
Weak Pattern of Integration
Slow
Fast
Slow Rates
Trait 1
Trait 2
Low Disparity

Figure 3.1: Testing hypothesis of climatic variability on morphological evolution.

Pattern of integration panel. Testing a pattern of integration hypothesis for carnivoran jaws. Circles represent example landmark coordinates, line width represents covariation association strength (small = low covariation between landmarks, large = high covariation between landmarks), dashed lines indicate modules where covariation between landmarks within a module is greater than covariation between landmarks in another module. Magnitude of integration panel, testing degree of covariation over whole jaw. Circles represent example landmark coordinates, line width represents covariation association strength (small = low covariation between landmarks, large = high covariation between landmarks). Rate of morphological evolution. Rates of trait evolution mapped onto a phylogenetic tree, darker colors = faster rates. Morphological disparity, hypothetical morphospace illustrating range of morphology exhibited by taxa. Arrows represent potential for moving into unexplored regions of morphospace, gray arrows = low potential (i.e., thinner line of least resistance), black arrows = higher potential. I ultimately found no support for a ramus-corpus pattern of integration in both climate variability regions, but found support for a high magnitude of integration, faster rates of morphological evolution, and higher disparity in low climatic variability regions.

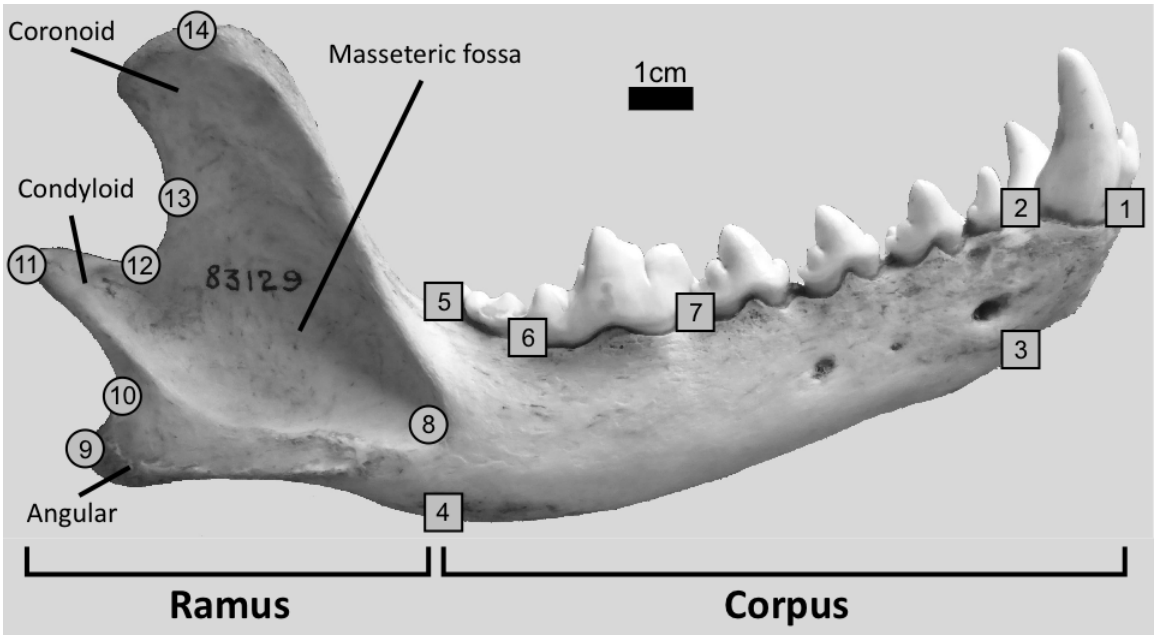

Figure 3.2: Landmarked mammalian jaw (African wild dog, *Lycaon pictus*)

Copus, dental bearing region; ramus, dental bearing region. Three processes on the ramus (coronoid, condyloid and angular) are sites for muscle attachment. The temporalis muscle inserts onto the coronoid process while the masseter muscle inserts onto the masseteric fossa and the pterygoid onto the angular process. Corpus module landmarks are represented by circles, ramus module landmarks are represented by squares. Landmark positions: 1 - most anterior point on the dentary; 2 - distal extreme of the lower canine; 3 - Ventral edge of the left-right dentary suture; 4 - Ventral base of ramus; 5 - Dorsal base of ramus; 6 - posterior portion of carnassial molar; 7 - anterior portion of carnassial molar; 8 - anterior border of masseteric fosa; 9 - distal extreme of angular process; 10 - most concave point between angular and condyloid processes; 11 - distal extreme of condyloid process; 12 - most concave point of mandibular notch; 13 - Most concave point between condyloid and coronoid processes; 14 - dorsal edge of coronoid process.

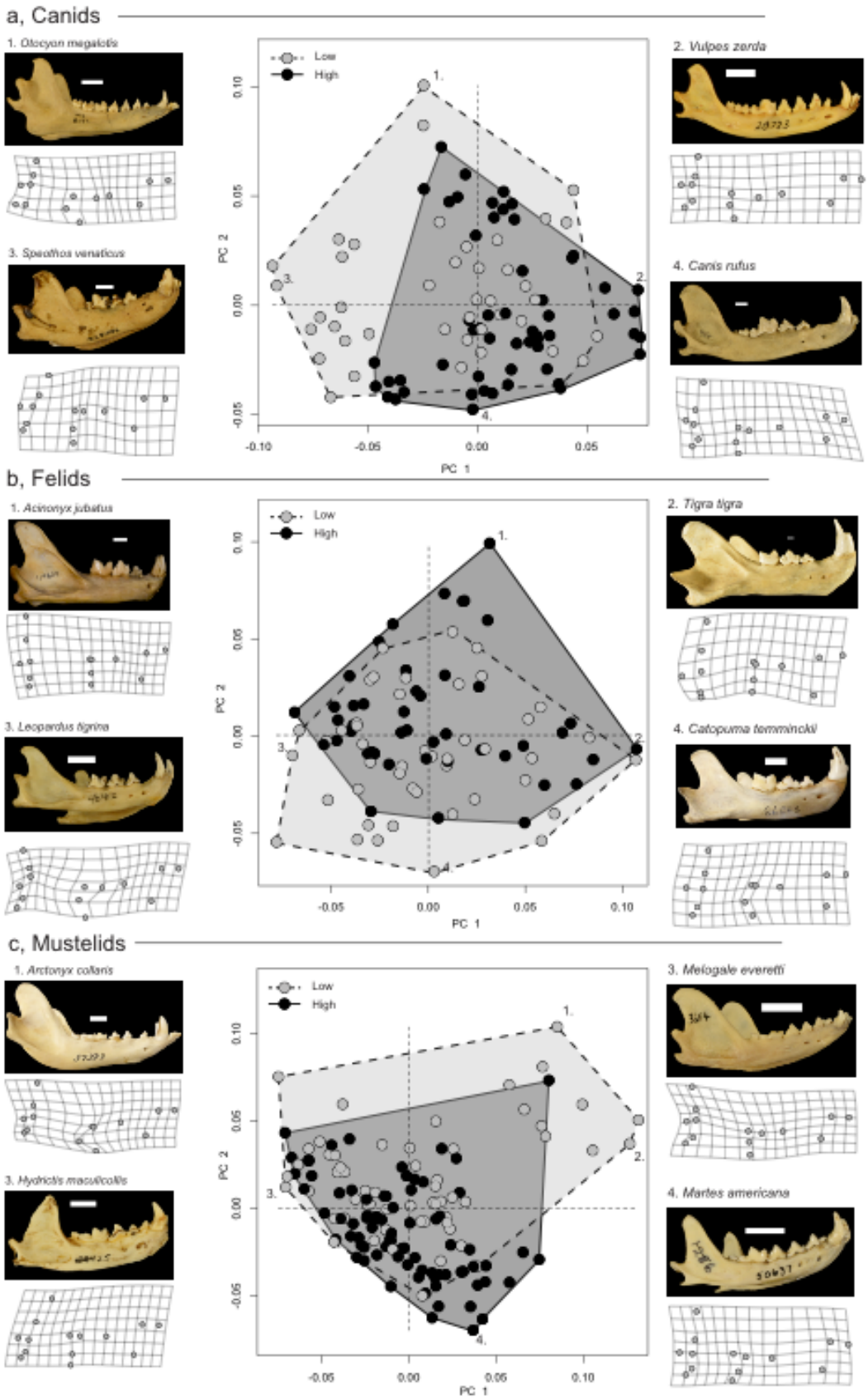
a, Canids
1. Otocyon megalotis
2. Vulpes zerda
3. Speothos venaticus
4. Canis rufus
Low
High
PC 1
PC 2
b, Felids
1. Acinonyx jubatus
2. Tigra tigra
3. Leopardus tigrina
4. Catopuma temminckii
c, Mustelids
1. Arctonyx collaris
3. Hydrictis maculicollis
3. Melogale everetti
4. Martes americana

Figure 3.3: Patterns of morphospace occupation in three carnivoran clades

Patterns of morphospace occupation in three carnivoran clades. Canids (a), Felids (b) and Mustelids (c) positions determined from separate PC analyses of the jaw landmark data. Numbers 1-4 located on the morphospace refers to the surrounding example specimen images and warps. White scale bar = 1cm.

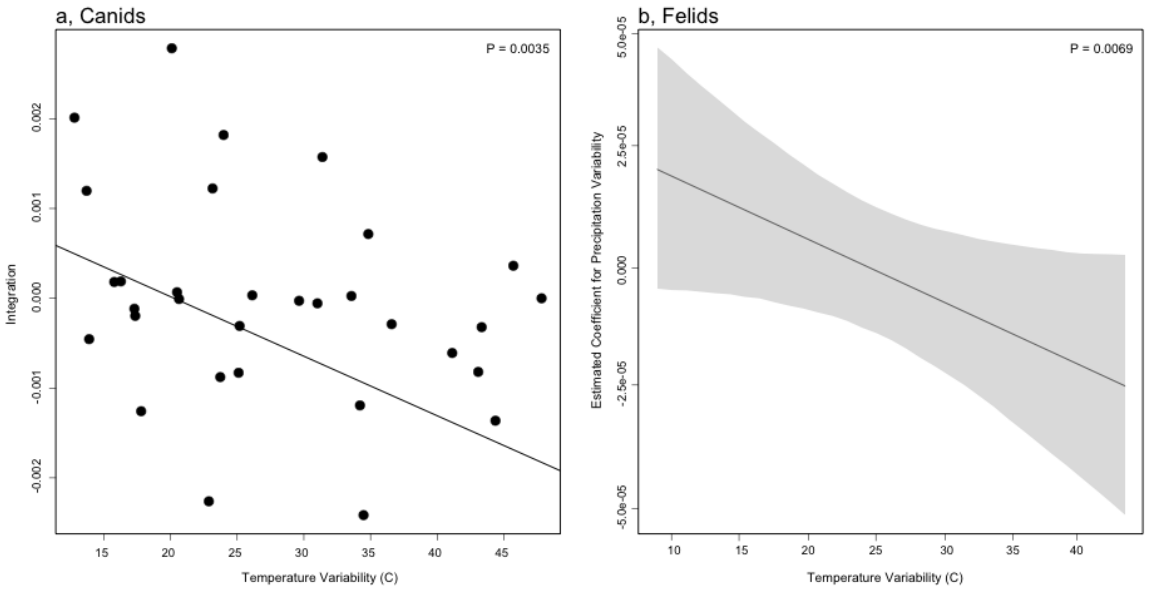

Figure 3.4: Regression plots for significant associations between climatic variability (current climate model) and integration.

a, Canids, PGLS regression of phenotypic integration by temperature variability. With increasing temperature variability, the level of integration decreases. b, Felids, estimated coefficient of precipitation variability on integration by temperature variability. With increasing temperature variability, the magnitude of the coefficient of precipitation variability on integration decreases.

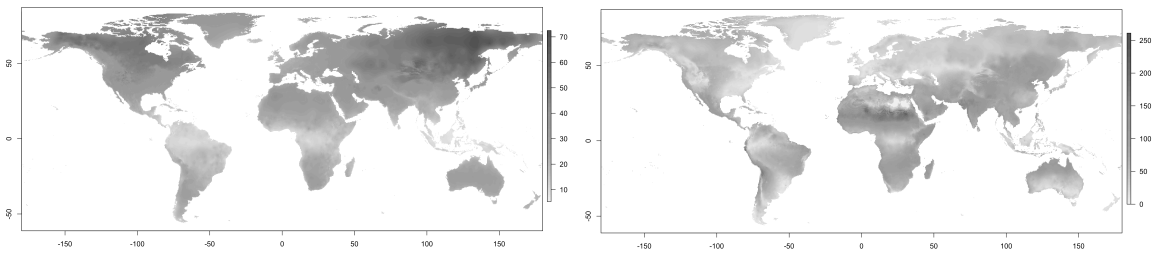

Figure 3.5: Distribution of temperature and precipitation variation around the world.

Images downloaded from WorldClim v1.4 and generated in R. Darker colors indicate regions of greater variation, lighter colors indicate regions of lower variation. Left, Temperature variation (temperature range); right, precipitation variation (coefficient of variation).

Clade	Temperature Variation (P)	Precipitation Variation (P)	Temperature * Precipitation variation (P)
Canid	**0.003**	0.337	0.749
Felid	0.464	0.513	**0.039**
Mustelid	0.801	0.733	0.406

Table 3.1: Integration against climate phylogenetic regression

Data for PGLS regression between the magnitude of integration and temperature-precipitation values gathered from the current climate model. (P) refers to the significance of the phylogenetic regression model. Significant associations ($\alpha<0.05$) are shown in bold type.

Clade	Variability	Group	Disparity (Proc)	Disparity (P)	Rates (σ^2)	Rates (P)	Integration pattern (r)	Integration pattern (P)	MANOVA (F)	MANOVA (P)
Canid	Temperature	Low	0.00410	**0.027**	2.25E-05	**0.037**	0.84	**0.005**	2.7528	0.558
		High	0.00258		1.53E-05		0.795	**0.013**		
	Precipitation	Low	0.00332	0.684	2.05E-05	0.396	0.904	**0.001**	0.87595	0.463
		High	0.00369		1.75E-05		0.822	**0.011**		
Felid	Temperature	Low	0.00402	0.647	2.52E-05	0.11	0.959	**0.001**	3.0158	0.305
		High	0.00452		1.91E-05		0.87	**0.014**		
	Precipitation	Low	0.00337	0.061	2.59E-05	**0.05**	0.965	**0.001**	1.6937	0.649
		High	0.00523		1.89E-05		0.92	**0.001**		
Mustelid	Temperature	Low	0.00752	**0.012**	3.80E-05	**0.01**	0.799	**0.002**	4.9888	**0.023**
		High	0.00408		2.74E-05		0.685	**0.019**		
	Precipitation	Low	0.00564	0.678	4.05E-05	**0.001**	0.742	**0.006**	1.0939	0.351
		High	0.00627		2.43E-05		0.801	**0.001**		

Table 3.2: Data for integration, rates of morphological evolution, and disparity

Bold type indicates significance (α<0.05). Disparity (Proc) refers to the observed Procrustes variances for a group and Disparity (P) refers to the significance associated with pairwise differences between groups. Rates (σ2) refers to the phylogenetic Brownian rate for a group and Rates (P) refers to the significance level of the observed ratio of maximum to minimum evolutionary rates (i.e., σ^2 low variability/σ^2 high variability). Integration pattern (r) refers to the correlation

between the ramus and corpus partitions and Integration pattern (P) refers to the significance of that correlation. MANOVA (F) refers to the F-statistic from the pMANOVA comparing jaw PC scores from taxa in low vs. high variability groupings and MANOVA (P) refers to the significance level based on the F-statistic.

CHAPTER 4

THE INFLUENCE OF REPRODUCTIVE CONSTRAINTS IN SHAPING THE PHENOTYPIC INTEGRATION AND MORPHOLOGICAL EVOLUTION OF MAMMALIAN JAWS

Introduction

Marsupial and placental mammals have independently invaded herbivorous, omnivorous, and carnivorous dietary niches (Price et al. 2012) despite the fact that they have very different modes of reproduction. Placental mammals invest in long periods of gestation followed by relatively short periods of lactation. In contrast, marsupials are born after a short period of gestation and then climb to the mother's pouch where they attach to a nipple and suckle for a long period of time (Smith 2001; Goswami et al. 2011; Kelly and Sears 2011). The marsupial life history strategy is reflected in a bias in the timing of muscle and bone development among different regions of the marsupial body. The cranial region of the marsupial neonate is exceptionally well-developed, especially the forelimbs, cranium, jaws, and cervical vertebrae. The anterior portion of the cranium and jaw ossifies much earlier relative to placental mammals, and is accompanied by early development of the jaw musculature (Sanchez-villagra and Smith 1997). In comparison to placental neonates, marsupial neonates have less well-developed hindlimbs and posterior axial skeleton (Smith 2001). This differential development prioritizes the tools a

marsupial neonate needs to survive in early life – strong forelimbs to climb to the pouch and a well-developed jaw for the ability to suckle.

The developmental sequence of the marsupial skull has been proposed to have evolutionary consequences for the disparity (morphological diversity), rates of morphological evolution, and pattern of modularity in marsupials. Nevertheless, the morphological variation observed among all mammalian dentaries reflects their associations with different feeding strategies and diets (Sanchez-villagra and Smith 1997; Anthwal and Tucker 2012). In all mammals the cranial portion of the dentary (the corpus) bears the teeth and caudal portion (the ramus) bears processes that provide surfaces for muscle attachments (angular and coronoid processes, (Figure 4.1). The masseter, temporalis, and ptergygoid muscle groups attach to these processes and control jaw closing. The ramus also has a condyloid process, or condyle, that participates in the jaw joint (Figure 4.1). Despite these anatomical similarities, there is a widely held hypothesis that the shape of marsupial dentaries should exhibit less variation than placental dentaries because they must be fully functional at birth (Prevosti et al. 2012; Echarri and Prevosti 2014).

Hallgrímsson (2009) drew an analogy to a well-used writing tablet to explain how the interaction of multiple developmental process can influence the pattern and magnitude of phenotypic integration – the strength of covariation among sets of anatomical traits or landmarks (Klingenberg 2008; Goswami and Polly 2010; Goswami et al. 2014). When writing on a tablet, multiple impressions of previous texts are still visible as new text is written. In much the same way, the final morphology of the mammalian dentary exhibits a complex covariation structure

that can be traced to overlapping genetic, temporal, and mechanical influences that occur during development (Klingenberg et al. 2003; Monteiro and Nogueira 2010). Within the mammalian jaw there are multiple modules, or subsets of anatomical landmarks that are more correlated with one another than with other subsets of landmarks (Figure 4.1). Modules typically form when there is a combination of selection for functionally correlated traits and genetic pleiotropy for those traits (Blows 2007). An anatomical structure, such as the dentary, can exhibit different magnitudes of phenotypic integration (i.e., correlations among anatomical landmarks can be strong or weak), and different patterns of phenotypic integration (i.e., regions within a structure can be partitioned into subsets that can differ in composition among individuals or across species). The magnitudes and patterns of phenotypic integration can have implications for the ability of an anatomical structure to respond to selection (Pigliucci 2008; Le Rouzic et al. 2013). The phenotypic evolution of an anatomical structure must proceed along a path delimited by the covariation between landmarks; this is known as the line of least resistance. In highly integrated structures, where magnitudes of integration are high and covariance between modules is strong, phenotypic evolution is constrained to proceed along a thin line of least resistance that allows only a limited range morphological variation (Drake and Klingenberg 2010; Klingenberg 2010). When the magnitude of phenotypic integration is low and there are many modules that can evolve independently, then the line of least resistance is very wide. The wider range of potential morphological diversity could allow access to more niches

(Wagner et al. 2007) and thereby influence the rate of morphological evolution (Goswami et al. 2014).

Given the need to suckle at an early developmental stage, the marsupial cranial skeleton experiences a strong mechanical influence during its initial stages of development (Smith 2006). The ability to suckle is initially provided by the flexibility of the Meckel's cartilage and the powerful tongue and hyoid muscles (hyoglossus, genioglossus, and geniohyoideus) until well-developed jaw closing muscles differentiate around 6 days after birth (Smith 1994). Accordingly, much of the development of craniofacial bones and muscles in marsupials occurs while the young are suckling. For example, in newborn opossums (*Monodelphis domestica*), only the corpus (anterior portion of the dentary) has begun to ossify and the ramus (posterior portion of the dentary) ossifies after birth. The delayed development and attachment of jaw closing muscles to the processes on the dentary changes the local mechanical environment. This is in stark contrast to newborn mice (*Mus musculus*), in which almost all cranial bones and muscles in their jaws undergo ossification and differentiation *in utero*, before the jaw must function in suckling (Clark and Smith 1993).

As the dentary and its associated muscles grow, the mechanical environment and the interactions of multiple genes and cell types establishes the final morphology of the condyloid, coronoid, and angular processes. The same genetic processes affect the development of the condyloid, coronoid and angular processes of placentals and marsupials. The condyloid is highly conserved in mammals, and has been the primary jaw articulating process since the evolution of the dentary-

squamosal jaw joint in the Late Triassic - Early Jurassic (Gill et al. 2014). Multiple genes control the formation of the condyloid including Prx1, Runx2 and Dlx5. Knockout mutants in these genes have smaller condyloid, angular, and coronoid processes. These mutants also lack the squamosal bone and the temporo-mandibular joint, highlighting the pleiotropic effect of these genes (Richman and Mitchell 1996; Depew et al. 2002; Oka et al. 2008). Genes, muscle activity, and cellular interaction regulate the development of the angular and coronoid processes. The induction of the coronoid is controlled by Pax9 expression and its persistence requires mechanical stimulation from the developing temporalis muscle (Anthwal et al. 2015). Increased muscle loading then activates Sox9 expression which drives further growth of the coronoid. Angular process development is at least partially controlled by Tgfβ2, as expression is localized to tissue surrounding the developing angular but is absent from the condyloid and coronoid processes (Oka et al. 2007; Anthwal et al. 2008). Angular process development is also controlled by the differentiation and growth of the masseter and pterygoid muscles that attach to it. Angular and coronoid processes do not form in mouse models that lack jaw muscles, indicating that both processes require at least some mechanical force to promote ossification (Rot-Nikcevic et al. 2007). This is likely due to the absence of feedback between secondary cartilage and muscular action, as secondary cartilage responds to muscle activity by ossifying and contributing additional bone to the processes (Anthwal and Tucker 2012). In the opossum, secondary cartilage is absent in the coronoid and angular processes, which is unusual given most growth of the opossum dentary occurs after muscles have differentiated and are generating

mechanical force (Smith 1994; Anthwal et al. 2015). This suggests that the formation of secondary cartilage is not required to form bone in marsupial coronoid and angular processes but may be important in other placental mammals (Smith 1994, 2006). This opens the possibility that despite the different genetic underpinnings of the angular and coronoid processes, the mechanical loading experienced by marsupials during suckling could promote their being linked as a single module. Alternatively, the fact that angular and coronoid processes are fully formed before placental mammals begin to suckle may allow them to remain separate modules.

While several studies have investigated integration and disparity in marsupial and placental crania in the context of reproductive constraints, this is the first to assess the effects of developmental genetics and the mechanical environment during development on phenotypic integration and disparity in the dentaries of placental and marsupial mammals. Goswami (2006) found similar patterns of cranial phenotypic integration between marsupials and placentals. The pattern of integration is therefore not constrained within any therian order or dietary grouping, however the magnitude of integration is stronger in the oral region of marsupials relative to placentals. Goswami (2016), suggested that this resulted from the need to suckle as a neonate. Continuous suckling also served to limit the disparity of the marsupial viscerocranium, further highlighting the relationship between integration and disparity, and the influence reproduction has on shaping marsupial morphological evolution (Bennett and Goswami 2013). However, when only comparing marsupial and placental carnivores, cranial disparity is similar

(Goswami et al. 2011), indicting a skull shape required to consume a carnivorous diet can still evolve despite differences in reproductive strategy. A few studies have investigated differences in placental and marsupial dentary morphology with respect to diet and trophic niche (Meloro and O'Higgins 2011; Prevosti et al. 2012; Echarri and Prevosti 2014), and some concluded that the dentaries of extant marsupials exhibit less disparity (Prevosti et al. 2012; Echarri and Prevosti 2014). Variation in dentary shape within the placental order Carnivora is primarily influenced by phylogeny, diet, and trophic niche (Meloro and O'Higgins 2011; Meloro et al. 2011). None of these studies of the dentary addresses the impacts of the underlying genetics or the effect of mechanical environment during development on the pattern of integration in the dentaries of marsupials and placental mammals.

Here I evaluate how the mode of reproduction in placental carnivorans and marsupial dasyuromorphs has influenced the pattern of integration in the dentary. I focus on carnivorans and dasyuropmorphs because these two orders of mammals share broadly similar diets, occupy relatively similar niches, and their jaw morphology is easily comparable. I use a 3D geometric morphometric approach to gather jaw shape data, and assess differences in morphological evolution using an explicit phylogenetic hypothesis and a large taxonomic sample. I compare the pattern of phenotypic integration in the dentaries' of carnivorans and dasyuropmorphs to investigate whether the distribution of modules and the magnitude of covariation among modules are associated with genetic or functional processes that play out during development. I hypothesize that the requirement for

marsupial neonates to develop jaw musculature far in advance of dentary ossification will produce a jaw with stronger covariation among the ramal processes and between the ramus and the corpus. For placentals I hypothesize that the ramal processes and corpus incisor and molar regions will be more independent. This is because dentary ossification is essentially complete at birth, which reduced the influence of muscle-bone interactions on dentary development. If dasyuriomorphs exhibit fewer modules than carnivorans, then I predict they will also exhibit reduced disparity and rates of morphological evolution, as more regions of the jaw will undergo coordinated development in response to selection. Evidence supporting our hypotheses will suggest the mechanical loading experienced by the marsupial neonate's dentary and may constrain the clade's ability to fully occupy a carnivorous niche. Evidence against our hypotheses will suggest that marsupial development does not constrain the development of the full range of carnivore-like dentaries, and that similar disparity and rates of morphological evolution can be achieved with fewer or different modular partitions.

Methods

Specimen image collection

I obtained digital images of Carnivora and Dasyuromorphia dentaries from multiple museum collections using a stereo camera setup. The samples were evenly distributed within each phylogeny and reflected the major aspects of ecological and morphological diversity within each clade. I photographed the left dentary of 508 specimens from 248 species. I used specimens with known gender information

when possible, and the final sample contained 245 females, 257 males, and 6 with an unknown gender assignment (Table S4.1). I did not separate sexes as I found they greatly overlapped in PC morphospace (MANOVA, Carnivora, F=0.78, P=0.50; Dasyuromorphia, F=0.62, P=0.61; Caniformia, F=0.56, P=0.66; Feliformia, F=0.47, P=0.68). I used two cameras to gather stereo image data for the collection of 3D landmarks from 2D pictures. I used a pair of Nikon D5200 DSLR cameras tethered to a computer running the Windows freeware package digiCamControl v2.0.1. The cameras were set-up at 120º angles from each other pointing down over specimens. I used a 21x14 checkerboard square to calibrate the positions of the two cameras. The dentary was imaged in four different orientations for each camera view. Orientation 1 included many of the lingual structures of the jaw, orientation 2 included the buccal profile of the jaw, orientation 3 included the posterior process of the jaw, and orientation 4 included the ventral portion of the jaw.

Geometric Morphometric Analysis

I placed 12 landmarks across the jaw to fully encompass the shape of the ramus and corpus (Figure 4.2). I collected 3D landmarks from each aspect and view of a jaw using the Stereomorph package (v2.0) in R. Following landmark collection from the images, I merged the landmark coordinates together to compile a 3D representation of the coordinates in space. See Olsen and Westneat (2015) and StereoMorph v2.0 package help files on the R CRAN website for more information. After extracting landmark coordinates using Stereomorph I performed a general least squares Procrustes superimposition to remove the effects of size, and to translate and rotate the images so that they are in register (Rohlf 1998). I then

performed a Procrustes ANOVA on the centroid size and shape data and found a significant effect of allometry on shape ($r^2 = 0.051$, $F = 29.5$; $P=0.002$). To minimize the potential effects of allometry, I performed a regression of shape on geometric centroid size using the geomorph package (v3.0.1) in R to generate a landmark data set based on residuals (Adams and Otárola-Castillo 2013). I conducted a principal components (PC) analysis on the allometrically corrected landmark configurations to reduce the data into a series of orthogonal axes that represented the major axes of shape variation among the taxa. I extracted five PCs which represented over 70% of the total shape variation (Table S4.1). I plotted the first two PCs to provide a visual representation of the range of morphological variation within the sample.

Patterns of phenotypic integration

I used a new method termed EMMLi (evaluating modularity with maximum likelihood) to test different hypotheses of jaw modularity in our clades and analyse the strength of covariation between and within those modules (Goswami and Finarelli 2016). The method compares log-likelihoods of different landmark correlation matrices using the small size corrected Akaike Information Criterion (AICc) to determine the best fitting modularity hypothesis. I extracted vector congruence coefficient correlation matrices based on the landmarks to produce a 12 x 12 element matrix (Table S4.2). These correlation matrices provide a single number for covariance between landmarks, rather than three separate numbers for covariance in the x-, y-, and z- directions. Vector based matrices are considered more biologically significant as they treat the landmark as a single unit of information (Goswami and Finarelli 2016). I extracted separate correlation matrices

for each clade grouping (Dasyuriamorpha, Carnivora, Caniformia, Feliformia). EMMLi allows modules to either constrain or vary the value of ρ (hypothesized correlation coefficient) within and/or among each module by adding additional parameters. For models with more than two modules, EMMLi conducted four additional comparisons by either constraining or permitting within and between module covariation (1, ρ is constrained within modules and between modules; 2, ρ varies within modules but constrained between modules; 3, ρ is constrained within modules but varies between; 4, ρ varies within and between modules).

The proximal causes of differences in jaw morphology among species are the variation in genetic and developmental signals alongside developmental heterochrony (Klingenberg 1998; Anthwal and Tucker 2012). Previous research on rodent and bat mandibles identified modules that originate from the same mesenchymal condensations, are attachments for the same muscles, or bear similar tooth types such as molars or incisors (Klingenberg et al. 2003; Zelditch et al. 2008; Monteiro and Nogueira 2010). I investigated 7 different modularity partitions based on the genetic and functional development of the dentary and compared this to a null pattern with no modules. Our modular partitions were based on independent functional roles, the mechanical environment, secondary cartilage formation, and genetic interactions with mesenchymal cell condensations. I considered six of our module partitions as three pairs. For models within each of these three pairs, the corpus is either a single module or two modules representing the molar and incisor alveoli (Figure 4.3; Table S4.3).

I first tested a null model of jaw integration in which all landmarks covary together (Figure 4.3, Model 1). The first modularity partition divided the jaw into two regions, anterior and posterior, representing the corpus and ramus (Figure 4.3, Model 2). This partition is well supported in a number of rodent mandible studies (e.g. Klingenberg et al. 2003; Klingenberg 2009) and reflects the functional separation between the muscle-bearing and tooth-bearing regions of the dentary. The fist pair of module partitions (Figure 4.3, Models 3 and 4) is based on the idea that the simultaneous development of the growing masseter and temporalis muscles causes the angular and coronoid process to covary together. The condyloid is a separate module. Knockout mutants that lack muscle exhibit almost complete loss of the angular and coronoid processes due to the loss of the feedback provided by mechanical stimuli, indicting the importance of mechanical force in regulating process development (Rot-Nikcevic et al. 2007). Similarly, both corpus modules are based on the teeth that are present in the alveoli as the incisor region is ossified at birth prior to the molar region. In these hypotheses the corpus is either a single module or two modules representing the incisor and molar regions. The masseteric region is represented by one landmark at the anterior boarder of the fossa, and I code this as unintegrated with any module.

The second pair of module partitions is based on the localization of secondary cartilage in the ramus (Figure 4.3, Model 5 and 6). Ossification of the angular and condyloid depend on secondary cartilage formation in certain placental mammals (Clark and Smith 1993; Smith 1994). The condyloid and angular processes are also more robust to knockouts in genes such as Dlx5, Tbx1 and Pax9,

while the coronoid process is completely lost (Anthwal et al. 2015). These hypotheses divided the jaw into 3-4 modules. Again, the corpus is either one or two modules based on the incisor and molar regions. The ramus is divided into two modules, one uniting the angular and condyloid, and one for the coronoid. The masseteric region is represented by one landmark at the anterior boarder of the fossa, and I code this as unintegrated with any module.

The third pair of modules is based on the cell condensation model of Atchley and Hall (1991), whereby there are six independent mesenchymal condensations with different cellular properties that give rise to different morphologies (Figure 4.3, Model 7 and 8) (Ramaesh and Bard 2003). Many different genes independently control the modular structure I propose in models 7 and 8 including Tgf-β2, Pax9, Dlx5, Goosecoid, and Prx1. Tgf-β2 expression is localized to the angular process and knockout of this gene causes disruption to osteoblast differentiation and loss of the angular process (Anthwal et al. 2008). Pax9 is only expressed in the developing coronoid and knockout prevents the expression of sox9 and scleraxis that are required for attachment of the temporalis muscle. Without attachment of the temporalis, the coronoid does not form (Rot-Nikcevic et al. 2007; Anthwal et al. 2015). Knockout of the Dlx5, Goosecoid and Prx1 genes can cause reduction of all the dentary processes and loss of the tempo-mandibular joint (Richman and Mitchell 1996). Similarly, both corpus modules are based on genes such as Satb2 that can cause major shortening of the corpus region and loss of the incisors (Britanova et al. 2006). Module hypotheses 7 and 8 divide the jaw into 4-5 modules. The corpus is either a single module or two modules representing the molar and

incisor-bearing regions and the ramus is divided into one module for each of the three processes. The masseteric region is represented by one landmark at the anterior boarder of the fossa, and I code this as unintegrated with any module.

Rates of Morphological Evolution and Morphological Disparity

I used comparative methods to examine morphological evolution in a phylogenetic context using a time-calibrated mammalian super-tree (Fritz et al., 2009). I pruned the supertree to include only the 237 species for which I had data. If the marsupial mode of reproduction limits the disparity in dentary shape, then I expect placental mammals to occupy a much larger region of morphospace. I used Procrustes variance to compare disparity between different groupings of mammals (Adams and Otárola-Castillo 2013). Procrustes variance measures the dispersion of all individuals from the consensus shape. Our first grouping compared disparity between dasyuromorph marsupials and fissiped carnivoran placentals (i.e., carnivorans excluding pinnipeds). The second grouping further divided placentals into caniforms and feliforms, and compared them both to dasyuromorphs. I separated caniforms, feliforms and dasyuromorphs because they originated within a similar time frame (~40-50 million years ago), represent monophyletic groups, and exhibit similar behaviours and dietary breadth within their groupings. I used the *morphol.disparity* function in the R geomorph package to conduct the Procrustes variance analysis (Adams and Otárola-Castillo 2013).

I compared the rates of morphological evolution between clades (dasyuromorphs vs fissiped carnivorans; dasyuromorphs vs caniforms vs feliforms) using the Procrustes-fitted jaw shape data. I used a method that calculates a

phylogenetically corrected rate based on a species distance approach (Adams 2014). The ratio of the maximum to minimum evolutionary rate is used as a test statistic, and differences between clades are determined by comparing observed data to simulated tip data under a BM model that uses a single rate for all species. I use the *compare.evol.rates* function in the R geomorph package to perform rate comparisons (Adams and Otárola-Castillo 2013).

Results

Patterns of Modularity

I found support for different patterns of modularity between placental and marsupial carnivores (Table 4.3). All carnivoran clades fit models with separate values of ρ (correlation coefficient) both within modules and between modules. Carnivoran jaws best supported a five module pattern with separate modules for each process of the ramus and with the corpus divided into incisor and molar regions (Model 6, posterior probability (PP = 1.00). When I divided carnivorans into caniforms and feliforms I found support for patterns of modularity that include independence of the processes on the ramus, but in caniforms the molar and incisor regions of the corpus are separate modules (Model 6, PP=0.96) while the corpus is a single module in feliforms (Model 5, PP=0.92). Dasyurimorphia jaws best fit a 3 module pattern with the coronoid and angular process in one module, and the condyloid and corpus representing the other two modules (Model 3, same ρ between modules, PP=0.42; model 3, separate ρ between modules, PP=0.22).

Jaw Morphology and Disparity

I found substantial overlap in morphospace among all clades and data subsets (i.e., dasyurimorphs, caniforms and feliforms) as defined by PC1, PC2, and PC3 (Figure 4.4, Table S4.1). In each morphospace the Dasyuromorphia appear to occupy a smaller area and are near the perimeter of the Carnivora shape space. Across all subsets, the first PC axis represents variation from an elongated to shortened jaw, a thin to wide condyloid process, and a low to high coronoid process (31.91% of shape variation). This axis primarily separates taxa with more robust jaws (e.g., *Sarcophilus*, *Mustela*, *Panthera*) from taxa with more slender jaws (e.g., *Sminthopsis*, *Vulpes*, *Eupleres*). The second PC represents variation from a medially projected angular process to a ventrally projected angular process (20.01% of shape variation). This axis separates all dasyurimorphs from the placentals. The third PC axis represents the position of the coronoid process, from a low, anterior position to a high, posterior position (8.75% of shape variation). This axis separates certain members of the caniforms and dasyurimorphs (e.g., *Gulo*, *Canis*, *Sarcophilus*) from certain feliforms (e.g., *Viverricula*, *Herpestes*).

I found no significant differences in disparity between dasyuromorphs and carnivorans (Procrustes variance (PV) Carnivora = 0.014, PV Dasyurimorphia = 0.011; $p = 0.192$). This relationship holds true even when I partition the carnivoran sample into caniforms and feliforms (PV Caniformia = 0.014, PV Feliformia = 0.012), and compare them dasyuromorphs (Table 4.2).

Morphological Evolution

I found significant differences in rates of morphological evolution among clades (Table 4.1). Caniforms ($\sigma^2 = 3.26*10^{-5}$) and dasyuromorphs ($\sigma^2 = 3.64*10^{-5}$) exhibit an approximately 3x faster rate of jaw evolution than feliforms ($\sigma^2 = 1.23*10^{-5}$). Dasyuromorphs display the fastest rates of jaw evolution, although their rate is indistinguishable from that of caniforms. When caniforms and feliforms are combined into the Carnivora, dasyuromorphs exhibit a significantly faster rate of morphological evolution (Dasyuriamorphia $\sigma^2 = 3.64*10^{-5}$, Carnivora $\sigma^2 = 2.29*10^{-5}$; $p<0.001$).

Discussion

I found a fundamental difference in the pattern of modularity between dasyuromorph marsupials and placental carnivorans. Dasyuromorphs exhibited a more integrated pattern with fewer modules than carnivorans. Specifically, the data support the hypothesis that muscle activity during early neonatal development affects the pattern of modularity. I found no evidence to suggest that the marsupial mode of reproduction has constrained disparity and rates of morphological evolution in the dentaries of dasyuromorph marsupials. Feliforms and caniforms experienced differences in the modularity pattern of the corpus region, while their ramus regions exhibited similar modularity patterns. Caniforms and dasyuromorphs exhibit similar, rapid rates of morphological evolution; the evolution of dentary shape is exceptionally slow in feliforms. Taken together, these results suggest that the mode of reproduction of dasyuromorph marsupials has not

hindered their ability to exploit a terrestrial carnivorous niche, and that different patterns of phenotypic integration can produce similar disparity and rates of morphological evolution.

I found dasyuromorph marsupials and carnivoran placentals exhibit different patterns of phenotypic integration across the dentary. I suggest the difference in patterns of integration between dasyuromorph and carnivoran mammals is a result of the differences in their modes of reproduction. Marsupials and placentals appear to expresses a similar suite of genes during dentary development, but the mechanical environment experienced by marsupial neonates is vastly different and likely influences the final covariation structure of the dentray. The patterns of covariation in marsupial dentaries appear to be driven by the interaction between the jaw musculature and the bony processes they attach to during development (Sanchez-villagra and Smith 1997). Regions of the dentary that share muscle attachments, or are located in regions that experience similar loads from suckling, often share common patterns of integration and will develop as a single module (Zelditch et al. 2008). In contrast to the ramus of the marsupial dentary, which does not ossify until around day 4, much of the corpus is ossified at birth (Clark and Smith 1993; Smith 1994), and this may explain why there is high integration in the anterior region of the dasyuromorph jaw. The jaws of placental carnivorans are fully ossified and functional at birth. All three processes on the ramus are separate modules, indicating they covary independently. The independence of these processes reflects the developmental patterning of the placental mandible in the absence of strong mechanical influences. The condyloid module evolves

independently in both dasyuromorphs and carnivorans, allowing jaw dynamics to change as the coronoid and angular processes change shape (Santana et al. 2010). Coronoid shape variation influences the opening and closing action of the jaw, as a higher coronoid produces a greater mechanical advantage and an increased ability to elevate the jaw during a bite (Davis et al. 2010; Santana et al. 2010). Caniforms and feliforms exhibit differences in the covariation structure of the corpus, with feliforms retaining the corpus as a single module while the caniform corpus is divided into a separate incisor and molar modules. The single corpus module in feliforms may reflect the increased emphasis on the carnassial complex and specialization for hypercarnivory (Holliday and Steppan 2004; Van Valkenburgh 2007; Meloro et al. 2008). Caniforms and feliforms exhibit a striking conservation in their patterns of covariation in the ramus despite being separated by 55-65 million years (Fritz et al. 2009; Meredith et al. 2011). Previous authors have noted the conservation of covariation patterns among closely-related species (e.g., Young and Hallgrímsson 2005; Goswami 2006). This is not surprising given the large genetic and developmental changes required to affect patterns of covariation (Hallgrímsson et al. 2009) and the fact that such changes are typically deleterious and rare in natural populations (Hallgrímsson et al. 2007).

The Carnivora and Dasyuromorphia both occupy similar carnivorous ecological niches and exhibit similar morphological disparity but they exhibit different rates of morphological evolution. Marsupial carnivores are no less disparate than placental carnivorans, despite the need for marsupials to suckle at an earlier life stage. The slower rate of feliform evolution could be linked to their

relatively narrow diet, as almost all are carnivorous to hypercarnivorous (Holliday and Steppan 2004; Price et al. 2012). Caniforms, which have a similar rate of dentary evolution to dasyuromorphs, occupy many different dietary niches. This includes the hypercarnivorous *Martes* and *Mustela*, though the carnivorous *Canis* and *Vulpes*, to more omnivorous genera such as *Conepatus* and *Ursus*, and even herbivorous genera including *Ailurus* and *Potos* (Jones et al. 2009). Dasyuromorphs do not exhibit the same dietary breadth as caniforms. Most are carnivores (*Dasyurus* and *Dasycercus*) and insectivores (*Antechinus* and *Sminthopsis*) but there are myrmecophagous and hypercarnivorous species (*Myrmecobius* and *Sarcophilus*, respectively).

Integration is thought to enhance morphological evolution in certain directions but limit it in others. In theory, a dentary with more modules can evolve to occupy a wider range of morphological space because it can respond to selection in a more targeted manner by changing different modules depending on the selective pressures (Hallgrímsson et al. 2009; Klingenberg 2010). Despite the greater number of modules in carnivoran jaws, levels of disparity are equal among dasyuromorphs and carnivorans. This suggests that one of two different mechanisms is at work. One possibility is that building a carnivore-like jaw is a developmentally simple task that can be achieved with different patterns of integration. The carnivore-like jaw shape appears more ancestral (Grossnickle and Polly 2013), suggesting the developmental program has persisted throughout marsupial and placental evolution. Additionally, the pattern of integration I discovered may make it much more difficult for marsupials to evolve omnivorous

and herbivorous morphologies. Many omnivorous and herbivorous placental mammals lose or reduce the coronoid (e.g., bats, guinea pigs) or angular process (e.g., primates, ungulates), while no marsupials completely lose these processes. The marsupial coronoid is always present, while the angular process may become reduced but is never completely lost, possibly due to its role in the early development of the auditory system (Smith 2006). The evolution of marsupial dentaries lacking certain processes is unlikely because jaw function is essential from an early age. The second mechanism that may explain why disparity in dasyuromorphs and carnivorans is similar, even though dasyuromorphs have fewer modules, is that the direction of selection may be aligned with the dasyuromorph pattern of covariation and promoted the maximal amount of morphological evolution (i.e., Wagner et al. 2007). Simulation studies and a small number of empirical studies support the idea that the evolution of integrated structures with few modules can lead to morphological extremes (Goswami et al. 2014; Hu et al. 2016). The relationship between rates of morphological evolution and integration are more complicated to address. Simulation studies suggest that rates of morphological evolution are not influenced by patterns of phenotypic integration (Goswami et al. 2014). However, it may depend on the structure and clade analyzed (Hallgrímsson et al. 2009), and some evidence from empirical studies has suggested rates can be affected by integration (e.g., Claverie and Patek 2013; Hu et al. 2016).

Dasyuromorph and carnivoran dentaries exhibit broad morphological similarities and variation in both clades is primarily distributed along the elongated to shortened axis, as it is in rodents (Gomes Rodrigues et al. 2015), bats (Dumont et

al. 2012), and even squamates (Sanger et al. 2012), and fish (Cooper et al. 2016). The ubiquity of this axis among many vertebrate clades, including mammals, has typically been linked to diet, and specifically to the generation of bite force (Santana et al. 2012; Dumont et al. 2014). Muscle-bone interactions in the developing dentary are important for determining the morphology and disparity of the angular process in adults. Although it ultimately serves as a muscle attachment site, the marsupial angular is also associated with the early develpment of the hearing appartus (Maier 1990; Sánchez-Villagra et al. 2002; Anthwal and Tucker 2012). The coronoid process also exhibits a major range of shape variation from a high to a low position relative to the condyloid. Mechanical feedback between the coronoid and temporalis muscle can determine the final shape of the process. Marsupials and placentals display complete overlap in coronoid process morphology indicating that both can form similar shapes regardless of developmental differences. Similar coronoid shapes can be achieved between dasyuromorphs and carnivorans regardless of whether morphology of the process is primarily determined by muscular action, or by a combination of genes, muscles and development (Anthwal et al. 2015). The clustering of *Sarcophilus* with other placental taxa that exhibit high coronoids such as *Gulo* and *Crocuta* confirms the marsupial condition is as efficient at producing carnivores with strong bite forces as the Carnivora and they can fill the same niches (Wroe et al. 2005; Nogueira et al. 2009).

Conclusions

Cranial development occurs differently in marsupials and placentals due to their differences in reproductive strategies. Marsupials are born at earlier developmental stages than placental mammals. To compensate, marsupials undergo regional heterochrony, particularly in their facial and forelimb skeletons. Here I assess the impact of reproductive differences between placentals and marsupials on dentary morphological evolution. I compare two clades with similar diets, the marsupial dasyuromorphia and the placental carnivorans, and compare their patterns of phenotypic integration, disparity, and rates of morphological evolution. I find the patterns of integration in the dentaries of dasyuromorphs and carnivorans are very different. Integration in dasyuromorphs appears to be driven by muscle attachment sites, while carnivorans exhibit patterns of integration that appear to more closely reflect developmental and genetic processes. The requirement for marsupials to suckle and develop functional jaw musculature at an early life stage may have impacted the covariation structure of the dentary. Reproductive differences did not have any effect on disparity. Rates of morphological evolution are different between dasyuromorphs and carnivorans, but this trend is primarily driven by the slow rate in feliforms, which may reflect their exceptional dietary specialization. Despite differences in patterns of covariation, the dentaries of dasyuromorphs and carnivorans exhibit similar disparity and broadly similar rates of evolution, indicating that reproductive constraints have not limited the evolution of a 'carnivore-like' jaw shape in marsupial mammals.

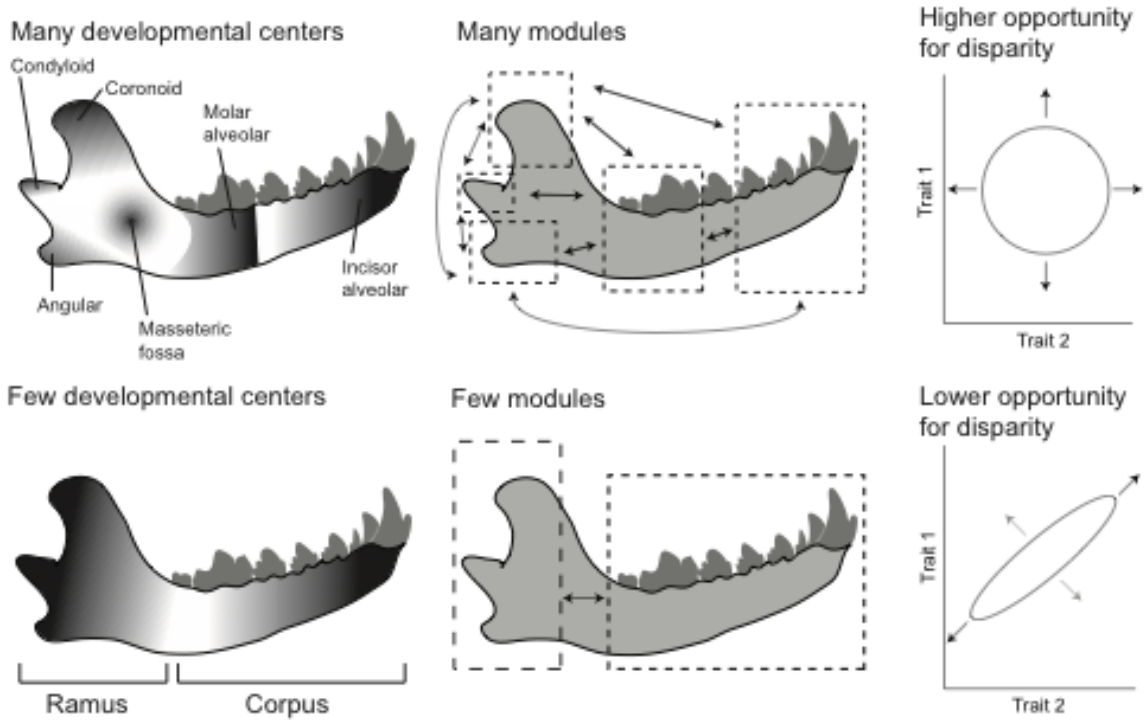

Figure 4.1: Proposed relationship between development, modularity, and disparity

An anatomical structure such as the dentary is shaped based on the interaction of multiple developmental centers. Developmental centers can arise due to independent control of cell condensations, genetic expression of certain genes, and muscle-bone interactions during development. Each of these centers can independently influence different morphological regions of the dentary. I call these developmentally independent regions modules, where morphological covariation within a module is stronger than between modules. In theory, a dentary with more modules means there is greater scope for increased morphological disparity because regions can independently evolve and more intricately respond to selective pressures.

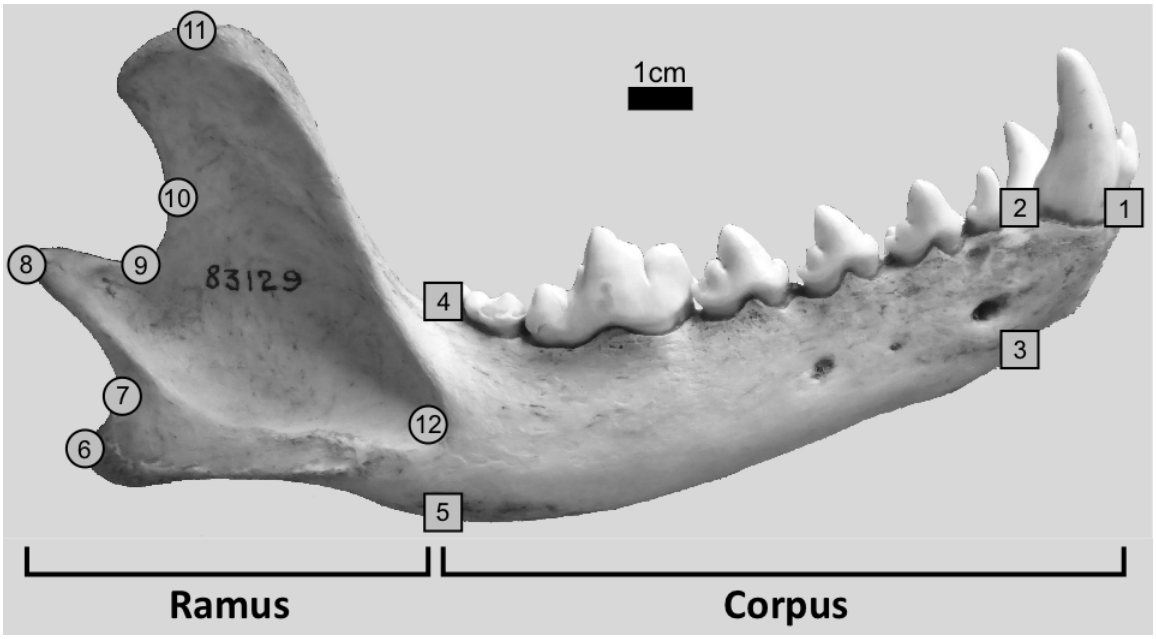

Figure 4.2: Landmark assignment on the mammalian dentary (African wild dog, *Lycaon pictus*)

The two primary modules, the corpus and ramus, represent the dental bearing and muscle bearing regions respectively. Corpus module landmarks are represented by circles, ramus module landmarks are represented by squares. Landmark positions: 1 - most anterior point on the dentary; 2 - distal extreme of the lower canine; 3 - Ventral edge of the left-right dentary suture; 4 - Dorsal base of the ramus; 5 - Ventral base of the ramus; 6 - distal extreme of the angular process; 7 - most concave point between angular and condyloid processes; 8 - distal edge of condyloid process; 9 - proximal edge of condyloid process; 10 - Most concave point between condyloid and coronoid processes; 11 - dorsal edge of the coronoid process; 12 - anterior border of the masseteric fossa.

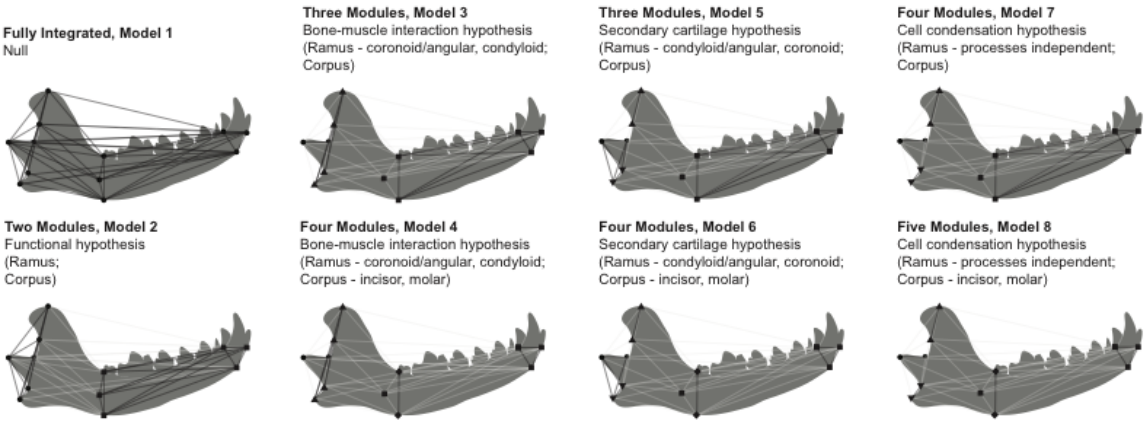

Figure 4.3: Modularity hypotheses

Model 1: no modularity, all landmarks covary together. Model 2: two modules, corpus and ramus. A common model observed in rodents (Klingenberg et al. 2003). Model 3: three modules, assignment based on mechanical stimulus provided by muscle attachment to the angular and coronoid process which are grouped together in a single module. Model 4: four modules, similar to model three but allows for the anterior and posterior regions of the corpus to covary independently. Model 5: three modules, allows for angular and condyloid to covary together due to the shared dependence of the angular and condylar process on secondary cartilage development. Model 6: similar to model five but allows for the anterior and posterior regions of the corpus to covary independently. Model 7, four modules, all processes on the ramus can covary. Model 8, five modules, similar to model seven but allows for the anterior and posterior regions of the corpus to covary independently.

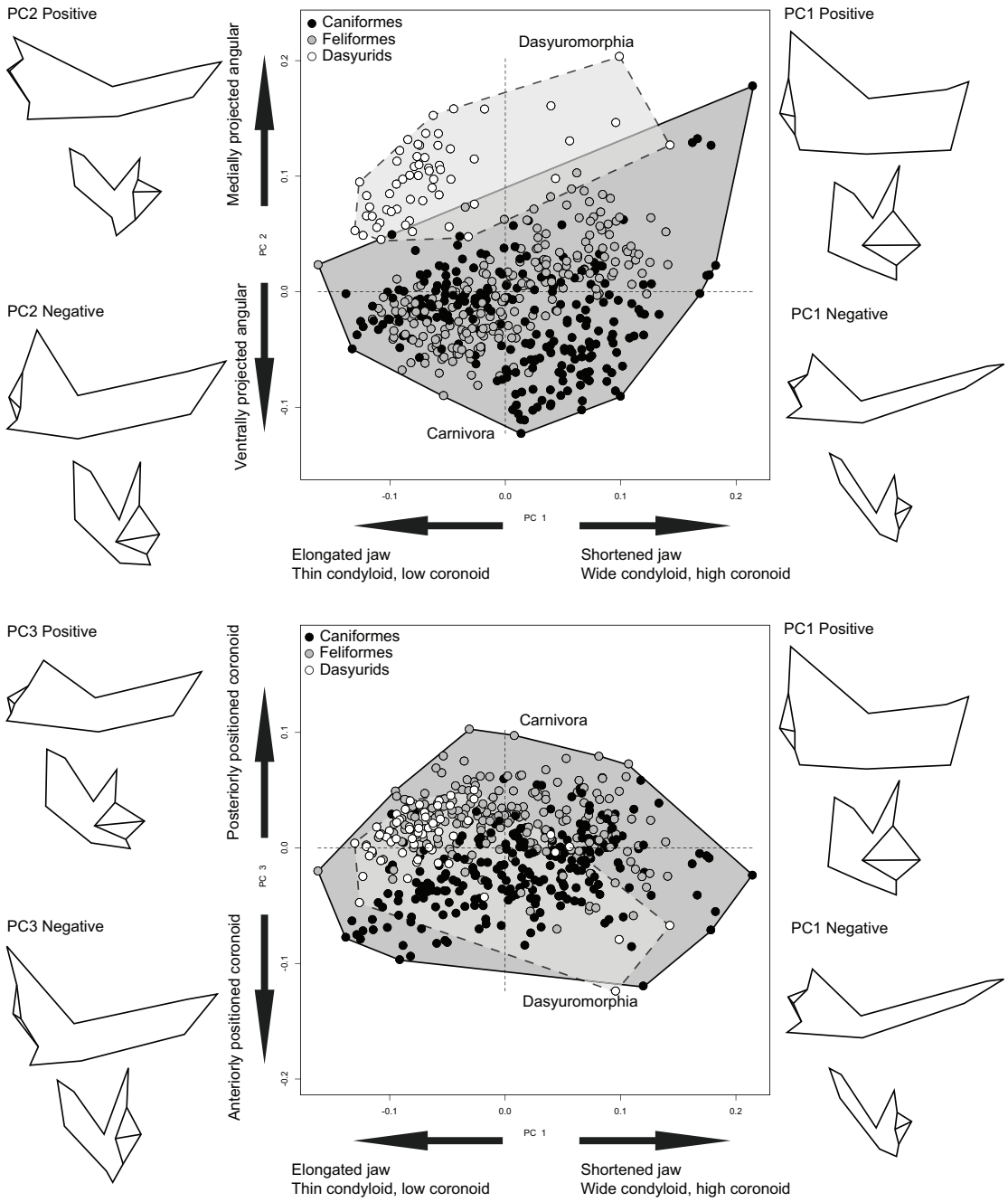

Figure 4.4: Morphospaces for the Carnivora and Dasyuromorphia.

Principal component (PC) scores from the first 3 axes are plotted for all individuals. Small black dots represent hypothetical trait values for ancestral nodes. Jaw wireframes illustrate the typical morphology of a jaw in that quadrant of morphospace for a given axis.

	Caniformia	Dasyuromorphia	Feliformia
Caniformia	X		
Dasyuromorphia	0.308	X	
Feliformia	**0.001**	**0.001**	X

Table 4.1: Comparisons of rates of morphological evolution

Statistical comparisons of rates of morphological evolution between marsupial and placental mammals. Bold type indicates significant differences in rates of morphological evolution between clades.

	Caniformia	Dasyuromorphia	Feliformia
Caniformia	X		
Dasyuromorphia	0.230	X	
Feliformia	0.297	0.666	X

Table 4.2: Comparisons of morphological disparity

Statistical comparisons of morphological disparity between marsupial and placental mammals.

Clade	Best Model	Model Log L	Posterior Probability
Carnivora	Cell condensation (modules; ramus - 3, corpus - 2) ρ separate within and between modules	1.00	1.00
Caniform	Cell condensation (modules; ramus - 3, corpus - 2) ρ separate within and between modules	1.00	0.96
Feliform	Cell condensation (modules; ramus - 3, corpus - 1) ρ separate within and between modules	1.00	0.92
Dasyuromorphia	Mechanical environment (modules, ramus - 2; corpus - 1) ρ separate within modules, similar between modules	1.00	0.42
Dasyuromorphia	Mechanical environment (modules, ramus - 2; corpus - 1) ρ separate within and between modules	0.53	0.22

Table 4.3: Best fitting modularity models for each placental and marsupial grouping

Taxa groupings with two entries for the Best Model indicate the two competing models were within 2 AICc units of each other. ρ is the hypothesized correlation coefficient. Models refer to the different modularity hypotheses set out in Figure 4.3. See Goswami and Finarelli (2016) for additional methodological details.

CHAPTER 5

CONCLUSIONS

My thesis set out to investigate the evolution of the mammalian feeding system with two primary aims. My first aim was to understand the influence of molar complexity on biomechanical performance in Triassic mammals. My second aim was to understand the role of phenotypic integration and climatic variability in shaping the morphological evolution of the jaw. In chapter 2 I built physical models of two Triassic mammals and found that the ability to damage a proxy food item was the major biomechanical parameter that increased with increasing complexity. In chapter 3 I found an association between climatic variability and phenotypic integration. Specifically, I found that carnivoran taxa in more climatically variable regions were less integrated and exhibited higher disparity and faster rates of morphological evolution. In chapter 4 I outlined differences in the pattern of jaw integration between marsupial and placental carnivores. In particular, I found that dasyuromorph marsupials had fewer modules and exhibited a pattern of integration on the jaw consistent with the early development of their cranial musculature. Despite this difference in integration, marsupial and placental carnivores exhibited broad similarity in their disparity and rates of morphological evolution.

My work on teeth tested the biomechanical implications of a transition from simple to complex tooth morphologies in Mesozoic mammals. This involved creating physical models of mammal tooth rows to test their functional efficiency in cutting

food with soft or hard material properties. I found that the *Morganucodon* and *Kuehneotherium* models differed in their biomechanical interactions with hard and soft foods. Specifically, *Morganucodon* was better able to process hard food while *Kuehneotherium* was better able to process soft foods. Perhaps more importantly, *Kuehneotherium* molars inflicted significantly more damage on food items regardless of their material properties, indicating the fundamental importance of the transition from a linear to a triangular arrangement of molar tooth cusps lies in the ability to maximize damage. These results demonstrate the implications of molar cusp re-arrangements for the biomechanics of early mammal teeth, and support other recent evidence that early mammals specialized on a diverse range of prey.

My work on carnivoran jaws tested the association between jaw integration and climatic variability. I found that canid and felid taxa in more climatically variable regions were less integrated and exhibited higher disparity and faster rates of morphological evolution. High climatic instability (i.e., large fluctuations in temperature and precipitation between seasons) may favor a reduction in phenotypic integration, because this permits the jaw to be more evolvable. Canids and felids living in climatically variable regions therefore have greater potential to more quickly respond to changing environmental conditions than their climatically stable counterparts. This suggests that climate may have a profound influence on the evolvability of species and contributes to a growing body of data that can inform how phenotypes may respond to climate change.

My work on marsupial and placental jaws tested the impact of different life history strategies on phenotypic integration and disparity. Marsupial neonates are born without a fully developed oral apparatus but immediately begin suckling in the pouch. This mechanical environment is vastly different to placental mammals, which exhibit simultaneous development of dentary muscles and bones that only function after they are fully developed. I found that dasyuromorphs exhibited fewer modules and higher integration between the angular and coronoid processes, the primary attachment sites for the masseter, temporalis, and pterygoid muscles, and between the molar and incisor alveoli. Carnivorans are free from this constraint as each process on the dentary can evolve independently. Despite differences in integration, dasyuromorphs and carnivorans display similar levels of disparity and rates of morphological evolution. This pattern of integration in dasyuromorphs may result from the overwhelming influence of muscles on the developing ramus and the rapid ossification of the corpus.

In conclusion, I show how one particular module of the feeding system, the teeth, and under high selection for maximizing damage. I then go on to show in another module, the jaw, how climatic variability and early life history events can shape the disparity and the rate of morphological evolution via phenotypic integration. Taken together, my work suggests the mammalian feeding system is highly modular and the distribution of this modularity is based on phylogeny and the environment.

APPENDIX A

SUPPLEMENTARY INFORMATION FOR CHAPTER 2

Kuehneotherium and *Morganucodon* measurements

Eighteen measurements were obtained from 2D images of teeth in buccal and occlusal views (Figure S2.1, Table S2.1). The measurements include cusp heights, widths, lengths, distances between cusps, and angles between cusps, which served as parameters for the computer aided design (CAD) models. The CAD models were constructed using angles, cones, cubes and cuboids. All cusps were treated like cones on a main 'base' that was considered to be the cingulum, where the tooth would have met the gum-line.

Physical models

Design of Computer Aided Design Models

The design of the CAD models was based on the measurements of *Morganucodon* and *Kuehneotherium* molar teeth. Despite their apparent simplicity, the teeth of early mammals are still geometrically complex. I needed to simplify this geometry to produce CAD models that could be parameterized. To isolate the major morphological differences between the molars of the two species, I performed *t*-tests between each of the molar variables (Table S2.3). The next step was to understand which variables were correlated so I could reduce the number of

parameters in the CAD models. I assessed covariation among variables using Pearson's correlations (Table S2.2).

I selected three primary variables to change in the CAD model on the basis of the *t*-test and correlation results: cusp-*b* height, notch angle and cusp angle. I calculated species-specific means for each of these variables. Cusp-*b* height was significantly different between the two species and was correlated with a number of the other width and height measures. I selected notch angle because it differed significantly between *Morganucodon* and *Kuehneotherium*. The two notch angles in each species, between cusps a-b and a-c, are similar within each species (*Morganucodon* a-b = 70.2º; *Morganucodon* a-c = 72.2º; and, *Kuehneotherium* a-b = 48.9º; *Kuehneotherium* a-c = 49.7º). Therefore, I used mean notch angle for each species in the models (*Morganucodon* notch = 71º and *Kuehneotherium* notch = 49º). I chose to incorporate cusp angle into the models because it was significantly different between species and was not consistently correlated with any other variable. I then calculated species specific means for the three main variables (*b*-cusp height, notch angle, cusp angle), and calculated means between the two species for each of the remaining 15 variables. I fixed the *a*-cusp to a value of 1 and scaled all other linear variables to this central cusp (Table S2.4). I then increased the size of each variable by a factor of ten prior to printing the teeth in 3D. The final measurement parameters used for the construction of the CAD models can be viewed in Table S2.5.

Both *Morganucodon* and *Kuehneotherium* also have smaller cusps, *d* (distal) and *e* (mesial), at the border of the molar cingulum. These cusps often exhibit wear

due to shearing forces, suggesting they are indeed involved in food processing (Crompton and Jenkins, 1968). I omitted these cusps from our models because they were difficult to measure and likely play only a small role in food processing. Mills (1971) suggests their main role is in interlocking the tooth row together (Figure S4).

Construction of Computer Aided Design Models

The cusps were created using a series of three concentric ovals with their dimensions obtained from the raw measurements (Figure S2.5). The ovals sat in three different planes, one oval sat at the base of the cusp, one halfway and one at the top. The height and width of the cusp was determined from measurements gathered from the mammal teeth. I used the interpolation function to extend a surface through each of the ovals to create the surface of the cusp. I duplicated this process for each of the three cusps and moved them into species-specific positions (i.e., triangular arrangement for *Kuehneotherium*, and linear arrangement for *Morganucodon*). Each molar on the molar row sat upon a long thick base-plate. To achieve the correct notch angles (angle between the apex and valley of adjacent cusps) for cusps *b* and *c*, cusps had to be rotated, meaning part of their geometry become 'submerged' into the base-plate. The size of the base-plate accounted for this so that no solid geometry emerged from the plate.

Proxy food item construction

Gel formulation

Food items used in occlusion experiments consisted of a gel encased in a thin polymer film. The thin film used was a poly(ethylene terephthalate) film (Hostaphan®, Mitsubishi Polyester Film GmbH).

The gel used to replicate the soft food item was a triblock copolymer. The polymer content of the triblock gel was a triblock copolymer of poly(methyl methacrylate) [PMMA] and poly(n-butyl acrylate) [PnBA]. The materials were received from Kuraray Co. with quoted molecular weight of 25k-116k-25k g/mol of PMMA-PnBA-PMMA. The solvent content of the triblock gel was 2-ethyl hexanol (Sigma Aldrich). To create the materials 15wt% of polymer was dissolved in solvent and heated to 100 °C. When cooled to room temperature, the PMMA end blocks microphase segregate into micellar domains due to the incompatibility with the solvent at lower temperatures. The PMMA micellar domains serve as physical crosslinks. The modulus and fracture properties of these gels are largely determined by the length of the PnBA block and the volume fraction of polymer in the gel (Seitz et al., 2007). These gels are thermoreversible; if damage occurs while the gel is a solid, the gel can be heated again above 90 °C to erase the damage and cooled again to room temperature to create a new sample.

The gel used to replicate a hard food item was a poly(dimethyl siloxane) [PDMS] elastomer (Sylgard 184®, Dow-Corning, Inc). The two parts of prepolymer:crosslinker were mixed in a 40:1 ratio and cured at 70ºC for 2 hours.

Cuticle film construction

A polyethylene terephthalate (PET) film from Mitsubishi Polyester Film GmbH (Hostaphan® TT) template was used to encase each gel. Templates were cut

out from paper using the dimensions outlined in Figure S6. These templates were used to cut out all PET films for future testing. Films were cut on a glass slide using a razor blade.

PDMS gel sample construction

PDMS was poured into a plastic mold, cured using the previously specified conditions, and cut to the correct size using a razor. A PET film was wrapped around the cured samples (Figure S6a). PDMS/PET adhesion was qualitatively much stronger than the Triblock/PET adhesion and thus, did not need to be liquid and cool on the PET film to prevent delamination of PET during testing. PDMS gel cures clear and provided an easy surface to see the size and pattern of fractures through the PET film.

Triblock gel sample construction

A glass mold was built using stacks of glass slides cut to the dimensions outlined in Figure S7. The PET was placed inside the glass mold with sections *B*-*F* contacting the interior of the glass mold, and section *A* was left outside of the mold to act as the top lid. Solid triblock pieces were placed on top of the PET film inside the glass mold. I used 2g of triblock gel in each sample which would precisely fill volume of the glass mold. The glass mold with the PET and triblock were placed on a hot plate at 120°C, allowing the triblock gel to melt and assume the shape of the glass mold. Once the triblock was fully melted I folded over section *A* of the PET film to form the lid. This ensured the liquid triblock was fully encased inside the PET film and would adhere to it. I removed the glass mold from the hot plate, allowing the triblock to cool and solidify ready for testing. The triblock-PET complex was far

more difficult to visualize the patterns and sizes of fracture in the PET film. Despite this, the sizes and patterns of PET fracture were consistent with what I observed with the PDMS gel.

Mechanical properties of proxy food items and individual materials

Rational

The ability of an entire insect to resist compressive force during biting depends on the tensile strength of the film, the tensile stiffness of the cuticle, and the compressive stiffness of the insect contents. However, the material properties and geometry of insect cuticle, specifically the Young's modulus (E) and cuticle thickness (t), can vary dramatically among and even within individual insects (E ~ 1 kPa - 20 GPa, t ~ 1 μm - 200 μm (Vincent and Wegst, 2004)). As a reference, wing cuticle can exhibit an E of ~ 5 GPa and thickness on average between 0.5 μm – 100 μm (Combes, 2010). Using these reported values of cuticle modulus and cuticle thickness, an average effective tensile stiffness (E*t) for can range from 2.5 kN/m – 500 kN/m. In using the effective tensile stiffness, I are able to represent the thickness and Young's modulus of the cuticle in a single value. Considering this stiffness range, I constructed proxy food items consisting of a "cuticle" polyethylene terephthalate (PET) film (E = 4.4 GPa, t = 6.45 μm) giving an effective tensile stiffness of 30 kN/m. In designing our hard and soft food items our aim was to select material properties for each based on values gathered from the literature (i.e., Evans and Sansom 1998, Vincent and Wegst, 2004). The properties that I chose for our

hard and soft food items were based, in part, on what is possible to do with the polymers and also to represent the range of values reported for numerous insects.

Young's modulus of individual materials

Young's modulus of each proxy food substrate was tested using micro-indentation and deep indentation. Young's modulus of the proxy food film was measured using tensile testing. Fracture energy of the proxy food items was measured using deep indentation.

Micro-indentation consists of a probe indenting the surface of a flat material and recording the force vs. displacement response. This indentation test is performed using a flat-punch probe of known radius and a material of a known thickness, where the probe indents the material to a displacement that is less than 10% of the layer thickness. In this small strain limit, assuming the material is incompressible, the Young's modulus, E, can be determined from the measured compliance, or inverse stiffness, of the test by:

$$C = \frac{d\delta}{dF} \qquad (S.1a)$$

$$E = \frac{3}{8aC}\left[1 + 1.33\left(\frac{a}{t}\right) + 1.33\left(\frac{a}{t}\right)^3\right]^{-1} \qquad (S.1b)$$

where δ is the displacement of the sample surface, F is the measured force, a is the radius of the flat-punch probe, E is the Young's modulus of the sample, and t is the thickness of the undeformed sample (Crosby and Shull, 1999). The tests were conducted using a custom built apparatus where displacement is actuated and the force is measured with a load cell. The displacement actuator was an EXFO IW-820 Nanopositioner from Burleigh instruments. Tests were conducted at a displacement

rate of 0.01 mm/s. The force was measured using a custom-built load cell consisting of a single-plate capacitive electrode and a grounded aluminum cantilever as the other capacitive electrode. For all indentation tests, the compliance of this cantilever-capacitor load cell was incorporated into the calculations. The single-plate capacitive electrode was a D-510.021 from PI GmbH & Co. The flat-punch probe used was a polished piece of steel drill stock with a diameter of 1.5 mm. For each test, a least squares linear fit was applied to the force vs. displacement data to determine a linear compliance. At least 7 tests each were performed on the PDMS gel and the triblock gel to determine the Young's modulus using Equation S.1b. The Young's modulus of the PDMS gel was determined to be 57.8 ± 2.4 kPa. The Young's modulus of the triblock gel was determined to be 13.9 ± 0.9 kPa.

Tensile testing was used to measure the Young's modulus of the proxy food film with an Instron 5564 universal tensile testing machine. Samples were cut to a size of 50 x 15 x 0.006 mm and tested at a rate of 0.17 mm/s. The Young's modulus averaged over 10 samples was 4.40 +/- 0.65 GPa.

Fracture properties of proxy food items

Deep-indentation, or indentation where the displacement imposed on a sample of infinite thickness is much larger than the length scale of the indenter ($\delta \gg a$), can be used to measure both the Young's modulus and the fracture energy of a sample (Fakhouri and Crosby, 2015). Using a spherically tipped indenter and the same custom-built indentation apparatus at a displacement rate of 0.1 mm/s, the force vs. displacement response for deep indentation can be related to the material properties and geometry by:

$$P = k'Ed^2 + \frac{8}{3}ERd \qquad (S.2)$$

where P is the force measured, k' is an empirical constant determined to be 0.26, E is the Young's modulus of the sample, d is the displacement of the sample surface, and R is the radius of curvature of the spherical probe. Using Equation S.2, a non-linear least squares fit of a quadratic equation was applied to the force vs. displacement curve to determine the Young's modulus of the sample. Using this technique, the moduli of the PDMS and triblock gels were determined to be 61.6 ± 3.4 kPa and 15.5 ± 1.3 kPa, respectively. These values are in good agreement with values determined by micro-indentation.

The puncture force of a sample can be related to the geometry and fracture properties by:

$$P_c = K\Gamma R \qquad (S.3)$$

where P_c is the critical force at puncture, K is an empirical constant determined to be 0.5, Γ is the fracture nucleation energy of the material, and R is the cross-sectional radius of the indenter. The fracture force is designated as the point at which there is a sharp drop in force in the force vs. displacement response due to the failure of the sample. With a known cross-sectional radius of 0.035 mm, fracture nucleation energy can be calculated from the measured fracture force using Equation S.3. Samples tested include free-standing PDMS gel and triblock gel, film-encased PDMS gel and triblock gel, and free-standing PET film. Table S2.6 summarizes the results of all sample combinations tested with deep indentation.

These gel and film properties fall within materials data reported for insects (Vincent and Wegst, 2004). The PET film modulus measured 4.40 +/- 0.65 GPa

which falls within the 1-20 GPa reported for sclerotised cuticles. The triblock (13.9 ± 0.9 kPa) and PDMS (57.8 ± 2.4 kPa) also fall within the reported range for soft insect cuticle (1 kPa-50 MPa).

As with other modeling techniques (e.g., finite element analysis (Dumont et al. 2009)), only by simplifying this complex insect system can I hone in on some of the biomechanical parameters that may vary as a result of morphological differences between the two early mammals. Despite the overlap in compressive stiffness between our gel insects and real insects I acknowledge that fracture and crack propagation could be subtly different between the homogeneous films and gels compared to the anisotropic insect cuticle and internal organs. However, I are confident that our simulated materials behaved similar to real insects.

The printed teeth may also deform during testing, but this deformation is assumed to be minimal given the material properties and geometry of the teeth and sample. I specifically chose the PET film as our cuticle, and I punctured using ABS printed teeth to minimize deformation and wear of the printed teeth. There is variation in energy among trials and no directional trend in increasing energy from one trial to the next indicating that wear is minimal (Figure S2.8). I visually inspected the models during the experiments and did not see any degradation in the models over time.

Scanning information for main text Figure 2.2

Morganucodon watsoni: NHMUK PV M92538, an isolated right lower molar (identified as m4). Scanned on a Bruker Skyscan 1172 micro-computed tomography

system in the Department of Archaeology and Anthropology at the University of Bristol.

Kuehneotherium praecursoris: NHMUK PV M98603, an isolated right lower molar (mid-row). Scanned using synchrotron radiation X-ray tomographic microscopy at the Swiss Light Source TOMCAT beamline.

Specimen repositories: Natural History Museum, London (NHMUK) and University Museum of Zoology, Cambridge (UMZC).

Occlusion experiments with proxy food items

Upper and lower tooth rows were fixed into a materials testing machine prior to puncture testing. The upper tooth row sat on an adjustable base-plate that could be moved to come into occlusion with the lower tooth row. The lower tooth row was fixed into an immovable clamp. A maximum displacement of 8.5mm was used for the soft food item and 10.6mm for the hard food item. These distances ensured that the teeth punctured the gel but did not come into contact with the base-plate, which could have damaged the models and/or the load cell. The soft food hard was slightly thinner than the hard food due to how the polymer complexes were constructed. For that reason I could not compare between hard and soft foods, only across species within those categories. All puncture tests were performed using an Instron 5500R universal tensile testing machine (Figure S2.9). The crosshead was moved at a displacement rate of 0.15 mm/s. The Instron load cell reported the compressive forces during the puncture experiments. I recorded energy, time (displacement), and force at the point of first fracture for both gel food items, and

performed *t*-tests to identify differences in these biomechanical parameters between *Morganucodon* and *Kuehneotherium* (Table S2.7-S2.8).

Proxy food item destruction

I quantified destruction of the PDMS/PET and triblock/PET composites. The patterns and lengths of fracture were similar among gels within each species. The gel/PET composites were loaded into the materials testing machine (See Figure S2.9), and subjected to compressive force by the occluding teeth. Following the trial the gel composite was removed and imaged with a digital camera (Figure S2.10-S2.11). The length of each puncture fracture present in the PET film was recorded using Image-J and the sum of lengths was calculated for each trial. A *t*-test was used to detect for significant differences in PET film puncture length between *Morganucodon* and *Kuehneotherium* (Table S2.10).

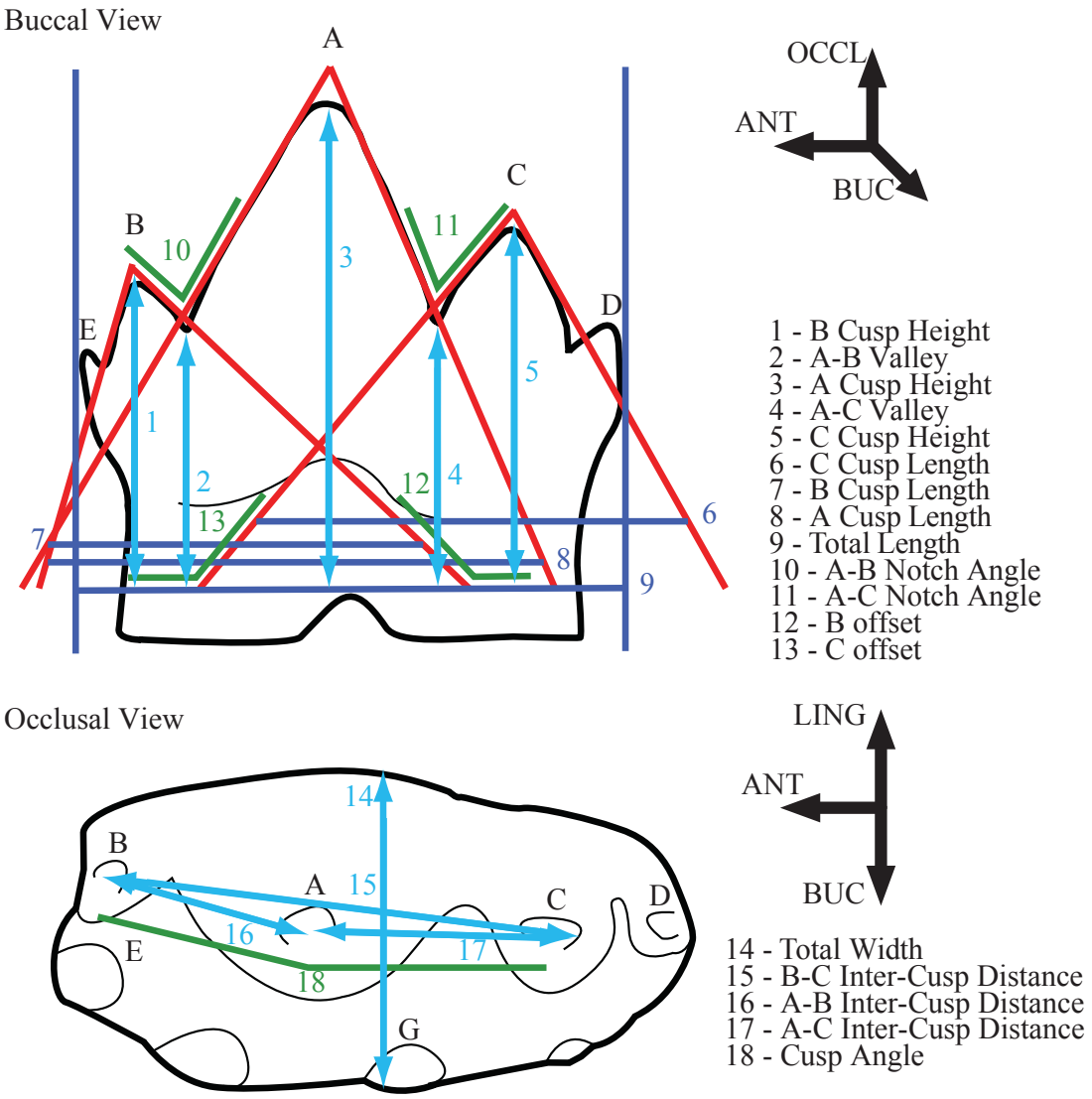

Figure S2.1. Molar measurements used in this study

The light blue vertical lines indicate heights of the cusps (in buccal view) or inter-cusp distances (occlusal view). Dark blue lines indicate lengths of cusps. Green lines indicate angle measurements in both views. Cusps would be built as cones in the CAD program - these cones are represented by the red triangles. OCCL, occlusal; ANT, anterior; BUC, buccal; LING, lingual.

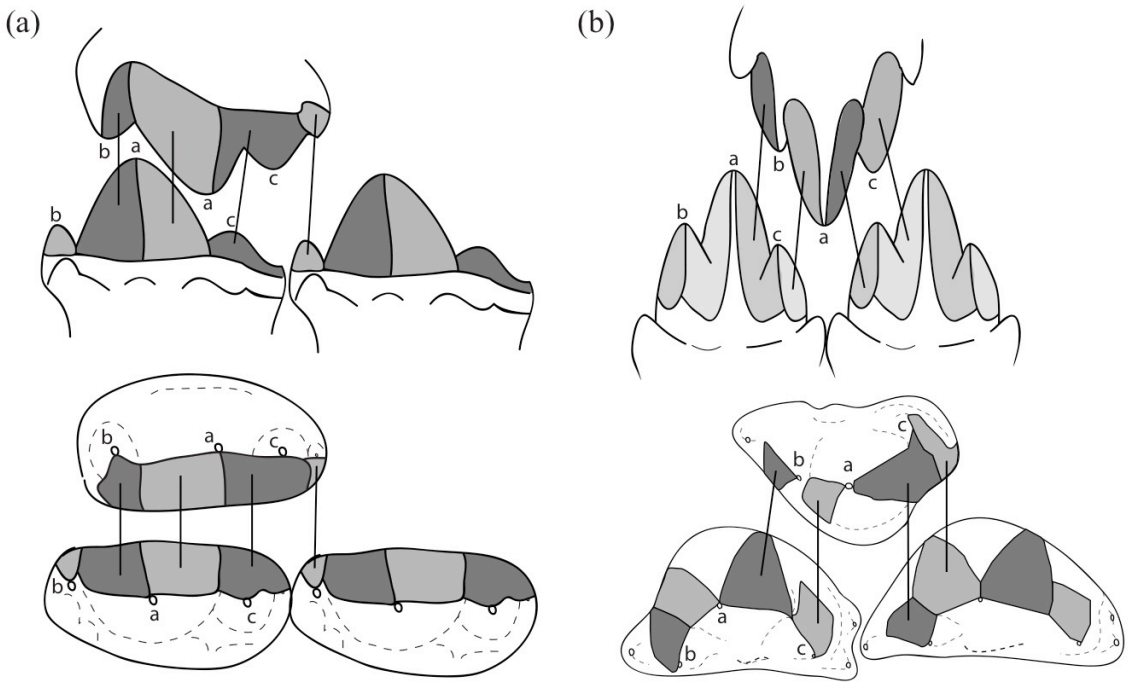

Figure S2.2. Occlusion in *Morganucodon* and *Kuehneotherium*

(a) Lateral (top) and occlusal (bottom) view of *Morganucodon*. (b) Lateral (top) and occlusal (bottom) view of *Kuehneotherium*. Colours represent occluding surfaces. Letters represent cusp name.

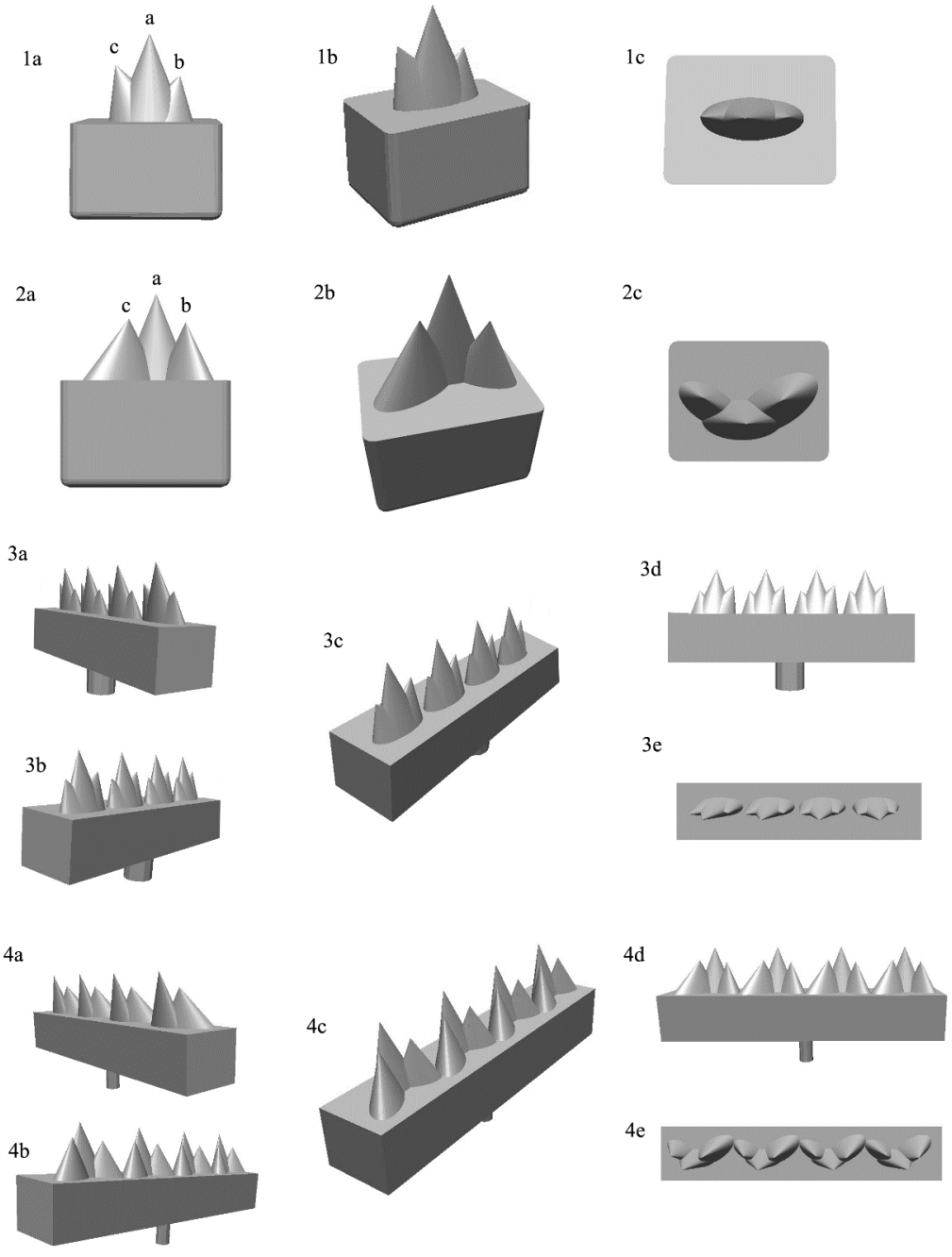

Figure S2.3. *Morganucodon* and *Kuehneotherium* CAD model examples for tooth rows and individual teeth

1a, front (buccal); 1b, default; and 1c, top (occlusal) view of a single *Morganucodon* molar. 2a, front (buccal); 2b, default; and 2c, top (occlusal) view of a single *Kuehneotherium* molar. 3a-b side (lingual-buccal); 3c, default; 3d, front (buccal); and 3e, top (occlusal) view for *Morganucodon* tooth row. 4a-b side (lingual-buccal); 4c, default; 4d, front (buccal); and 4e, top (occlusal) view for *Kuehneotherium* tooth row. The lingual surface of both molars (3a/4a) is at 90° vertical to the base-plate to allow corresponding upper and lower molar rows to occlude.

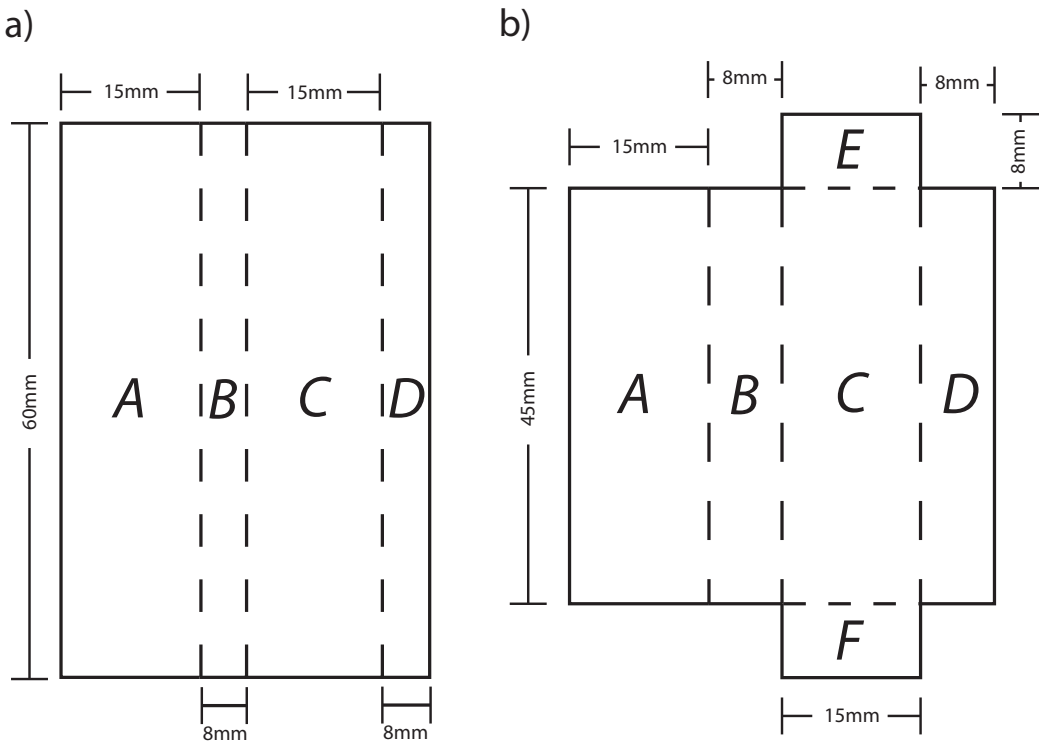

Figure S2.4. PET film template dimensions

a, PDMS film template. b, Triblock film template. Dotted lines indicate folding lines. Letters are referred to in the main text.

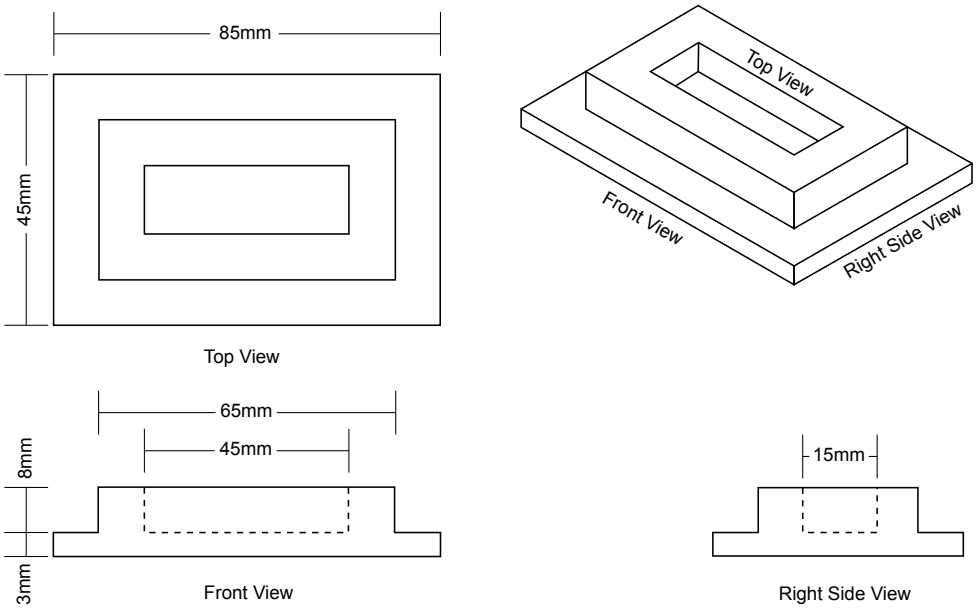

Figure S2.5. Triblock mold dimensions

Engineering drawing illustrating the geometry of the glass triblock mold.

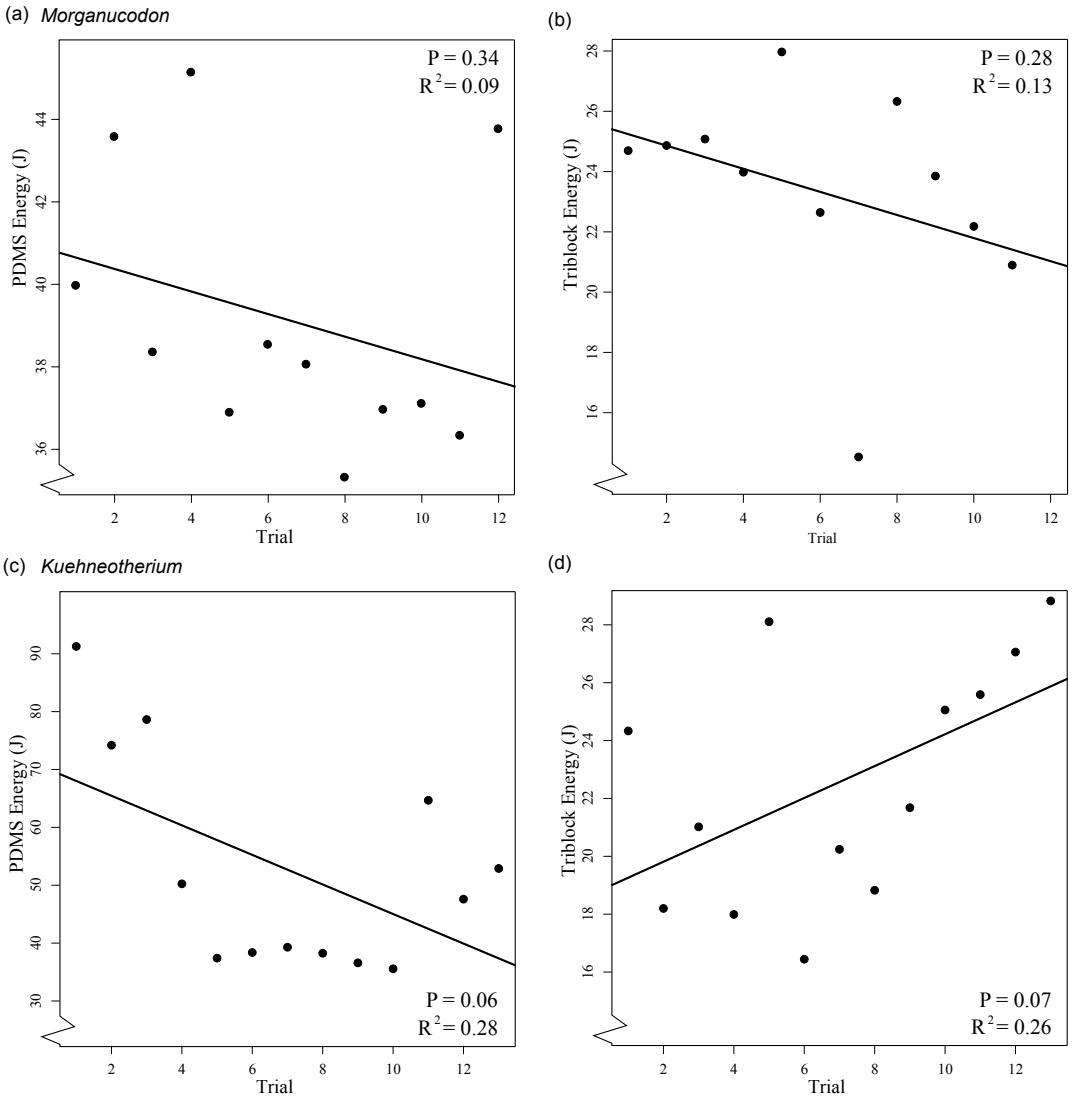

Figure S2.6. Effects of repeated model testing on energy

(a) PDMS and (b) triblock energy by trial for *Morganucodon*. (c) PDMS and (d) triblock energy by trial for *Kuehneotherium*. No model exhibits significant increases in energy with each trial as would be expected if the models were being worn. Energy calculated as area under the force displacement curve at the completion of the trial.

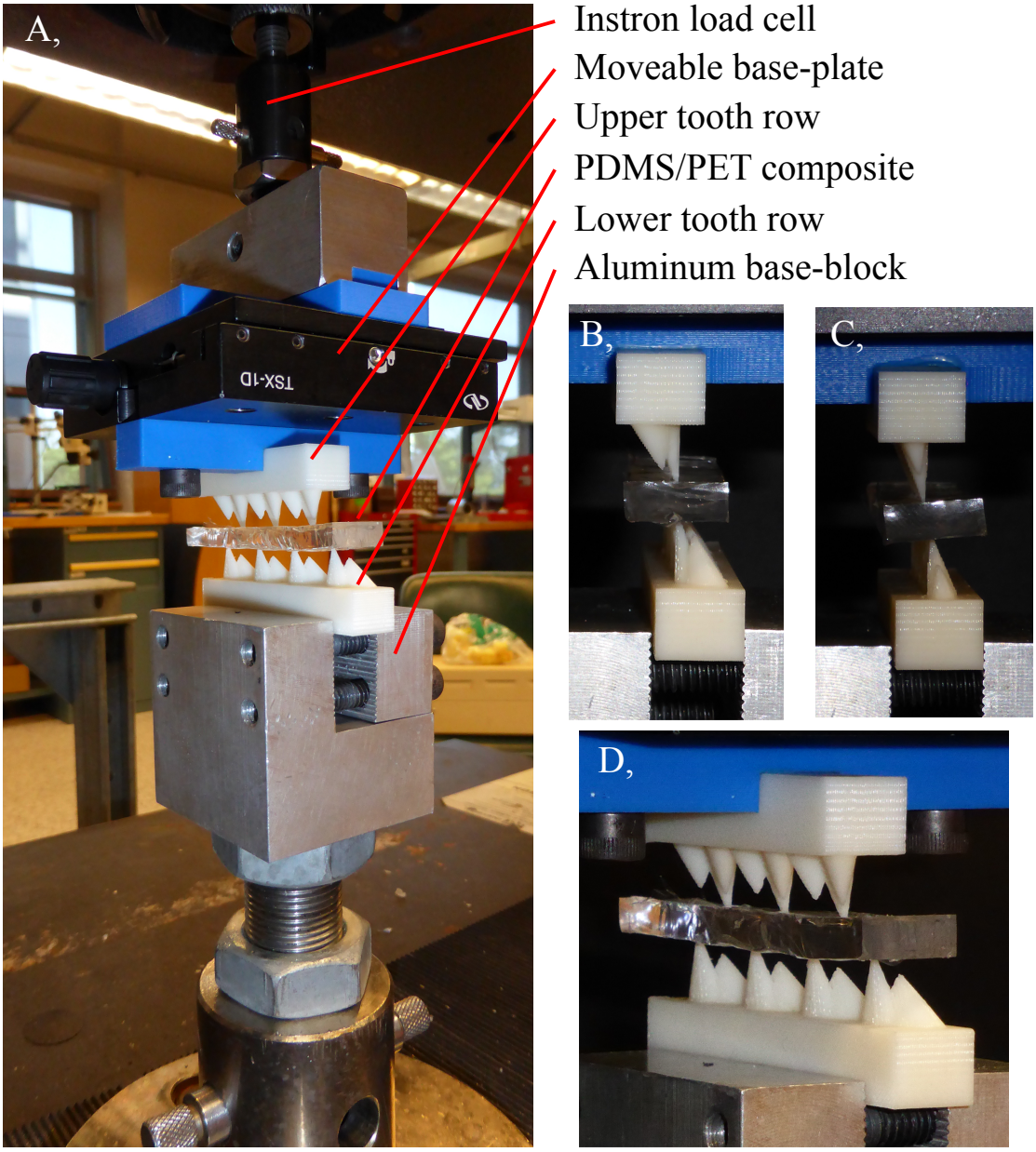

Figure S2.7. Materials testing set-up

A, Full testing rig; B, *Kuehneotherium* end view; C, *Morganucodon* end view; D, *Kuehneotherium* lateral view; E, *Morganucodon* lateral view.

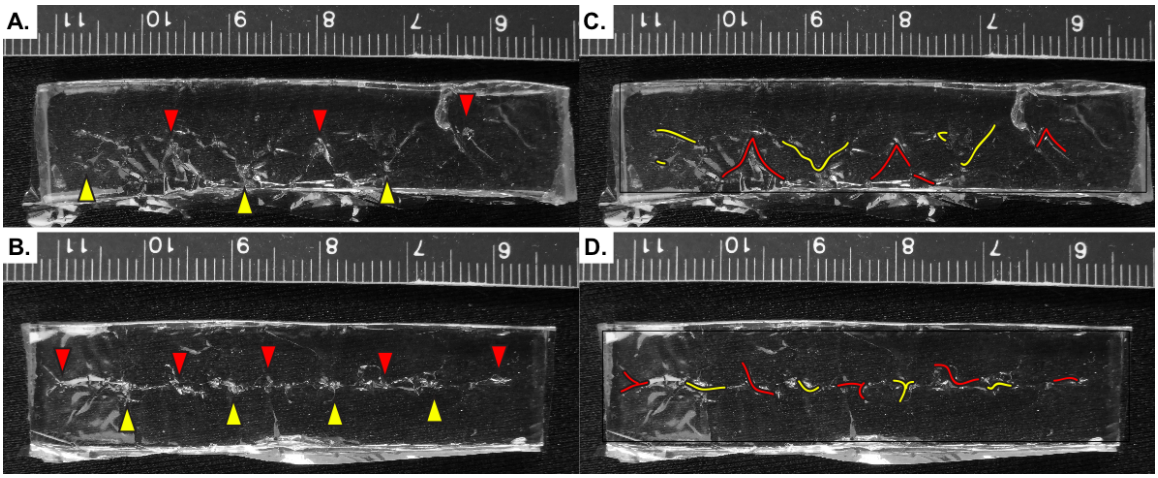

Figure S2.8. PDMS/PET destruction testing

A. Puncture point of the primary cusp for *Kuehneotherium*; B. Puncture point of the primary cusp for *Morganucodon*; C. Highlighted areas where fracture in the PET film occurred in *Kuehneotherium*; D. Highlighted areas where fracture in the PET film occurred in *Morganucodon*. Red colors indicate fracture/puncture by upper tooth row; yellow colors indicate fracture/puncture by lower tooth row.

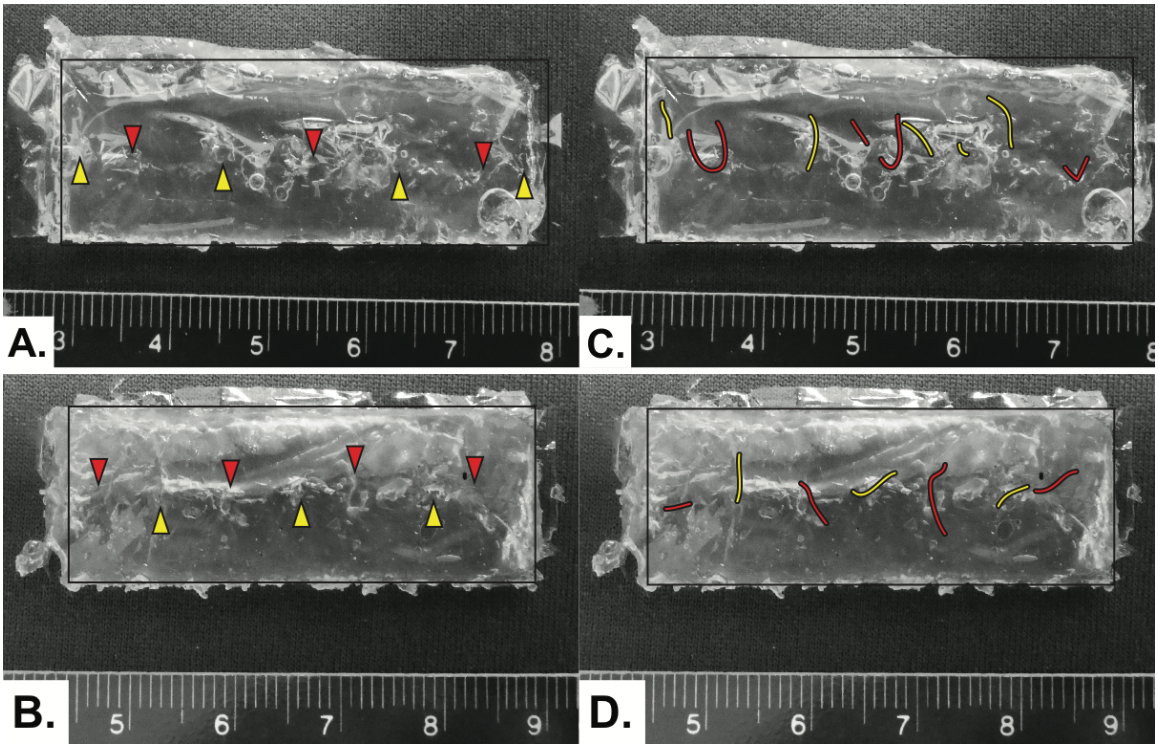

Figure S2.9. Triblock/PET destruction testing

A. Puncture point of the primary cusp for *Kuehneotherium*; B. Puncture point of the primary cusp for *Morganucodon*; C. Highlighted areas where fracture in the PET film occurred in *Kuehneotherium*; D. Highlighted areas where fracture in the PET film occurred in *Morganucodon*. Red colors indicate fracture/puncture by upper tooth row, yellow colors indicate fracture/puncture by lower tooth row.

Species	Speciemen	HeightA	HeightB	HeightC	ValleyAB	ValleyAC	WidthA	WidthB	WidthC	WidthTotal	NotchAB	NotchAC	bOffset	cOffset	LengthTotal	InterAB	InterAC	InterBC	CuspAngle
Keuhneotherium	NHMUK PV M92773	1.29	0.84	0.74	0.56	0.58	0.93	0.50	0.62	0.93	47.84	56.94	114.65	127.95	0.68	0.42	0.37	0.64	106.78
Keuhneotherium	NHMUK PV M92774	1.61	1.14	1.03	0.91	0.92	1.14	0.81	0.78	1.16	52.14	46.93	120.78	117.46	0.73	0.44	0.33	0.65	115.12
Keuhneotherium	NHMUK PV M92775	1.19	0.80	0.72	0.58	0.57	0.78	0.55	0.59	0.85	49.82	47.05	120.61	122.78	0.51	0.35	0.28	0.52	111.86
Keuhneotherium	NHMUK PV M92776	1.62	1.13	0.99	0.85	0.85	1.22	0.82	0.89	1.22	55.52	50.26	119.62	125.74	0.74	0.57	0.38	0.77	105.02
Keuhneotherium	NHMUK PV M19117	1.31	0.92	0.89	0.69	0.75	0.85	0.67	0.70	0.96	47.31	45.53	117.07	122.24	0.59	0.28	0.34	0.59	145.00
Keuhneotherium	NHMUK PV M19121	1.30	0.90	0.88	0.76	0.71	0.96	0.58	0.69	1.07	40.23	45.73	110.70	112.95	0.69	0.37	0.35	0.61	119.40
Keuhneotherium	NHMUK PV M19128	1.08	0.79	0.69	0.58	0.58	0.80	0.54	0.57	0.90	44.93	46.17	114.32	118.10	0.52	0.30	0.29	0.50	115.76
Keuhneotherium	NHMUK PV M19131	1.11	0.78	0.78	0.60	0.66	0.97	0.60	0.65	0.96	58.25	52.52	127.48	119.00	0.44	0.28	0.30	0.53	132.90
Keuhneotherium	NHMUK PV M19170	1.37	0.95	0.77	0.75	0.66	0.85	0.66	0.71	0.84	46.91	52.62	118.92	128.03	0.52	0.35	0.28	0.52	110.20
Keuhneotherium	NHMUK PV M19198	1.19	0.76	0.75	0.55	0.58	0.92	0.52	0.58	0.93	52.92	49.20	119.87	121.35	0.62	0.37	0.38	0.67	132.36
Keuhneotherium	NHMUK PV M24977	1.40	0.91	0.85	0.74	0.73	0.92	0.65	0.79	1.00	42.10	53.40	114.98	125.82	0.49	0.40	0.34	0.63	117.07
Morganucodon	UMZC Eo.D.32	0.99	0.50	0.62	0.33	0.42	1.23	0.65	0.96	1.53	66.29	78.41	135.25	134.64	0.56	0.54	0.42	0.97	179.39
Morganucodon	UMZC Eo.D.33	1.20	0.55	0.80	0.43	0.53	1.36	0.74	0.87	1.67	62.92	71.11	131.27	124.82	0.64	0.47	0.61	1.08	176.64
Morganucodon	UMZC Eo.D.43	1.04	0.56	0.69	0.39	0.51	1.19	0.71	1.01	1.47	71.97	77.06	136.14	136.28	0.78	0.49	0.69	1.17	176.99
Morganucodon	UMZC Eo.D.79	1.39	0.83	0.79	0.65	0.54	1.61	0.87	1.18	1.93	66.13	74.75	128.77	139.32	0.77	0.63	0.59	1.22	175.80
Morganucodon	UMZC Eo.D.134	1.10	0.65	0.77	0.47	0.54	1.49	0.79	1.01	1.71	67.10	80.69	130.98	130.85	0.67	0.42	0.68	1.10	173.82
Morganucodon	UMZC Eo.D.183	1.32	0.74	0.86	0.61	0.57	1.54	0.90	1.02	1.75	72.89	69.38	131.82	130.60	0.72	0.42	0.71	1.13	177.28
Morganucodon	UMZC Eo.D.293a	1.18	0.57	0.80	0.41	0.50	1.27	0.68	0.91	1.68	66.33	62.18	133.78	121.39	0.69	0.43	0.58	1.02	178.44
Morganucodon	UMZC Eo.D.293i	1.36	0.71	0.85	0.57	0.65	1.43	0.84	1.19	1.62	78.74	74.36	146.57	132.90	0.69	0.43	0.72	1.14	172.41
Morganucodon	UMZC Eo.D.293k	1.31	0.57	0.80	0.43	0.57	1.29	0.75	1.17	1.58	68.10	78.82	140.74	134.87	0.73	0.57	0.61	1.18	172.99
Morganucodon	UMZC Eo.D.293L	1.36	0.73	0.89	0.58	0.61	1.63	0.90	1.15	1.86	78.74	71.07	139.12	133.00	0.86	0.59	0.68	1.26	176.07
Morganucodon	UMZC Eo.D.293m	1.35	0.65	0.96	0.54	0.58	1.56	0.89	0.89	1.86	73.93	56.24	136.31	116.55	0.74	0.41	0.83	1.22	170.88

Table S2.1: Specimens used and raw measurements.

Morg Corr	HeightA	HeightB	HeightC	ValleyAB	ValleyAC	WidthA	WidthB	WidthC	WidthTotal	NotchAB	NotchAC	bOffset	cOffset	LengthTotal	InterAB	InterAC	InterBC	CuspAngle
HeightA	1	0.7602	0.8312	0.8641	0.8133	0.7548	0.8341	0.4971	0.7267	0.4668	-0.3864	0.2307	-0.0786	0.5658	0.1427	0.5296	0.7062	-0.5455
HeightB	0.7602	1	0.5421	0.9729	0.627	0.8695	0.8621	0.5825	0.7698	0.4349	-0.0856	-0.0892	0.2604	0.5633	0.1909	0.4314	0.6434	-0.2889
HeightC	0.8312	0.5421	1	0.6959	0.8091	0.7255	0.8074	0.0843	0.6936	0.5428	-0.6678	0.2143	-0.5255	0.5207	-0.2982	0.7883	0.6088	-0.6321
ValleyAB	0.8641	0.9729	0.6959	1	0.7263	0.9006	0.9319	0.5081	0.8021	0.4948	-0.2386	-0.0147	0.1022	0.5665	0.0956	0.5388	0.6793	-0.383
ValleyAC	0.8133	0.627	0.8091	0.7263	1	0.6142	0.7766	0.5271	0.4185	0.7225	-0.1943	0.5254	-0.0561	0.5703	-0.1516	0.7474	0.699	-0.6914
WidthA	0.7548	0.8695	0.7255	0.9006	0.6142	1	0.9283	0.3076	0.9177	0.408	-0.2839	-0.1533	-0.0623	0.5018	0.0839	0.5135	0.6364	-0.3985
WidthB	0.8341	0.8621	0.8074	0.9319	0.7766	0.9283	1	0.3834	0.7771	0.5975	-0.3025	0.0463	-0.04	0.6036	-0.0182	0.704	0.7605	-0.5161
WidthC	0.4971	0.5825	0.0843	0.5081	0.5271	0.3076	0.3834	1	0.1302	0.4329	0.504	0.4491	0.7464	0.453	0.5545	0.0413	0.5322	-0.2761
WidthTotal	0.7267	0.7698	0.6936	0.8021	0.4185	0.9177	0.7771	0.1302	1	0.1579	-0.4736	-0.3415	-0.2249	0.4695	0.1494	0.3757	0.5348	-0.2775
NotchAB	0.4668	0.4349	0.5428	0.4948	0.7225	0.408	0.5975	0.4329	0.1579	1	-0.1959	0.6879	0.0402	0.5504	-0.1411	0.6182	0.5734	-0.4022
NotchAC	-0.3864	-0.0856	-0.6678	-0.2386	-0.1943	-0.2839	-0.3025	0.504	-0.4736	-0.1959	1	0.0515	0.8433	-0.195	0.4265	-0.4541	-0.1267	0.1619
bOffset	0.2307	-0.0892	0.2143	-0.0147	0.5254	-0.1533	0.0463	0.4491	-0.3415	0.6879	0.0515	1	0.0801	0.1327	-0.0596	0.2275	0.2114	-0.4384
cOffset	-0.0786	0.2604	-0.5255	0.1022	-0.0561	-0.0623	-0.04	0.7464	-0.2249	0.0402	0.8433	0.0801	1	0.1472	0.6795	-0.3829	0.1727	0.2263
LengthTotal	0.5658	0.5633	0.5207	0.5665	0.5703	0.5018	0.6036	0.453	0.4695	0.5504	-0.195	0.1327	0.1472	1	0.311	0.5659	0.8886	-0.2613
InterAB	0.1427	0.1909	-0.2982	0.0956	-0.1516	0.0839	-0.0182	0.5545	0.1494	-0.1411	0.4265	-0.0596	0.6795	0.311	1	-0.4942	0.3148	0.2392
InterAC	0.5296	0.4314	0.7883	0.5388	0.7474	0.5135	0.704	0.0413	0.3757	0.6182	-0.4541	0.2275	-0.3829	0.5659	-0.4942	1	0.6691	-0.7166
InterBC	0.7062	0.6434	0.6088	0.6793	0.699	0.6364	0.7605	0.5322	0.5348	0.5734	-0.1267	0.2114	0.1727	0.8886	0.3148	0.6691	1	-0.5689
CuspAngle	-0.5455	-0.2889	-0.6321	-0.383	-0.6914	-0.3985	-0.5161	-0.2761	-0.2775	-0.4022	0.1619	-0.4384	0.2263	-0.2613	0.2392	-0.7166	-0.5689	1

Morg P-Value	HeightA	HeightB	HeightC	ValleyAB	ValleyAC	WidthA	WidthB	WidthC	WidthTotal	NotchAB	NotchAC	bOffset	cOffset	LengthTotal	InterAB	InterAC	InterBC	CuspAngle
HeightA	0	0.0066	0.0015	6.00E-04	0.0023	0.0072	0.0014	0.1198	0.0113	0.1477	0.2405	0.4949	0.8182	0.0697	0.6756	0.0939	0.0151	0.0826
HeightB	0.0066	0	0.085	0	0.039	5.00E-04	6.00E-04	0.06	0.0056	0.1813	0.8023	0.7941	0.4393	0.0712	0.574	0.1853	0.0327	0.3888
HeightC	0.0015	0.085	0	0.0174	0.0026	0.0115	0.0027	0.8053	0.0179	0.0844	0.0247	0.5269	0.0969	0.1005	0.3731	0.0039	0.0468	0.0369
ValleyAB	6.00E-04	0	0.0174	0	0.0114	2.00E-04	0	0.1105	0.003	0.1218	0.4799	0.9659	0.7649	0.0692	0.7797	0.0873	0.0215	0.245
ValleyAC	0.0023	0.039	0.0026	0.0114	0	0.0444	0.0049	0.0957	0.2002	0.012	0.567	0.097	0.8699	0.067	0.6563	0.0082	0.0167	0.0184
WidthA	0.0072	5.00E-04	0.0115	2.00E-04	0.0444	0	0	0.3575	1.00E-04	0.2129	0.3975	0.6526	0.8555	0.1158	0.8062	0.1062	0.0353	0.2247
WidthB	0.0014	6.00E-04	0.0027	0	0.0049	0	0	0.2444	0.0049	0.0522	0.3659	0.8925	0.9071	0.0493	0.9576	0.0156	0.0066	0.1041
WidthC	0.1198	0.06	0.8053	0.1105	0.0957	0.3575	0.2444	0	0.7028	0.1835	0.1139	0.1658	0.0083	0.1618	0.0767	0.9041	0.092	0.4112
WidthTotal	0.0113	0.0056	0.0179	0.003	0.2002	1.00E-04	0.0049	0.7028	0	0.6429	0.1412	0.3041	0.5062	0.1451	0.661	0.2548	0.0901	0.4086
NotchAB	0.1477	0.1813	0.0844	0.1218	0.012	0.2129	0.0522	0.1835	0.6429	0	0.5637	0.0193	0.9067	0.0793	0.6791	0.0426	0.0651	0.22
NotchAC	0.2405	0.8023	0.0247	0.4799	0.567	0.3975	0.3659	0.1139	0.1412	0.5637	0	0.8804	0.0011	0.5657	0.1908	0.1606	0.7105	0.6344
bOffset	0.4949	0.7941	0.5269	0.9659	0.097	0.6526	0.8925	0.1658	0.3041	0.0193	0.8804	0	0.8148	0.6974	0.8618	0.501	0.5325	0.1774
cOffset	0.8182	0.4393	0.0969	0.7649	0.8699	0.8555	0.9071	0.0083	0.5062	0.9067	0.0011	0.8148	0	0.6658	0.0215	0.2451	0.6116	0.5033
LengthTotal	0.0697	0.0712	0.1005	0.0692	0.067	0.1158	0.0493	0.1618	0.1451	0.0793	0.5657	0.6974	0.6658	0	0.3518	0.0696	3.00E-04	0.4377
InterAB	0.6756	0.574	0.3731	0.7797	0.6563	0.8062	0.9576	0.0767	0.661	0.6791	0.1908	0.8618	0.0215	0.3518	0	0.1223	0.3457	0.4787
InterAC	0.0939	0.1853	0.0039	0.0873	0.0082	0.1062	0.0156	0.9041	0.2548	0.0426	0.1606	0.501	0.2451	0.0696	0.1223	0	0.0244	0.0131
InterBC	0.0151	0.0327	0.0468	0.0215	0.0167	0.0353	0.0066	0.092	0.0901	0.0651	0.7105	0.5325	0.6116	3.00E-04	0.3457	0.0244	0	0.0678
CuspAngle	0.0826	0.3888	0.0369	0.245	0.0184	0.2247	0.1041	0.4112	0.4086	0.22	0.6344	0.1774	0.5033	0.4377	0.4787	0.0131	0.0678	0

Kueh Corr	HeightA	HeightB	HeightC	ValleyAB	ValleyAC	WidthA	WidthB	WidthC	WidthTotal	NotchAB	NotchAC	bOffset	cOffset	LengthTotal	InterAB	InterAC	InterBC	CuspAngle
HeightA	1	0.959	0.8713	0.9009	0.868	0.7831	0.8746	0.8965	0.77	0.0908	0.0647	-0.0412	0.2337	0.6701	0.8064	0.4185	0.7256	-0.3969
HeightB	0.959	1	0.8974	0.9538	0.9261	0.7678	0.9404	0.8834	0.7863	0.1022	-0.0989	-0.0109	0.0862	0.6358	0.6962	0.2574	0.5855	-0.3478
HeightC	0.8713	0.8974	1	0.9036	0.9769	0.8232	0.8956	0.8553	0.9054	0.1495	-0.2223	0.0384	-0.1677	0.6361	0.5797	0.4264	0.6721	-0.0201
ValleyAB	0.9009	0.9538	0.9036	1	0.9359	0.7094	0.9201	0.8813	0.7712	-0.0198	-0.1802	-0.0422	-0.0781	0.5162	0.5773	0.1521	0.4859	-0.2647
ValleyAC	0.868	0.9261	0.9769	0.9359	1	0.797	0.9497	0.8682	0.864	0.1675	-0.2129	0.1021	-0.142	0.533	0.5342	0.2751	0.5656	-0.0573
WidthA	0.7831	0.7678	0.8232	0.7094	0.797	1	0.7659	0.7624	0.9271	0.4621	0.0964	0.2187	-0.0614	0.6871	0.7806	0.548	0.7996	-0.2506
WidthB	0.8746	0.9404	0.8956	0.9201	0.9497	0.7659	1	0.8956	0.7726	0.2941	-0.1524	0.2428	0.0448	0.4307	0.5761	0.157	0.5119	-0.1597
WidthC	0.8965	0.8834	0.8553	0.8813	0.8682	0.7624	0.8956	1	0.7884	0.0935	0.0977	0.0191	0.2099	0.4218	0.7038	0.3556	0.6496	-0.268
WidthTotal	0.77	0.7863	0.9054	0.7712	0.864	0.9271	0.7726	0.7884	1	0.214	-0.1655	-0.016	-0.2627	0.7101	0.7108	0.5576	0.776	-0.1591
NotchAB	0.0908	0.1022	0.1495	-0.0198	0.1675	0.4621	0.2941	0.0935	0.214	1	0.1585	0.8942	0.1114	0.0457	0.184	0.0794	0.2206	0.1221
NotchAC	0.0647	-0.0989	-0.2223	-0.1802	-0.2129	0.0964	-0.1524	0.0977	-0.1655	0.1585	1	0.1494	0.7075	-0.1401	0.247	0.172	0.1409	-0.3508
bOffset	-0.0412	-0.0109	0.0384	-0.0422	0.1021	0.2187	0.2428	0.0191	-0.016	0.8942	0.1494	1	0.0943	-0.3094	-0.097	-0.2664	-0.1009	0.2302
cOffset	0.2337	0.0862	-0.1677	-0.0781	-0.142	-0.0614	0.0448	0.2099	-0.2627	0.1114	0.7075	0.0943	1	-0.1076	0.3163	0.1291	0.1692	-0.3505
LengthTotal	0.6701	0.6358	0.6361	0.5162	0.533	0.6871	0.4307	0.4218	0.7101	0.0457	-0.1401	-0.3094	-0.1076	1	0.7109	0.6862	0.7663	-0.3008
InterAB	0.8064	0.6962	0.5797	0.5773	0.5342	0.7806	0.5761	0.7038	0.7108	0.184	0.247	-0.097	0.3163	0.7109	1	0.5873	0.8416	-0.6632
InterAC	0.4185	0.2574	0.4264	0.1521	0.2751	0.548	0.157	0.3556	0.5576	0.0794	0.172	-0.2664	0.1291	0.6862	0.5873	1	0.8962	0.0529
InterBC	0.7256	0.5855	0.6721	0.4859	0.5656	0.7996	0.5119	0.6496	0.776	0.2206	0.1409	-0.1009	0.1692	0.7663	0.8416	0.8962	1	-0.1845
CuspAngle	-0.3969	-0.3478	-0.0201	-0.2647	-0.0573	-0.2506	-0.1597	-0.268	-0.1591	0.1221	-0.3508	0.2302	-0.3505	-0.3008	-0.6632	0.0529	-0.1845	1

Kueh P-Value	HeightA	HeightB	HeightC	ValleyAB	ValleyAC	WidthA	WidthB	WidthC	WidthTotal	NotchAB	NotchAC	bOffset	cOffset	LengthTotal	InterAB	InterAC	InterBC	CuspAngle
HeightA	0	0	5.00E-04	2.00E-04	5.00E-04	0.0044	4.00E-04	2.00E-04	0.0056	0.7905	0.8502	0.9043	0.4891	0.0241	0.0027	0.2002	0.0115	0.2269
HeightB	0	0	2.00E-04	0	0	0.0058	0	3.00E-04	0.0041	0.7649	0.7723	0.9747	0.801	0.0355	0.0173	0.4448	0.0584	0.2945
HeightC	5.00E-04	2.00E-04	0	1.00E-04	0	0.0019	2.00E-04	8.00E-04	1.00E-04	0.6609	0.5111	0.9106	0.6221	0.0354	0.0616	0.191	0.0235	0.9533
ValleyAB	2.00E-04	0	1.00E-04	0	0	0.0145	1.00E-04	3.00E-04	0.0054	0.9539	0.5959	0.902	0.8195	0.104	0.0629	0.6552	0.1297	0.4315
ValleyAC	5.00E-04	0	0	0	0	0.0033	0	5.00E-04	6.00E-04	0.6225	0.5297	0.7651	0.677	0.0914	0.0905	0.4129	0.0698	0.8671
WidthA	0.0044	0.0058	0.0019	0.0145	0.0033	0	0.006	0.0064	0	0.1525	0.778	0.5182	0.8577	0.0195	0.0046	0.0809	0.0031	0.4573
WidthB	4.00E-04	0	2.00E-04	1.00E-04	0	0.006	0	2.00E-04	0.0053	0.3801	0.6547	0.4719	0.8959	0.1861	0.0636	0.6448	0.1074	0.6391
WidthC	2.00E-04	3.00E-04	8.00E-04	3.00E-04	5.00E-04	0.0064	2.00E-04	0	0.0039	0.7845	0.7751	0.9555	0.5355	0.1963	0.0157	0.2832	0.0305	0.4255
WidthTotal	0.0056	0.0041	1.00E-04	0.0054	6.00E-04	0	0.0053	0.0039	0	0.5275	0.6267	0.9628	0.4352	0.0144	0.0142	0.0747	0.005	0.6403
NotchAB	0.7905	0.7649	0.6609	0.9539	0.6225	0.1525	0.3801	0.7845	0.5275	0	0.6416	2.00E-04	0.7444	0.8939	0.5881	0.8164	0.5145	0.7206
NotchAC	0.8502	0.7723	0.5111	0.5959	0.5297	0.778	0.6547	0.7751	0.6267	0.6416	0	0.6611	0.0149	0.6812	0.4641	0.6131	0.6794	0.2902
bOffset	0.9043	0.9747	0.9106	0.902	0.7651	0.5182	0.4719	0.9555	0.9628	2.00E-04	0.6611	0	0.7828	0.3546	0.7766	0.4285	0.7677	0.4959
cOffset	0.4891	0.801	0.6221	0.8195	0.677	0.8577	0.8959	0.5355	0.4352	0.7444	0.0149	0.7828	0	0.7527	0.3434	0.7053	0.619	0.2906
LengthTotal	0.0241	0.0355	0.0354	0.104	0.0914	0.0195	0.1861	0.1963	0.0144	0.8939	0.6812	0.3546	0.7527	0	0.0142	0.0197	0.0059	0.3687
InterAB	0.0027	0.0173	0.0616	0.0629	0.0905	0.0046	0.0636	0.0157	0.0142	0.5881	0.4641	0.7766	0.3434	0.0142	0	0.0575	0.0012	0.0261
InterAC	0.2002	0.4448	0.191	0.6552	0.4129	0.0809	0.6448	0.2832	0.0747	0.8164	0.6131	0.4285	0.7053	0.0197	0.0575	0	2.00E-04	0.8772
InterBC	0.0115	0.0584	0.0235	0.1297	0.0698	0.0031	0.1074	0.0305	0.005	0.5145	0.6794	0.7677	0.619	0.0059	0.0012	2.00E-04	0	0.5871
CuspAngle	0.2269	0.2945	0.9533	0.4315	0.8671	0.4573	0.6391	0.4255	0.6403	0.7206	0.2902	0.4959	0.2906	0.3687	0.0261	0.8772	0.5871	0

Table S2.2: Significance of Pearson's correlations for both taxa

Variable	T-test P-value	K Mean	M Mean
HeightA	0.26822505	1.3147	1.2364
HeightB	4.40347E-05	0.9003	0.6395
HeightC	0.551669103	0.8278	0.8012
ValleyAB	0.000612455	0.6886	0.4908
ValleyAC	0.001651276	0.6901	0.5476
WidthA	2.36354E-07	0.9396	1.4174
WidthB	0.000932124	0.6269	0.7922
WidthC	4.95045E-07	0.6887	1.0321
WidthTotal	6.3075E-11	0.9832	1.6966
NotchAB	1.15372E-08	48.9068	70.2840
NotchAC	2.0182E-08	49.6679	72.1872
bOffset	4.58488E-08	118.0897	135.5223
cOffset	0.002943062	121.9480	130.4723
LengthTotal	0.006351129	0.5925	0.7121
InterAB	0.003585971	0.3763	0.4913
InterAC	8.75687E-09	0.3294	0.6452
InterBC	3.95089E-12	0.6026	1.1345
CuspAngle	3.63821E-12	119.2237	175.5185

Table S2.3: T-tests to determine primary differences between tooth morphologies

Species	Speciemen	HeightA	HeightB	HeightC	ValleyAB	ValleyAC	WidthA	WidthB	WidthC	WidthTotal	NotchAB	NotchAC	bOffset	cOffset	LengthTotal	InterAB	InterAC	InterBC	CuspAngle
Keuhneotherium	NHMUK PV M92773	1	0.65	0.58	0.44	0.45	0.72	0.39	0.48	0.72	47.84	56.94	114.65	127.95	0.53	0.33	0.29	0.49	106.78
Keuhneotherium	NHMUK PV M92774	1	0.71	0.64	0.57	0.57	0.71	0.51	0.48	0.72	52.14	46.93	120.78	117.46	0.45	0.27	0.20	0.41	115.12
Keuhneotherium	NHMUK PV M92775	1	0.67	0.61	0.49	0.48	0.65	0.46	0.50	0.72	49.82	47.05	120.61	122.78	0.43	0.29	0.24	0.44	111.86
Keuhneotherium	NHMUK PV M92776	1	0.69	0.61	0.53	0.52	0.75	0.51	0.55	0.75	55.52	50.26	119.62	125.74	0.45	0.35	0.24	0.47	105.02
Keuhneotherium	NHMUK PV M19117	1	0.71	0.68	0.53	0.57	0.65	0.51	0.54	0.74	47.31	45.53	117.07	122.24	0.45	0.21	0.26	0.45	145.00
Keuhneotherium	NHMUK PV M19121	1	0.69	0.68	0.58	0.55	0.74	0.45	0.53	0.83	40.23	45.73	110.70	112.95	0.53	0.28	0.27	0.47	119.40
Keuhneotherium	NHMUK PV M19128	1	0.73	0.64	0.53	0.54	0.74	0.50	0.53	0.83	44.93	46.17	114.32	118.10	0.48	0.28	0.26	0.46	115.76
Keuhneotherium	NHMUK PV M19131	1	0.70	0.71	0.54	0.59	0.87	0.54	0.58	0.86	58.25	52.52	127.48	119.00	0.40	0.25	0.27	0.47	132.90
Keuhneotherium	NHMUK PV M19170	1	0.70	0.56	0.55	0.48	0.62	0.48	0.52	0.62	46.91	52.62	118.92	128.03	0.38	0.26	0.20	0.38	110.20
Keuhneotherium	NHMUK PV M19198	1	0.63	0.63	0.46	0.49	0.77	0.44	0.49	0.78	52.92	49.20	119.87	121.35	0.52	0.31	0.32	0.56	132.36
Keuhneotherium	NHMUK PV M24977	1	0.65	0.61	0.53	0.52	0.66	0.46	0.56	0.71	42.10	53.40	114.98	125.82	0.35	0.29	0.24	0.45	117.07
Morganucodon	UMZC Eo.D.32	1	0.50	0.62	0.33	0.43	1.24	0.66	0.97	1.54	66.29	78.41	135.25	134.64	0.56	0.55	0.42	0.98	179.39
Morganucodon	UMZC Eo.D.33	1	0.46	0.66	0.36	0.45	1.13	0.62	0.73	1.40	62.92	71.11	131.27	124.82	0.54	0.39	0.51	0.90	176.64
Morganucodon	UMZC Eo.D.43	1	0.54	0.66	0.37	0.49	1.15	0.68	0.97	1.41	71.97	77.06	136.14	136.28	0.75	0.47	0.66	1.13	176.99
Morganucodon	UMZC Eo.D.79	1	0.59	0.56	0.47	0.39	1.15	0.62	0.85	1.38	66.13	74.75	128.77	139.32	0.55	0.45	0.43	0.88	175.80
Morganucodon	UMZC Eo.D.134	1	0.59	0.70	0.42	0.49	1.35	0.72	0.92	1.55	67.10	80.69	130.98	130.85	0.61	0.38	0.61	0.99	173.82
Morganucodon	UMZC Eo.D.183	1	0.56	0.65	0.46	0.43	1.16	0.68	0.77	1.33	72.89	69.38	131.82	130.60	0.54	0.32	0.53	0.85	177.28
Morganucodon	UMZC Eo.D.293a	1	0.48	0.68	0.35	0.43	1.08	0.58	0.78	1.43	66.33	62.18	133.78	121.39	0.59	0.37	0.49	0.86	178.44
Morganucodon	UMZC Eo.D.293i	1	0.52	0.63	0.42	0.48	1.06	0.62	0.88	1.20	78.74	74.36	146.57	132.90	0.50	0.31	0.53	0.84	172.41
Morganucodon	UMZC Eo.D.293k	1	0.43	0.61	0.33	0.43	0.99	0.58	0.90	1.21	68.10	78.82	140.74	134.87	0.56	0.44	0.47	0.90	172.99
Morganucodon	UMZC Eo.D.293L	1	0.53	0.66	0.43	0.45	1.20	0.66	0.84	1.36	78.74	71.07	139.12	133.00	0.63	0.43	0.50	0.93	176.07
Morganucodon	UMZC Eo.D.293m	1	0.48	0.71	0.40	0.43	1.15	0.65	0.65	1.37	73.93	56.24	136.31	116.55	0.55	0.30	0.61	0.90	170.88

Table S2.4: Height *A* scaled measures for all variables.

Constants	Measures
HeightA	1
HeightB	
HeightC	0.6401
ValleyAB	0.4582
ValleyAC	0.4844
WidthA	0.9340
WidthB	0.6422
WidthC	0.6824
WidthTotal	1.0663
NotchAB	
NotchAC	
LengthTotal	0.5155
InterAB	0.3433
InterAC	0.3882
InterBC	0.6922
CuspAngle	
bOffset	126.8
cOffset	126.2

Variables	Species	Measures
Notch AB/AC (°)	Keuhneotherium	49
	Morganucodon	71
Height B (cm)	Keuhneotherium	0.6846
	Morganucodon	0.5172
Cusp Angle (°)	Keuhneotherium	119
	Morganucodon	176

Table S2.5: Input parameters to construct 3D CAD models

Sample	Fracture Force (mN)	Fracture Energy (N/m) x 10^3
PDMS Gel	50.4 ± 5.8	2.88 ± 0.33
Triblock Gel	5.4 ± 0.3	0.31 ± 0.02
PET Film	227.9 ± 6.3	13.02 ± 0.36
PDMS/PET Composite	264.3 ± 5.0	15.11 ± 0.29
Triblock/PET Composite	189.1 ± 22.2	10.81 ± 1.27

Table S2.6: Material properties data for the proxy insect food items

Type	Species	Force (N)	Disp (mm)	Energy (J)
MF	K	20.08	10.52	89.81
MF	K	16.73	10.51	72.66
MF	K	16.34	10.61	78.64
MF	K	17.21	10.61	50.24
MF	K	10.21	10.61	37.40
MF	K	11.41	10.61	38.37
MF	K	10.92	10.61	39.28
MF	K	15.22	10.39	61.62
MF	K	12.67	10.61	47.60
MF	K	13.73	10.61	52.90
MF	M	10.84	10.61	39.94
MF	M	11.57	10.41	41.44
MF	M	10.87	10.61	38.33
MF	M	11.89	10.61	45.11
MF	M	10.02	10.61	36.87
MF	M	9.81	10.61	38.51
MF	M	10.21	10.61	38.03
MF	M	10.54	10.61	35.29
MF	M	9.94	10.44	35.39
MF	M	10.18	10.61	37.08
MF	M	9.53	10.61	36.31
MF	M	12.97	10.61	43.74

Type	Species	Force (N)	Disp (mm)	Energy (J)
F2F	K	11.93	4.33	19.41
F2F	K	8.11	3.68	13.04
F2F	K	8.71	3.68	12.75
F2F	K	5.52	3.85	9.80
F2F	K	5.49	3.94	9.51
F2F	K	4.98	3.84	8.39
F2F	K	4.87	4.00	9.13
F2F	K	7.29	3.73	11.06
F2F	K	5.71	3.71	8.56
F2F	K	5.36	3.83	9.13
F2F	M	2.68	2.58	4.19
F2F	M	2.18	3.11	4.81
F2F	M	2.41	2.51	4.00
F2F	M	2.33	2.99	4.92
F2F	M	2.25	2.36	3.65
F2F	M	2.02	2.12	3.02
F2F	M	2.17	2.45	3.75
F2F	M	2.22	1.96	2.68
F2F	M	2.69	2.42	3.90
F2F	M	2.49	2.61	3.99
F2F	M	2.26	2.40	3.94
F2F	M	3.36	5.28	10.85

Maximum Force (MF)	Force	Displacement	Energy
T-test (Pvalue)	0.00097	0.75231	0.00304
Kmean	14.45244	10.56544	56.85254
Mmean	10.69803	10.57524	38.83707

Force to Fracture (F2F)	Force	Displacement	Energy
T-test (Pvalue)	0.000002	0.00066	0.00002
Kmean	6.79919	3.85806	11.07739
Mmean	2.42230	2.73129	4.47583

Table S2.7: Hard food (PDMS) maximum force and force to fracture statistical comparisons

Type	Species	Force (N)	Disp (mm)	Energy (J)
MF	K	5.47	5.84	7.90
MF	K	7.78	7.53	15.44
MF	K	7.81	7.96	14.72
MF	K	7.67	6.85	17.84
MF	K	5.46	6.91	8.82
MF	K	8.02	7.57	16.05
MF	K	5.92	7.65	15.40
MF	K	7.96	8.00	21.54
MF	K	7.86	6.75	16.74
MF	K	7.22	7.97	22.38
MF	K	9.04	5.58	12.34
MF	K	8.85	6.47	16.12
MF	M	9.46	8.50	24.65
MF	M	9.89	8.51	24.83
MF	M	9.54	8.46	24.64
MF	M	11.89	8.51	23.94
MF	M	12.69	8.51	27.93
MF	M	7.38	8.51	22.60
MF	M	8.17	8.47	14.49
MF	M	10.18	8.51	26.29
MF	M	9.83	7.82	19.58
MF	M	8.56	7.61	15.83
MF	M	7.50	8.51	20.86

Type	Species	Force (N)	Disp (mm)	Energy (J)
F2F	K	5.47	5.84	7.90
F2F	K	6.59	6.71	10.35
F2F	K	7.50	8.06	15.47
F2F	K	7.27	6.03	12.59
F2F	K	5.46	6.91	8.78
F2F	K	7.23	6.72	10.70
F2F	K	5.15	6.47	9.59
F2F	K	6.38	6.83	12.02
F2F	K	7.20	6.06	12.17
F2F	K	6.04	5.41	9.41
F2F	K	9.04	5.58	12.34
F2F	K	8.85	6.47	16.12
F2F	M	6.65	6.99	13.45
F2F	M	5.43	6.67	11.26
F2F	M	8.23	7.66	17.91
F2F	M	6.64	7.11	12.16
F2F	M	8.64	7.39	16.87
F2F	M	5.13	6.65	12.35
F2F	M	5.32	7.28	8.33
F2F	M	3.59	5.25	7.54
F2F	M	5.80	6.51	10.41
F2F	M	8.56	7.61	15.83
F2F	M	6.52	7.28	13.26

Maximum Force (MF)	Force	Displacement	Energy
T-test (Pvalue)	0.0019	0.0001	0.0009
Kmean	7.4218	7.0890	15.4398
Mmean	9.5532	8.3542	22.3313

Force to Fracture (F2F)	Force	Displacement	Energy
T-test (Pvalue)	0.4691	0.0876	0.3294
Kmean	6.8490	6.4228	11.4531
Mmean	6.4111	6.9455	12.6690

Table S2.8: Soft food (triblock) maximum force and force to fracture statistical comparisons

Hard (PDMS)	
Trial	Sum
K1	7.352
K2	6.325
K3	6.045
K4	8.5
K5	8.327
K6	7.803
K7	5.106
K8	4.428
K9	4.754
K10	3.478
M1	5.305
M2	4.839
M3	4.585
M4	3.827
M5	5.258
M6	3.651
M7	4.545
M8	4.912
M9	5.454
M10	5.58
M11	4.435
M12	4.171
T-test (p)	0.01182
K mean	6.21
M mean	4.71

Soft (Triblock)	
Trial	Sum
K1	3.820
K2	4.673
K3	3.371
K4	5.076
K5	4.498
M1	3.086
M2	1.939
M3	1.395
M4	1.884
M5	3.151
M6	1.933
M7	1.165
M8	2.581
M9	2.549
M10	1.373
M11	2.205
T-test (p)	0.00003
K mean	4.29
M mean	2.11

Table S2.9: Soft and hard food damage statistics for both taxa

APPENDIX B

SUPPLEMENTARY INFORMATION FOR CHAPTER 3

Genus	Speces	Institution	Catalogue	Sex	Clade	TempVar	PrecipVar	PC1	PC2	PC3	PC4
Acionyx	jubatus	MCZ	13667	U	Fel	High	High	0.00529	0.07292	-0.01757	-0.03611
Acionyx	jubatus	MCZ	20047	M	Fel	High	High	0.01470	0.06913	-0.02828	-0.01978
Acionyx	jubatus	MCZ	26467	U	Fel	High	High	0.02749	0.05943	-0.02620	-0.02594
Acionyx	jubatus	MCZ	27497	U	Fel	High	High	0.02784	0.09956	-0.01764	-0.01353
Acionyx	jubatus	MCZ	27498	U	Fel	High	High	0.01532	0.06910	-0.01900	-0.00673
Aonyx	capensis	AMNH	55230	M	Mus	Low	High	-0.04279	-0.01821	0.02037	0.04164
Aonyx	capensis	MCZ	22686	U	Mus	Low	High	-0.06350	0.02990	-0.01290	-0.00766
Aonyx	cinerea	AMNH	101467	F	Mus	Low	High	0.07744	0.04809	0.04142	0.02233
Aonyx	congica	MCZ	31621	U	Mus	Low	High	0.01027	0.05360	-0.00329	0.03650
Aonyx	congica	MCZ	31622	F	Mus	Low	High	0.00925	-0.00773	-0.00009	0.00311
Arctonyx	collaris	AMNH	57373	U	Mus	Low	High	-0.04648	0.03150	-0.02132	0.00541
Arctonyx	collaris	MCZ	24832	F	Mus	Low	High	0.04292	-0.06471	0.01226	-0.00805
Arctonyx	collaris	MCZ	35894	M	Mus	Low	High	-0.00138	0.01894	-0.01938	-0.01189
Arctonyx	collaris	MCZ	35932	M	Mus	Low	High	-0.01752	0.03771	-0.00171	-0.03992
Atelorynus	microtus	AMNH	95285	F	Can	Low	Low	0.02942	0.00211	-0.00371	-0.02778
Canis	adjustus	AMNH	160989	F	Can	Low	High	-0.07028	0.00908	-0.01794	-0.03632
Canis	adustus	MCZ	23090	F	Can	Low	High	0.02611	0.00223	-0.01591	-0.02771
Canis	adustus	MCZ	37939	F	Can	Low	High	-0.01244	0.00120	-0.00348	0.00753
Canis	adustus	MCZ	45890	F	Can	Low	High	-0.02155	-0.01116	0.01018	0.00671
Canis	aureus	MCZ	12608	F	Can	High	High	0.01273	-0.04091	0.00241	-0.00202

Canis	aureus	MCZ	12609	M	Can	High	High	-0.02027	-0.01570	0.02431	0.02464
Canis	aureus	MCZ	12610	F	Can	High	High	-0.06855	0.02964	0.00270	0.00719
Canis	aureus	MCZ	8613	F	Can	High	High	0.00388	0.02485	-0.01939	0.03278
Canis	latrans	MCZ	42784	F	Can	High	Low	-0.03889	0.01458	0.03335	-0.01184
Canis	latrans	MCZ	43271	U	Can	High	Low	-0.00757	-0.02853	0.01186	0.00618
Canis	latrans	MCZ	51044	F	Can	High	Low	0.00041	0.03519	-0.02453	-0.03446
Canis	latrans	MCZ	51045	M	Can	High	Low	-0.01435	-0.01716	-0.02022	0.00391
Canis	latrans	MCZ	68	M	Can	High	Low	-0.02034	-0.01882	-0.01196	0.03812
Canis	lupus	MCZ	46554	M	Can	High	Low	-0.01773	-0.04727	-0.07403	0.03072
Canis	lupus	MCZ	50511	F	Can	High	Low	0.00345	-0.02886	-0.01223	0.00926
Canis	lupus	MCZ	51411	M	Can	High	Low	0.01985	-0.00738	-0.00553	-0.03987
Canis	lupus	MCZ	51602	U	Can	High	Low	-0.05847	0.01010	0.04519	-0.01108
Canis	lupus	MCZ	67250	F	Can	High	Low	0.02282	0.04556	-0.02269	0.01596
Canis	mesomelas	MCZ	31957	U	Can	Low	High	-0.05859	0.03479	-0.07284	0.03364
Canis	mesomelas	MCZ	31960	M	Can	Low	High	0.06732	0.05784	0.00473	0.01870
Canis	mesomelas	MCZ	35425	F	Can	Low	High	-0.03477	0.04051	-0.03709	-0.00347
Canis	mesomelas	MCZ	35430	M	Can	Low	High	0.00047	-0.00852	-0.01065	-0.01300
Canis	rufus	MCZ	21531	F	Can	High	Low	-0.01293	-0.00053	-0.03019	0.01381
Canis	rufus	MCZ	25372	M	Can	High	Low	0.01865	0.00393	-0.01838	0.01267
Canis	rufus	MCZ	25375	F	Can	High	Low	0.02956	0.00915	0.01913	0.00527
Canis	rufus	MCZ	9114	M	Can	High	Low	0.00765	-0.03615	-0.02411	-0.00012
Canis	simensis	AMNH	81001	M	Can	Low	High	0.01004	-0.00455	0.01560	0.00089
Caracal	caracal	MCZ	20048	U	Fel	High	High	0.04351	0.05226	-0.00694	-0.00786
Caracal	caracal	MCZ	20049	F	Fel	High	High	0.01567	0.05088	-0.03079	-0.01248
Caracal	caracal	MCZ	58305	U	Fel	High	High	-0.07228	-0.02453	-0.01206	-0.03734
Catopuma	temminckii	AMNH	84393	M	Fel	Low	Low	0.02593	0.03466	0.02198	0.02976
Cerdocyon	thous	MCZ	16038	F	Can	Low	Low	0.00342	-0.07142	-0.01393	-0.03059
Cerdocyon	thous	MCZ	16039	F	Can	Low	Low	0.01591	-0.00617	-0.01417	-0.02521
Cerdocyon	thous	MCZ	27904	U	Can	Low	Low	0.07977	0.04213	-0.00983	0.02874
Cerdocyon	thous	MCZ	30958	M	Can	Low	Low	-0.05638	0.02760	-0.00276	-0.01954
Chrysocyon	brachyurus	MCZ	28615	M	Can	Low	High	-0.02624	-0.03053	0.01800	-0.00525
Chrysocyon	brachyurus	MCZ	51456	M	Can	Low	High	-0.06469	0.02566	0.01551	0.01822
Chrysocyon	brachyurus	MCZ	51457	M	Can	Low	High	-0.04186	0.02114	0.05331	0.00985
Cuon	alpinus	AMNH	101773	F	Can	Low	High	-0.02408	0.00172	-0.03639	0.01628
Cuon	alpinus	MCZ	19566	U	Can	Low	High	-0.01566	0.03712	-0.04057	-0.00325
Cuon	alpinus	MCZ	30382	U	Can	Low	High	-0.03868	0.06081	-0.05994	-0.00256
Cuon	alpinus	MCZ	35919	M	Can	Low	High	0.07800	0.08270	0.01113	0.00291
Cuon	alpinus	MCZ	35929	U	Can	Low	High	0.05854	0.07212	0.02920	0.01661
Dusicyon	australis	AMNH	235204	U	Can	Low	Low	0.08662	0.10601	0.01365	0.01096
Eira	barbara	MCZ	1827	U	Mus	Low	High	0.01354	0.01593	0.01467	-0.03287

Eira	barbara	MCZ	30968	F	Mus	Low	High	0.00138	-0.02178	-0.00294	0.01558
Eira	barbara	MCZ	32044	M	Mus	Low	High	0.02163	0.00854	0.01342	-0.01211
Eira	barbara	MCZ	485	U	Mus	Low	High	-0.00408	-0.00688	0.00935	-0.01373
Enhydra	lutris	MCZ	63308	F	Mus	Low	Low	-0.00102	0.03162	-0.01269	-0.01474
Enhydra	lutris	MCZ	63312	M	Mus	Low	Low	0.00464	-0.00478	-0.02532	0.01190
Enhydra	lutris	MCZ	63314	F	Mus	Low	Low	-0.01606	-0.02728	-0.01103	0.04421
Felis	bengalensis	MCZ	24843	F	Fel	High	High	-0.00283	-0.04088	0.00787	0.01421
Felis	bengalensis	MCZ	26923	F	Fel	High	High	0.00658	-0.04039	0.03279	-0.00033
Felis	bengalensis	MCZ	36028	U	Fel	High	High	-0.00191	-0.01143	0.02172	0.00964
Felis	bengalensis	MCZ	36034	U	Fel	High	High	0.00026	-0.03269	0.01432	0.01466
Felis	chaus	UMMZ	122370	U	Fel	High	High	0.00281	-0.03920	0.00658	0.01240
Felis	colocolo	MCZ	19224	U	Fel	High	High	-0.04668	-0.03722	0.01459	-0.03052
Felis	colocolo	MCZ	19501	U	Fel	High	High	-0.04723	-0.02630	0.01661	-0.02873
Felis	libyca	MCZ	22690	U	Fel	High	High	-0.03761	-0.04308	0.01500	0.01358
Felis	libyca	MCZ	32263	U	Fel	High	High	-0.03537	-0.03446	0.01178	-0.00172
Felis	libyca	MCZ	35421	U	Fel	High	High	-0.04122	-0.04199	0.01366	0.00735
Felis	libyca	MCZ	44285	U	Fel	High	High	0.03790	-0.03658	-0.04014	0.02940
Felis	manul	UMMZ	177415	M	Mus	Low	Low	0.00076	-0.01084	-0.02542	-0.00165
Felis	margarita	UMMZ	118429	U	Mus	Low	High	0.00153	-0.01119	-0.00613	0.00351
Felis	nigripes	AMNH	214381	U	Mus	Low	High	-0.00484	-0.01602	0.00783	-0.01985
Felis	pardus	MCZ	26137	U	Mus	Low	High	-0.03373	-0.03980	-0.00246	0.01107
Felis	pardus	MCZ	37593	U	Mus	Low	High	0.01367	-0.03647	-0.00063	0.01247
Felis	planiceps	MCZ	6282	M	Mus	High	High	-0.04061	-0.03505	-0.01099	0.00725
Felis	planiceps	MCZ	6303	F	Mus	High	High	-0.00240	-0.04767	0.02332	0.03914
Felis	serval	MCZ	23093	F	Mus	High	High	-0.00793	0.02174	0.00896	-0.01435
Felis	serval	MCZ	31620	M	Mus	High	High	-0.01362	0.03211	0.03412	-0.01820
Felis	serval	MCZ	34106	U	Mus	Low	High	0.02516	0.02616	-0.00307	-0.00650
Felis	silvestris	MCZ	34851	U	Mus	Low	High	0.00043	0.01676	-0.02210	0.01954
Felis	silvestris	MCZ	37521	M	Mus	Low	High	-0.00062	0.00247	-0.04015	0.02496
Felis	silvestris	MCZ	37522	U	Mus	Low	High	-0.00381	-0.00572	-0.05755	0.00313
Felis	silvestris	MCZ	37628	M	Mus	High	High	-0.00524	0.02646	-0.02322	0.00330
Felis	viverrinus	MCZ	5292	U	Mus	Low	High	-0.01511	-0.01113	0.07328	-0.00238
Felis	viverrinus	MCZ	57926	F	Mus	Low	High	-0.01026	0.01937	0.07032	0.01700
Felis	viverrinus	MCZ	6329	F	Mus	Low	High	-0.02225	0.00894	0.09119	0.02197
Felis	yagouaroundi	MCZ	30730	M	Mus	Low	High	-0.06056	-0.01644	-0.01077	0.01088
Felis	yagouaroundi	MCZ	42787	M	Mus	Low	High	-0.06232	-0.00108	0.02369	0.00538
Felis	yagouaroundi	MCZ	B8428	U	Mus	Low	High	-0.04971	-0.01332	-0.00727	0.00836
Felis	yagouaroundi	MCZ	B9095	U	Fel	Low	Low	-0.07198	-0.00569	-0.00081	0.00816
Galictis	cuja	AMNH	235992	U	Fel	Low	Low	-0.04321	0.03096	-0.07168	-0.05321
Galictis	vittata	MCZ	20233	M	Fel	Low	Low	-0.03776	-0.00574	-0.05462	-0.05562

Galictis	vittata	MCZ	27487	F	Fel	Low	Low	-0.01958	0.00928	-0.05490	-0.04535
Galictis	vittata	MCZ	27488	M	Fel	Low	Low	0.00081	0.00144	-0.04185	-0.03734
Galictis	vittata	MCZ	6420	U	Fel	Low	Low	0.01853	-0.03081	-0.11655	0.06921
Gulo	gulo	MCZ	36260	U	Fel	Low	Low	0.03047	-0.02185	-0.11356	0.07783
Gulo	gulo	MCZ	47398	U	Fel	Low	Low	0.03984	-0.03385	-0.08412	0.07038
Gulo	gulo	MCZ	B8882	U	Fel	Low	Low	-0.04287	0.02835	-0.01661	-0.00268
Gulo	gulo	MCZ	B8962	M	Fel	Low	Low	-0.02967	-0.04093	-0.02251	-0.00463
Hydrictis	maculicollis	AMNH	51828	U	Fel	Low	Low	-0.04027	0.00107	-0.00510	-0.00944
Ictonyx	libuca	AMNH	70093	U	Fel	Low	Low	-0.03889	0.00466	-0.03328	0.01647
Ictonyx	striatus	AMNH	83753	U	Fel	Low	Low	-0.02064	0.05653	-0.00316	0.02457
Ictonyx	striatus	MCZ	14423	M	Fel	Low	Low	-0.03074	-0.01574	-0.00607	0.02310
Ictonyx	striatus	MCZ	14424	U	Fel	Low	Low	-0.03658	-0.03013	0.02529	-0.00008
Ictonyx	striatus	MCZ	35401	U	Fel	Low	Low	-0.02989	-0.01023	0.02206	-0.01210
Ictonyx	striatus	MCZ	4045	U	Fel	Low	High	-0.04955	0.01257	0.03450	0.00079
Ictonyx	striatus	MCZ	4047	U	Fel	Low	High	-0.03390	0.01545	0.01833	0.00676
Leopardus	colocolo	AMNH	243110	U	Fel	Low	High	-0.02824	-0.01088	0.03203	0.01074
Leopardus	geoffroyi	UMMZ	146504	M	Mus	High	Low	-0.00557	0.01972	0.00164	0.03892
Leopardus	guigna	MSUM	2116	F	Mus	High	Low	-0.02620	0.04861	0.04439	-0.00077
Leopardus	pardalis	MCZ	19759	M	Mus	High	Low	0.04972	-0.04428	0.00675	0.00006
Leopardus	pardalis	MCZ	6274	F	Mus	High	Low	0.04903	-0.00322	0.00441	-0.00177
Leopardus	pardalis	MCZ	B5647	F	Mus	Low	Low	-0.02996	-0.04675	-0.05538	-0.00361
Leopardus	pardalis	MCZ	B5648	M	Mus	Low	Low	-0.03534	-0.05438	-0.03371	-0.01569
Leopardus	tigrina	MCZ	20979	M	Mus	Low	Low	-0.02536	0.04402	0.00668	0.00286
Leopardus	tigrina	MCZ	28678	F	Mus	Low	Low	-0.01293	0.02926	-0.01361	0.03438
Leopardus	tigrina	MCZ	46412	U	Mus	Low	Low	-0.01656	0.01972	0.00885	0.00026
Leopardus	wiedii	MCZ	24058	F	Mus	Low	Low	-0.03080	-0.00954	-0.00893	-0.00176
Leopardus	wiedii	MCZ	51384	M	Mus	High	Low	-0.04733	-0.00385	-0.00254	-0.00726
Leopardus	wiedii	MCZ	5358	F	Mus	High	Low	-0.04661	0.00723	0.00338	-0.02149
Leopardus	wiedii	MCZ	6413	F	Mus	High	Low	-0.05328	-0.00562	0.05917	-0.00199
Lontra	longicaudis	AMNH	207729	M	Mus	High	Low	-0.00794	-0.02763	-0.01942	0.00616
Lontra	provocax	AMNH	33295	U	Mus	High	Low	0.00961	-0.01456	-0.05889	-0.00624
Lutra	canadensis	MCZ	B4995	U	Mus	Low	High	-0.00519	-0.02856	-0.03704	-0.01343
Lutra	canadensis	MCZ	B4998	M	Can	Low	Low	0.00111	-0.01156	0.00866	0.01959
Lutra	canadensis	MCZ	B6092	F	Can	Low	Low	-0.03468	-0.00606	-0.00887	0.00293
Lutra	canadensis	MCZ	B6093	M	Can	Low	Low	-0.01527	-0.02080	-0.01606	0.00866
Lutra	longicaudis	MCZ	1828	M	Can	Low	Low	-0.03130	0.02780	-0.01826	0.00361
Lutra	longicaudis	MCZ	28092	M	Can	High	Low	-0.02559	0.01027	0.00407	-0.02557
Lutra	longicaudis	MCZ	28637	F	Can	Low	High	-0.01366	-0.01236	0.01455	-0.01857
Lutra	longicaudis	MCZ	37845	U	Can	Low	High	-0.02280	0.00243	0.03355	-0.02680
Lutra	lutra	AMNH	206592	M	Can	Low	High	0.01416	0.00345	0.00894	0.00035

Lutra	lutra	MCZ	22243	M	Can	Low	High	-0.01024	-0.01447	-0.04465	0.02898
Lutra	lutra	MCZ	22244	U	Can	Low	High	-0.01062	-0.04557	-0.02724	0.03269
Lutra	lutra	MCZ	34577	U	Can	Low	High	-0.01098	-0.01787	0.01455	0.02425
Lutra	lutra	MCZ	57928	U	Can	Low	High	0.00963	-0.04962	-0.00267	0.01266
Lutra	maculicollis	MCZ	19973	M	Fel	High	Low	0.01647	0.01659	0.04862	0.02073
Lutra	maculicollis	MCZ	26837	F	Fel	High	Low	0.01552	0.01296	0.04858	0.01728
Lutra	maculicollis	MCZ	39425	M	Fel	High	Low	0.00699	-0.00769	0.04073	0.03107
Lutrogale	perspicillata	AMNH	99610	F	Fel	High	Low	0.02156	-0.00495	0.02919	0.01956
Lycalopex	sechurae	AMNH	46532	U	Fel	High	Low	0.01567	0.00257	0.02922	0.00745
Lycalopex	vetulus	AMNH	133927	M	Fel	High	Low	-0.04543	0.00090	0.00266	0.00500
Lycaloplex	culpaeus	MCZ	38359	M	Fel	High	Low	-0.02926	0.02978	-0.02153	0.03587
Lycaloplex	culpaeus	MCZ	42719	F	Fel	High	Low	-0.00280	-0.00903	0.00762	-0.02324
Lycaloplex	griseus	MCZ	19590	M	Fel	High	Low	0.02456	-0.03177	-0.03308	0.02462
Lycaloplex	griseus	MCZ	26924	M	Fel	High	Low	0.01914	-0.00073	-0.01837	0.00770
Lycaon	pictus	AMNH	83129	M	Mus	High	Low	-0.02516	-0.05523	0.00166	-0.01079
Lycaon	pictus	MCZ	13233	M	Mus	High	Low	-0.03670	0.00627	-0.01506	-0.02089
Lycaon	pictus	MCZ	13234	F	Mus	High	Low	-0.07099	-0.01370	0.01076	-0.00367
Lycaon	pictus	MCZ	22362	F	Mus	High	Low	-0.06737	0.00009	-0.02610	-0.00920
Lycaon	pictus	MCZ	37596	F	Mus	High	High	-0.03892	-0.04211	0.02464	-0.00279
Lynx	canadensis	MCZ	34520	U	Mus	High	High	-0.05417	-0.00649	0.00073	-0.02442
Lynx	canadensis	MCZ	41397	F	Mus	High	High	-0.03777	0.00327	0.00072	0.00416
Lynx	canadensis	MCZ	50522	U	Mus	High	High	-0.05195	-0.03606	0.02048	-0.00221
Lynx	canadensis	MCZ	50527	F	Mus	High	High	-0.06112	0.01131	0.02343	0.02054
Lynx	lynx	MSUM	34837	M	Mus	High	High	-0.05861	0.02821	-0.00989	0.00634
Lynx	pardinus	AMNH	169492	F	Mus	High	Low	-0.04937	-0.00280	0.00788	0.01926
Lynx	rufus	MCZ	42047	U	Mus	High	Low	-0.03402	-0.01625	0.00927	0.01722
Lynx	rufus	MCZ	42048	F	Mus	High	Low	-0.04347	-0.00596	0.01598	0.03668
Lynx	rufus	MCZ	42050	F	Mus	High	Low	-0.03741	0.02149	-0.00744	0.00890
Lynx	rufus	MCZ	42054	M	Mus	High	Low	-0.03118	0.00524	0.03659	0.03063
Martes	americana	MCZ	50636	M	Mus	High	Low	-0.04383	-0.01963	0.00067	0.02806
Martes	americana	MCZ	50637	U	Mus	High	Low	-0.04062	0.00893	0.03662	-0.01100
Martes	americana	MCZ	50638	U	Mus	High	Low	-0.06662	0.02021	0.02824	0.00401
Martes	americana	MCZ	50647	M	Mus	High	Low	-0.05861	0.02764	0.00986	0.01314
Martes	flavigula	AMNH	117619	U	Mus	High	Low	-0.03346	0.01059	0.04655	0.02394
Martes	flavigula	MCZ	23206	M	Mus	Low	High	-0.07113	0.01853	0.06044	-0.00881
Martes	flavigula	MCZ	24975	F	Mus	Low	Low	-0.04005	0.02385	0.04238	0.01136
Martes	flavigula	MCZ	24976	M	Mus	Low	Low	-0.07201	0.01239	0.02626	-0.00662
Martes	flavigula	MCZ	28601	F	Mus	Low	Low	0.00561	0.00180	-0.01403	0.02228
Martes	foina	AMNH	70182	M	Mus	Low	Low	0.03410	-0.02111	0.01056	0.02429
Martes	martes	AMNH	36633	M	Mus	High	High	0.05436	-0.01428	-0.04583	0.01568

Martes	melampus	AMNH	184575	F	Mus	Low	Low	0.04791	-0.02548	-0.02120	0.01167
Martes	pennanti	MCZ	50623	M	Mus	Low	High	-0.05632	-0.03259	-0.01201	-0.01101
Martes	pennanti	MCZ	50624	F	Mus	Low	Low	-0.06535	-0.00983	-0.02379	-0.00560
Martes	pennanti	MCZ	50630	M	Mus	Low	Low	-0.07614	-0.01114	-0.02862	0.00174
Martes	pennanti	MCZ	50632	M	Mus	Low	Low	-0.06720	-0.04217	-0.01163	-0.00626
Martes	zibellina	AMNH	97800	M	Mus	High	High	0.00902	-0.01439	0.02022	0.00798
Meles	meles	MCZ	14653	U	Mus	High	High	-0.00192	-0.01318	0.03088	-0.00644
Meles	meles	MCZ	19954	F	Mus	High	High	-0.01520	-0.00021	0.02710	-0.01442
Meles	meles	MCZ	22246	F	Mus	High	High	0.00455	-0.04422	0.00544	0.01337
Mellivora	capensis	MSUM	8093	M	Mus	High	High	0.02687	-0.00698	0.00349	0.02059
Melogale	everetti	MCZ	36113	M	Mus	High	High	-0.01307	0.01174	0.04645	-0.00773
Melogale	everetti	MCZ	36114	F	Mus	High	High	0.00789	0.03222	-0.00172	0.01104
Melogale	everetti	MCZ	36117	M	Mus	High	High	0.00919	0.00182	-0.00867	0.01089
Melogale	everetti	MCZ	36118	F	Mus	High	High	0.00231	-0.00340	0.02540	0.00332
Melogale	moschata	UMMZ	97616	M	Mus	High	High	-0.00416	-0.02357	0.03060	-0.01313
Melogale	orientalis	AMNH	102075	F	Mus	High	High	0.03746	-0.07118	0.03874	-0.01223
Melogale	personata	AMNH	87401	M	Mus	High	High	0.01349	-0.06392	0.03173	-0.01933
Mustela	africana	AMNH	61813	M	Mus	High	High	-0.01872	-0.02721	0.01802	-0.02596
Mustela	africana	MCZ	30802	M	Mus	Low	Low	-0.00932	0.00040	0.01164	-0.02337
Mustela	africana	MCZ	36324	F	Mus	High	Low	-0.01599	-0.00662	-0.02846	0.00277
Mustela	altaica	AMNH	117604	M	Mus	High	Low	-0.01328	-0.02231	-0.01929	-0.02130
Mustela	altaica	MCZ	23261	M	Mus	High	Low	0.01801	-0.00461	-0.01687	-0.03925
Mustela	altaica	MCZ	23262	U	Mus	High	Low	0.00563	-0.04025	0.02285	0.00066
Mustela	altaica	MCZ	23263	F	Mus	High	Low	0.01767	-0.03884	0.01201	-0.00608
Mustela	altaica	MCZ	38101	U	Mus	Low	High	-0.01071	-0.01905	0.01639	-0.01456
Mustela	erminea	MCZ	B7260	F	Mus	Low	High	-0.02795	-0.02144	0.00880	0.00757
Mustela	erminea	MCZ	B7261	M	Mus	Low	High	0.02758	0.02925	0.05627	0.01535
Mustela	erminea	MCZ	B7263	M	Mus	Low	Low	0.01910	0.03489	0.04726	0.01848
Mustela	erminea	MCZ	B9108	U	Mus	High	High	0.00829	0.01542	0.05841	0.02592
Mustela	eversmanii	AMNH	85382	M	Mus	High	High	-0.07621	0.07684	-0.03720	-0.01222
Mustela	eversmanni	MCZ	19893	M	Mus	High	High	0.12898	0.03778	0.02728	-0.00262
Mustela	eversmanni	MCZ	24984	U	Mus	High	High	0.10125	0.06070	-0.00721	-0.02018
Mustela	eversmanni	MCZ	40940	M	Mus	High	High	0.10727	0.03387	0.02218	-0.01213
Mustela	felipei	AMNH	63839	M	Mus	High	High	0.13395	0.05158	-0.02382	-0.03581
Mustela	frenata	MCZ	39585	M	Mus	High	High	0.08170	0.07477	-0.03571	-0.00590
Mustela	frenata	MCZ	43076	M	Mus	High	High	0.03295	0.00386	-0.03747	-0.01644
Mustela	frenata	MCZ	43807	M	Mus	Low	Low	0.02400	-0.01203	-0.05361	-0.01594
Mustela	frenata	MCZ	B6949	F	Mus	Low	Low	0.01349	-0.03772	-0.01392	-0.01861
Mustela	frenata	MCZ	B7759	M	Mus	High	Low	0.02144	-0.03874	0.00549	-0.01278
Mustela	kathiah	MCZ	38195	M	Mus	High	Low	0.03160	-0.03689	-0.01972	-0.02340

Mustela	kathiah	MCZ	44711	M	Mus	High	Low	0.04012	-0.04484	-0.01077	-0.01616
Mustela	kathiah	MCZ	24982	F	Mus	High	Low	0.07605	-0.02988	0.00762	0.00405
Mustela	lutreolina	AMNH	106670	U	Mus	High	Low	0.03541	-0.02405	-0.01390	0.00567
Mustela	nigripes	MCZ	43727	F	Mus	High	Low	0.03780	-0.03396	0.01471	0.00100
Mustela	nigripes	MCZ	57298	M	Mus	High	Low	0.05869	-0.04325	-0.00094	-0.01245
Mustela	nigripes	MCZ	B4184	U	Fel	Low	High	-0.03970	-0.00600	-0.04250	-0.01996
Mustela	nigripes	MCZ	42723	F	Mus	High	Low	-0.02625	-0.02268	-0.00727	-0.01576
Mustela	nivalis	MCZ	27437	F	Mus	High	Low	-0.01909	-0.00490	-0.02682	-0.02020
Mustela	nivalis	MCZ	34147	F	Mus	High	Low	0.02438	-0.02139	0.00513	-0.02060
Mustela	nivalis	MCZ	34148	M	Mus	High	Low	0.04450	-0.04294	0.01538	-0.01114
Mustela	nivalis	MCZ	3707	M	Can	High	High	0.03054	-0.03714	0.01926	-0.00888
Mustela	nudipes	AMNH	106065	M	Can	High	High	0.01726	-0.05720	-0.00131	-0.01685
Mustela	nudipes	MCZ	36747	F	Can	High	High	0.04497	-0.03351	-0.00521	-0.00631
Mustela	putorius	MCZ	B3701	F	Fel	High	High	0.00783	-0.05106	0.00506	0.00040
Mustela	putorius	MCZ	B3702	F	Can	Low	High	0.02227	-0.00841	-0.00221	0.00139
Mustela	sibirica	AMNH	60095	M	Can	Low	High	-0.00955	-0.02393	0.00330	-0.00001
Mustela	sibirica	MCZ	19895	F	Can	Low	High	-0.01331	0.00707	-0.01501	-0.02113
Mustela	sibirica	MCZ	24979	M	Fel	Low	High	-0.03258	-0.00899	-0.00993	-0.02429
Mustela	sibirica	MCZ	7104	F	Fel	Low	High	0.00127	0.01076	0.03377	-0.01049
Mustela	sibirica	MCZ	7106	M	Fel	Low	High	-0.01442	0.00716	-0.02530	-0.02520
Mustela	vison	MCZ	34165	F	Fel	Low	High	0.01514	-0.04015	-0.01584	-0.01147
Mustela	vison	MCZ	41362	M	Fel	Low	Low	0.06661	-0.02564	-0.01858	-0.00115
Mustela	vison	MCZ	41380	U	Fel	Low	Low	0.03593	-0.05737	0.01040	0.00454
Mustela	vison	MCZ	41381	U	Fel	Low	Low	0.01569	-0.04532	0.03050	-0.01588
Neofelis	nebulosa	AMNH	184931	M	Fel	High	High	0.02530	0.00631	-0.00266	-0.01881
Nyctereutes	procyonoides	MCZ	24853	M	Fel	High	High	0.00319	0.01701	0.03553	-0.00115
Nyctereutes	procyonoides	MCZ	24858	F	Fel	High	High	-0.00407	0.02406	0.00920	-0.02734
Nyctereutes	procyonoides	MCZ	24860	M	Fel	High	High	-0.03050	-0.02862	-0.02045	0.00740
Otocyon	megalotis	MCZ	25739	M	Fel	High	High	-0.00076	-0.03293	-0.02204	0.01199
Otocyon	megalotis	MCZ	8296	M	Fel	High	High	-0.02430	-0.00424	-0.00083	0.01976
Otocyon	megalotis	MCZ	8297	M	Fel	High	High	-0.02465	-0.00550	0.03286	0.00565
Panthera	leo	MCZ	31925	M	Fel	High	High	-0.01980	-0.00618	-0.02730	-0.00425
Panthera	leo	MCZ	31926	M	Fel	Low	High	-0.00638	-0.02818	0.03981	-0.00290
Panthera	leo	MCZ	36283	M	Mus	Low	High	-0.00281	-0.02323	0.03783	0.00491
Panthera	leo	MCZ	37656	M	Fel	High	High	-0.02926	-0.01714	0.04162	0.00459
Panthera	onca	MCZ	28621	M	Fel	High	High	-0.02468	0.05278	-0.02038	0.01470
Panthera	onca	MCZ	6976	F	Fel	High	High	-0.00573	0.05948	-0.03135	0.04010
Panthera	onca	MCZ	9371	F	Fel	High	High	-0.01314	0.04699	0.00167	0.02263
Panthera	pardus	MCZ	28666	M	Fel	High	High	0.00879	0.02960	-0.02132	0.02038
Panthera	pardus	MCZ	39737	U	Fel	Low	Low	-0.02475	0.10012	-0.01093	0.00900

Pardofelis	marmorata	AMNH	102844	F	Fel	Low	Low	-0.02490	0.08184	-0.00554	0.01354
Poecilogale	albinucha	AMNH	82442	U	Fel	Low	Low	0.06486	-0.03932	0.00605	0.00798
Prionailurus	planiceps	AMNH	35398	F	Fel	High	High	0.05864	-0.05373	0.02882	-0.00326
Prionailurus	rubiginosa	AMNH	150072	U	Fel	Low	High	0.08276	0.00207	-0.00374	0.00544
Prionsilurus	bengalensis	AMNH	205323	U	Fel	Low	High	0.10707	-0.00880	-0.00348	-0.00268
Profelis	aurata	AMNH	51998	U	Fel	Low	High	0.05352	-0.00973	0.00281	-0.00571
Pseudalopex	gymnocercus	UMMZ	124458	F	Fel	Low	Low	0.05070	-0.02089	0.01021	0.00589
Pteronura	brasiliensis	AMNH	98594	M	Mus	Low	Low	0.05164	0.01109	0.01330	-0.01807
Pteronura	brasiliensis	MCZ	27868	U	Mus	Low	Low	0.03944	-0.00932	0.00482	-0.00212
Puma	concolor	MCZ	30709	F	Fel	Low	Low	0.06899	0.00419	0.01066	0.01767
Puma	concolor	MCZ	30939	U	Fel	Low	Low	0.01247	-0.00390	-0.01675	-0.01674
Puma	concolor	MCZ	31074	M	Fel	Low	Low	-0.05208	0.03895	0.01571	0.00370
Puma	concolor	MCZ	31075	F	Fel	Low	Low	0.01409	0.02640	0.02023	0.02124
Puma	concolor	MCZ	63600	M	Fel	Low	Low	0.02618	0.03144	0.00783	0.02305
Speothos	venaticus	MCZ	28056	U	Fel	Low	Low	0.00877	-0.01297	0.01530	0.01304
Speothos	venaticus	MCZ	41096	U	Fel	Low	Low	0.05762	0.01709	0.01394	-0.01000
Speothos	venaticus	MCZ	42086	F	Fel	Low	Low	0.02832	-0.00668	-0.01319	-0.00809
Taxidae	taxus	MCZ	30175	U	Fel	Low	Low	-0.09372	0.01782	-0.00832	0.01507
Taxidae	taxus	MCZ	30422	F	Can	Low	Low	-0.09180	0.00880	-0.02313	-0.03336
Taxidae	taxus	MCZ	B9222	F	Can	Low	Low	-0.06195	0.02186	-0.02260	-0.01256
Taxidae	taxus	MCZ	B9223	U	Can	Low	Low	-0.04517	0.03691	0.01643	-0.01654
Tigra	tigra	MCZ	444	M	Mus	High	High	-0.02473	0.00523	-0.00172	-0.01536
Tigra	tigra	MCZ	5087	M	Mus	High	High	-0.07233	0.04410	-0.02225	-0.02140
Tigra	tigra	MCZ	8051	M	Mus	High	High	-0.05679	0.01902	-0.00764	-0.02568
Tigra	tigra	MCZ	9349	F	Mus	High	High	0.10690	-0.00363	-0.01306	-0.02928
Uncia	uncia	UMMZ	157859	F	Fel	High	High	0.07236	0.00832	-0.01246	-0.01404
Urocyon	cinereoargenteus	MCZ	12323	M	Can	High	Low	0.08503	-0.00936	-0.00966	-0.01121
Urocyon	cinereoargenteus	MCZ	29043	U	Can	High	Low	0.07633	-0.02309	0.01103	-0.01309
Urocyon	cinereoargenteus	MCZ	39020	M	Can	High	Low	0.06051	-0.02366	0.05436	0.01023
Urocyon	cinereoargenteus	MCZ	39021	F	Can	High	Low	-0.01674	0.07197	-0.00627	-0.01812
Urocyon	cinereoargenteus	MCZ	39026	F	Can	High	Low	0.01168	0.05162	0.01623	0.01451
Urocyon	cinereoargenteus	MCZ	39027	M	Can	High	Low	0.01154	0.04355	0.02733	0.00805
Urocyon	cinereoargenteus	MCZ	39028	U	Can	High	Low	-0.00933	0.04911	0.03749	0.00086
Urocyon	cinereoargenteus	MCZ	43017	M	Can	High	Low	0.01556	0.04602	0.02891	0.00743
Urocyon	littoralis	MCZ	7064	U	Can	Low	High	0.01660	0.03898	0.02129	0.00163
Urocyon	littoralis	MCZ	7065	U	Can	Low	High	0.00733	0.03986	0.03534	0.00831
Vormela	peregusna	AMNH	60103	U	Mus	High	Low	0.00659	0.04654	0.02583	-0.00547
Vulpes	bengalensis	UMMZ	75162	F	Can	High	High	0.03086	0.03926	-0.01353	-0.01247
Vulpes	chama	AMNH	148759	U	Can	High	High	0.04031	0.03747	-0.00386	0.00481
Vulpes	chama	MCZ	20077	F	Can	High	High	0.06195	-0.00414	-0.02488	-0.02613

Vulpes	chama	MCZ	37021	U	Can	High	High	0.04351	0.02241	0.01373	0.00533
Vulpes	corsac	UMMZ	118430	F	Can	High	Low	0.04298	0.02131	-0.00630	-0.01927
Vulpes	lagopus	MCZ	21808	M	Can	High	Low	0.02723	-0.01901	-0.00889	-0.01726
Vulpes	lagopus	MCZ	23602	F	Can	High	Low	0.02692	-0.01433	0.02284	-0.01567
Vulpes	lagopus	MCZ	47128	F	Can	High	Low	0.01517	-0.02950	-0.00020	-0.00951
Vulpes	lagopus	MCZ	52840	M	Can	High	Low	0.03685	-0.03612	-0.00637	-0.01323
Vulpes	macrotis	MCZ	37514	F	Can	High	Low	0.03144	-0.02930	0.01220	-0.02522
Vulpes	macrotis	MCZ	38619	F	Can	High	Low	0.07137	-0.00310	-0.00354	-0.00016
Vulpes	macrotis	MCZ	38620	F	Can	High	Low	0.07129	-0.01322	-0.00861	0.00611
Vulpes	macrotis	MCZ	38621	F	Can	High	Low	0.07396	-0.01477	0.01694	-0.02782
Vulpes	pallida	AMNH	82296	F	Can	Low	High	0.07384	-0.02253	-0.00597	0.00001
Vulpes	rueppellii	UMMZ	122374	F	Can	High	High	0.02354	-0.01684	-0.00344	-0.00502
Vulpes	velox	MCZ	B5681	M	Can	High	Low	0.01761	-0.01761	0.00633	-0.00771
Vulpes	velox	MCZ	B7719	F	Can	High	Low	0.03228	-0.00500	0.00882	-0.00976
Vulpes	vulpes	MCZ	14444	M	Can	High	Low	0.02487	-0.01206	-0.00552	0.01773
Vulpes	vulpes	MCZ	14445	F	Can	High	Low	0.03264	-0.01397	-0.00542	0.01434
Vulpes	vulpes	MCZ	22240	M	Can	High	Low	0.02027	0.01548	-0.00488	-0.00311
Vulpes	vulpes	MCZ	34784	M	Can	High	Low	0.00532	-0.01524	0.00413	-0.00716
Vulpes	vulpes	MCZ	46575	M	Can	High	Low	0.02717	-0.01551	-0.00285	-0.00599
Vulpes	vulpes	MCZ	46578	F	Can	High	Low	0.03761	-0.03802	0.00070	0.00955
Vulpes	zerda	MCZ	28723	M	Can	High	Low	0.07295	0.00684	-0.00182	-0.00546
Vulpes	zerda	MCZ	29617	U	Can	High	Low	0.05790	0.00774	-0.00885	0.00050

Table S3.1: Catalogue, gender, clade assignment, climatic grouping, and PC scores for the Carnivora

Species	PC1	PC2	PC3	PC4	Integration	TempBIO7	PrecipBIO15
Atelocynus_microtis	-0.05637622	0.027602218	-0.00276485	-0.01954245	0.00201146	128	41
Canis_adustus	0.01566138	0.001226823	0.0023115	-0.01427962	6.73E-05	204.92	91.42
Canis_aureus	-0.00412726	-0.00183112	-0.00992404	0.006910355	-5.64E-05	310.17	69.83
Canis_latrans	0.000981574	-0.0329175	0.01665616	0.010118552	-0.0002888	365.83	38.67
Canis_lupus	-0.04162365	-0.03661008	0.01432931	-0.00800823	-0.0008203	430.75	63.17
Canis_mesomelas	0.008838775	-0.01865617	-0.01596638	0.002851131	-8.54E-06	206.42	83.92
Canis_rufus	-0.01576471	-0.03974886	0.00231038	0.017483816	-0.0006302	303.67	20.33
Canis_simensis	0.01004115	-0.00454797	0.01560111	0.000888422	-0.0001168	172.92	79.83
Cerdocyon_thous	-0.00231122	0.009993935	-0.03575579	0.012730812	-0.0001962	173.58	60.25
Chrysocyon_brachyurus	-0.01587247	0.005727314	0.07826125	0.012197201	0.00278472	201	63.33
Cuon_alpinus	-0.06161232	-0.00132859	-0.00161125	0.005024008	0.00181853	239.83	99.17
Dusicyon_australis	-0.00757105	-0.02852827	0.01185856	0.006179263	-0.0004553	139	19.92
Lycalopex_culpaeus	0.019853706	-0.00965256	-0.0017374	0.02328587	-0.0008779	237.33	59.75
Lycalopex_griseus	0.051134357	-0.01988169	-0.03351366	0.013677482	0.00122326	231.58	51.42
Lycalopex_gymnocercus	0.012469423	-0.00390258	-0.0167466	-0.01673747	3.30E-05	261.33	38.75
Lycalopex_sechurae	0.019847032	-0.00738222	-0.00553002	-0.0398744	0.00018817	162.83	140.75
Lycalopex_vetulus	-0.0175225	0.037705989	-0.00170618	-0.03991659	-0.0012582	178	74.67
Lycaon_pictus	-0.06745748	-0.02405253	-0.01762277	-0.01169635	-0.0003083	251.83	105.08
Nyctereutes_procyonoides	-0.0145157	0.053082221	-0.01668528	0.025809329	-0.0013639	443.67	71.42
Otocyon_megalotis	-0.01362003	0.07052019	-0.01260005	0.014306224	-0.0022616	228.75	92.67
Speothos_venaticus	-0.08248844	0.016162226	-0.01801666	-0.01028254	0.00119659	137.08	54.75
Urocyon_cinereoargenteus	0.005403799	0.048454169	0.02326898	0.002150214	-0.0024155	344.75	59.33
Urocyon_littoralis	0.035585253	0.038362826	-0.0086937	-0.00382772	0.0001816	157.83	94.83
Vulpes_bengalensis	0.061947457	-0.0041439	-0.02487575	-0.02613493	0.00157282	313.92	117.5
Vulpes_chama	0.038636992	0.015277124	0.00123967	-0.01390329	-2.82E-05	296.42	73.17
Vulpes_corsac	0.027229509	-0.01901147	-0.00889117	-0.01726428	0.00036214	457.08	54.83
Vulpes_lagopus	0.027596904	-0.02731045	0.00711917	-0.01590563	-0.0003218	433.33	46.75
Vulpes_macrotis	0.07261451	-0.01340465	-0.00029616	-0.00546383	-0.0011932	342.08	61.58
Vulpes_pallida	0.043509313	0.052255671	-0.00694163	-0.00785871	-0.0008296	251.08	137.25
Vulpes_rueppellii	0.023539907	-0.01683664	-0.00343924	-0.00501816	2.53E-05	335.67	108.17
Vulpes_velox	0.024940929	-0.0113054	0.00757097	-0.00873915	-0.0006095	411.25	63.08
Vulpes_vulpes	0.024647596	-0.01321854	-0.00230757	0.004226432	-3.45E-07	478.25	62.58
Vulpes_zerda	0.065423183	0.007289459	-0.00533589	-0.00247638	0.00071545	348.33	61.58
Acinonyx_jubatus	0.018128612	0.074029636	-0.02173535	-0.02041698	-0.0019164	266.33	86.08
Caracal_caracal	0.001203591	0.026670162	0.01333806	-0.01301548	2.58E-05	298.5	72.17
Catopuma_temminckii	0.003415461	-0.07142326	-0.01393197	-0.03059188	-0.0009632	207.42	67.67
Felis_chaus	-0.0206359	0.056534373	-0.00316262	0.024566443	-0.0008564	309.33	110.67
Felis_margarita	-0.02620373	0.048609163	0.04438714	-0.00076506	0.00017276	349	73.75
Felis_nigripes	-0.03889415	0.014576072	0.0333459	-0.01184393	-0.0004926	307.92	81

Felis_silvestris	-0.03994843	-0.0006073	0.01975067	-0.00328818	0.00035073	277.5	81.92
Leopardus_colocolo	-0.02722045	-0.02101223	-0.00033068	0.008978758	-0.0001693	221.83	55.33
Leopardus_geoffroyi	-0.04543307	0.000902203	0.00265544	0.005003579	0.00040113	247.58	43.08
Leopardus_guigna	-0.02926339	0.029779579	-0.02153292	0.035867893	4.33E-05	216.75	59.83
Leopardus_pardalis	0.003937267	-0.02418877	-0.01054045	-0.00042652	-0.0001255	156.75	59.25
Leopardus_tigrinus	-0.0583526	-0.0024474	-0.0101337	-0.01125149	0.00060611	147.83	57.33
Leopardus_wiedii	-0.04570327	-0.02034751	0.01164183	-0.00631408	0.00017389	145.92	56.75
Leptailurus_serval	-0.01828188	0.030997874	0.00064056	0.01249866	0.00023116	207.08	90.75
Lynx_canadensis	-0.00088894	-0.01800062	0.02091089	0.000124994	-0.0001332	434.08	50.58
Lynx_lynx	0.026866665	-0.00698309	0.00348886	0.020586255	0.00031043	406.67	55.58
Lynx_pardinus	-0.01244043	0.001200191	-0.00348418	0.007525718	-9.88E-07	281.17	58.67
Lynx_rufus	0.001578974	0.010594638	0.01536592	0.004378603	-1.62E-05	404.42	53.33
Neofelis_nebulosa	0.012727759	-0.04091275	0.0024081	-0.00201638	-0.0001489	241.5	75.42
Otocolobus_manul	-0.00557245	0.019716081	0.0016417	0.038923198	-0.0001388	429.67	91.5
Panthera_leo	0.078329988	-0.02494301	0.00691136	0.001870236	0.00131447	181	85.75
Panthera_onca	0.051954547	-0.00650999	0.00877051	-0.00596195	0.0002061	132.58	55.42
Panthera_pardus	0.051796553	-0.0131592	0.00666186	0.003459214	0.00045692	250.5	90.5
Panthera_tigris	0.0851558	-0.00694023	-0.00603765	-0.01690553	0.00140168	260.25	77.67
Pardofelis_marmorata	0.01026623	0.053602695	-0.00329185	0.036504404	-0.0013076	188.83	71.5
Prionailurus_bengalensis	-0.03439593	-0.00451046	-0.01063596	0.004869108	7.56E-05	275.25	83.58
Prionailurus_planiceps	-0.02767677	-0.04946563	-0.05437498	0.003804824	-0.0011591	90.58	23.83
Prionailurus_rubiginosus	-0.07027602	0.009079253	-0.01794386	-0.03632057	4.51E-05	256.42	115.5
Prionailurus_viverrinus	-0.00117128	-0.02358184	-0.03845189	-0.00450426	-0.0003544	189.08	86.42
Profelis_aurata	0.02281903	0.045556393	-0.02268872	0.015964924	-0.0005374	141	60.58
Puma_concolor	0.026996637	0.011055746	0.0088209	0.007846511	-7.07E-05	203.33	51.33
Puma_yagouaroundi	-0.02003528	-0.00265236	-0.00863212	0.008696156	-1.12E-05	175.5	58.58
Uncia_uncia	0.060514958	-0.02365772	0.05435545	0.010228075	-0.0009237	391.58	92.42
Aonyx_capensis	-0.03425398	0.033611328	-0.05243395	0.011027263	-0.0008262	222.25	97.58
Aonyx_cinerea	-0.04278745	-0.01821483	0.02037391	0.041636605	0.00051152	212.5	90.08
Arctonyx_collaris	0.072618673	0.079669828	0.01467871	0.012295553	0.00195955	266.33	79.33
Eira_barbara	-0.02493354	0.008985387	-0.05576225	-0.04788129	-0.0015835	174.25	69.83
Enhydra_lutris	0.029613672	-0.02883654	-0.10474752	0.072473991	-0.0090083	191	28
Galictis_cuja	0.000412333	0.035188878	-0.02452907	-0.03445741	-0.0005362	250.83	52.5
Galictis_vittata	-0.01197395	0.000947531	0.01527865	-0.01764949	-0.0004074	136.83	60.33
Gulo_gulo	-0.00555162	-0.03188236	-0.01500122	0.02464702	-0.0001434	481.33	53.25
Hydrictis_maculicollis	-0.06041645	0.01621873	0.04356727	-0.00378674	0.00016222	168.08	71.08
Ictonyx_libyca	0.029558346	0.009153544	0.01912897	0.005273283	0.00016529	289.25	111.17
Ictonyx_striatus	0.017025164	0.009022005	0.03638576	0.020975884	-0.0002956	225.25	98.33
Lontra_canadensis	-0.05077973	0.005116743	0.00767091	0.015839032	0.00104391	450.58	48.75
Lontra_longicaudis	-0.03040305	0.005196439	0.00528399	0.027409318	0.0002445	134.58	46.33

Lontra_provocax	-0.0203351	-0.01882127	-0.01196478	0.038120423	-0.0001843	143.75	19
Lutra_lutra	-0.05357111	0.019402249	0.02479503	0.007457095	0.00065023	439.33	42.17
Lutrogale_perspicillata	-0.04185728	0.021137235	0.05330959	0.009854702	-0.0007808	238	102
Martes_americana	0.007016607	-0.04647063	0.02977485	-0.01766105	-0.0015589	456	43.5
Martes_flavigula	-0.00439101	-0.00283826	-0.01447156	-0.01860887	-0.0001902	271.75	61.67
Martes_foina	0.007645695	-0.0361518	-0.02410886	-0.00011984	-0.0004141	394.92	74
Martes_martes	0.003446487	-0.0288637	-0.01222965	0.009258165	-0.0003304	342.67	31.83
Martes_melampus	-0.02155444	-0.01115797	0.01018191	0.006712371	0.00010173	324.33	31.33
Martes_pennanti	-0.00383904	-0.02989289	0.01501286	-0.0031028	-0.0004317	407.08	32.5
Martes_zibellina	-0.02624302	-0.03053212	0.01800474	-0.00524585	-0.0002911	548.42	52.33
Meles_meles	0.018322771	0.026522142	0.05398051	0.019915246	-0.0006186	297.83	32.5
Mellivora_capensis	-0.07620719	0.076844158	-0.03720064	-0.01221817	-0.0009958	240	104.5
Melogale_everetti	0.117864116	0.045982317	0.00460814	-0.01768632	0.0063109	89.92	33.25
Melogale_moschata	0.081697856	0.074772989	-0.03571104	-0.00589677	0.0020303	269.75	63.75
Melogale_orientalis	0.077435496	0.048093056	0.04141851	0.022332115	0.0025564	119.33	45.08
Melogale_personata	0.0797677	0.042127712	-0.00983172	0.028736987	0.00195297	215.75	90.58
Mustela_africana	0.01467261	-0.00289919	-0.04042083	-0.00619055	-0.0004883	124.67	48.5
Mustela_altaica	0.029915429	-0.04457905	-0.00533081	-0.01579993	-0.000515	483	109.58
Mustela_erminea	0.051984675	-0.0327835	0.00187578	-0.00043281	0.00026373	529.58	57
Mustela_eversmanii	-0.01728148	-0.00993795	-0.02269202	-0.02028055	-0.0001019	434.25	64.5
Mustela_felipei	0.018648888	0.003925397	-0.01837636	0.012669468	-0.0003772	109.25	25.83
Mustela_frenata	0.032328729	-0.03843387	0.00665258	-0.01275732	-0.0003061	346.5	35.08
Mustela_kathiah	0.006847971	-0.02779922	0.00205335	0.000596215	-0.0002822	239.5	80.75
Mustela_lutreolina	-0.04647584	0.031499704	-0.02132179	0.005407643	0.00047595	122.75	36.25
Mustela_nigripes	-0.01476008	0.003997884	-0.0041169	-0.0202767	-0.0004227	414.17	53.5
Mustela_nivalis	0.033343091	-0.04211998	0.00161976	-0.00599064	-0.0002801	430.08	54.58
Mustela_nudipes	0.017274584	-0.00070941	-0.001379	-0.00785391	9.21E-05	99.5	35.5
Mustela_putorius	-0.00043947	0.020532913	0.02236525	-0.01424232	-0.0004421	344.08	30.42
Mustela_sibirica	-0.02299749	-0.00615314	-0.00951237	0.008267923	0.00023596	499.83	50.75
Neovison_vison	-0.01456443	-0.01868111	0.02299004	0.000584903	-0.0003598	446.5	45.42
Poecilogale_albinucha	0.015673074	0.050879487	-0.030785	-0.01247659	-0.0008566	186.75	75.17
Pteronura_brasiliensis	-0.05838334	0.032306633	0.01561036	0.010960055	0.00060815	137.42	53.08
Taxidea_taxus	-0.04975598	0.026316632	-0.00379487	-0.01974528	0.00019639	387.08	56.25
Vormela_peregusna	0.000473763	-0.00851798	-0.01065029	-0.01299634	-0.000211	442.17	38.58

Table S3.2: Species mean PC scores, integration, and climatic variability values for the Carnivora

APPENDIX C

SUPPLEMENTARY INFORMATION FOR CHAPTER 4

Genus	Species	Institution	CatNo	Gender	TwoGroup	ThreeGroup	PC1	PC2	PC3	PC4
Ailuropoda	melanoleuca	AMNH	110451	F	Car	Can	0.02381	-0.10259	-0.03636	0.08014
Ailuropoda	melanoleuca	AMNH	147745	M	Car	Can	0.02691	-0.03685	-0.04395	0.04276
Ailurus	fulgens	AMNH	146682	M	Car	Can	0.12660	0.00682	-0.04106	-0.03907
Ailurus	fulgens	AMNH	146778	F	Car	Can	0.05393	-0.08585	0.00681	0.01831
Aonyx	capensis	AMNH	51853	F	Car	Can	0.17454	0.01404	-0.00680	-0.03244
Aonyx	capensis	AMNH	52104	M	Car	Can	0.16855	-0.00159	-0.00480	-0.01642
Aonyx	cinerea	AMNH	101638	M	Car	Can	0.09539	-0.08580	0.02934	-0.01739
Aonyx	cinerea	AMNH	106626	F	Car	Can	0.09404	-0.02595	0.00262	-0.00367
Arctonyx	collaris	AMNH	110460	F	Car	Can	-0.00113	0.03777	0.05980	-0.08372
Arctonyx	collaris	AMNH	57373	M	Car	Can	0.01272	0.02832	0.00084	-0.08321
Atelocynus	microtis	AMNH	100095	M	Car	Can	0.01279	0.03743	-0.03441	-0.03557
Atelocynus	microtis	AMNH	95285	F	Car	Can	-0.02488	-0.01100	0.03153	-0.01387
Bassaricyon	alleni	AMNH	98709	F	Car	Can	0.00693	0.05725	0.01204	-0.01763
Bassaricyon	alleni	FMNH	65788	M	Car	Can	-0.05141	0.01401	-0.02223	0.00536
Bassaricyon	gabbii	AMNH	140334	F	Car	Can	0.04898	0.05789	-0.02177	-0.02014
Bassaricyon	neblina	AMNH	42351	M	Car	Can	0.02008	0.06146	-0.02062	-0.03375
Bassaricyon	neblina	FMNH	70721	F	Car	Can	-0.02740	0.02060	-0.02003	0.02743
Bassariscus	astutus	NMNH	116181	F	Car	Can	-0.04509	-0.00303	-0.02779	-0.02041
Bassariscus	astutus	NMNH	125571	M	Car	Can	-0.05889	0.00528	-0.03738	-0.01720
Bassariscus	sumichrasti	AMNH	135926	M	Car	Can	-0.03123	-0.01704	0.02313	-0.00977
Bassariscus	sumichrasti	AMNH	135927	F	Car	Can	0.01841	0.03080	0.01783	-0.02960
Bassariscus	sumichrasti	NMNH	340736	M	Car	Can	-0.01518	-0.01385	-0.01251	-0.00950
Bassariscus	sumichrasti	NMNH	340737	F	Car	Can	-0.01752	-0.00320	-0.02828	-0.00170

Canis	adustus	AMNH	116333	M	Car	Can	-0.07385	-0.00635	-0.02035	-0.03024
Canis	adustus	AMNH	160997	F	Car	Can	-0.09750	-0.00553	-0.01479	-0.01715
Canis	aureus	AMNH	88708	F	Car	Can	-0.03952	-0.00670	-0.03739	-0.02964
Canis	aureus	AMNH	88712	M	Car	Can	-0.01897	-0.00979	-0.04997	-0.03724
Canis	himalayensis	NMNH	198457	M	Car	Can	-0.08849	-0.03829	-0.08441	0.00508
Canis	himalayensis	NMNH	198458	F	Car	Can	-0.09141	-0.04842	-0.09667	-0.00376
Canis	indica	NMNH	16146	U	Car	Can	-0.05928	-0.02213	-0.08254	0.00606
Canis	latrans	AMNH	24812	F	Car	Can	-0.05280	-0.00802	-0.03693	-0.03731
Canis	latrans	AMNH	24860	M	Car	Can	-0.04852	-0.02504	-0.04716	-0.02189
Canis	lupus	AMNH	16850	M	Car	Can	-0.02255	-0.03302	-0.07010	-0.00630
Canis	lupus	AMNH	98227	F	Car	Can	-0.01649	-0.00690	-0.06578	-0.00094
Canis	mesomelas	AMNH	114176	F	Car	Can	-0.07689	-0.00777	-0.02991	-0.02715
Canis	mesomelas	AMNH	205145	M	Car	Can	-0.05205	-0.00274	-0.03700	-0.01396
Canis	rufus	AMNH	4609	M	Car	Can	-0.02229	-0.00854	-0.04368	-0.02040
Canis	rufus	NMNH	234426	F	Car	Can	-0.08193	-0.04080	-0.09367	0.00221
Canis	rufus	NMNH	234427	M	Car	Can	-0.08109	-0.04086	-0.05982	0.00607
Canis	simensis	AMNH	81001	M	Car	Can	-0.07758	-0.00840	-0.04432	-0.01070
Canis	simensis	AMNH	81034	F	Car	Can	-0.06024	0.00083	-0.05100	-0.01466
Cerdocyon	thous	AMNH	14853	M	Car	Can	-0.04185	0.00887	-0.02936	-0.03710
Cerdocyon	thous	AMNH	75790	F	Car	Can	-0.05230	0.02135	-0.02476	-0.06203
Chrysocyon	brachyurus	AMNH	36962	M	Car	Can	-0.03484	-0.00208	-0.05063	-0.00098
Chrysocyon	brachyurus	FMNH	28311	F	Car	Can	-0.13812	-0.00174	-0.07730	-0.00170
Conepatus	chinga	NMNH	194320	F	Car	Can	0.00643	-0.00687	-0.04186	0.00574
Conepatus	chinga	NMNH	194322	M	Car	Can	0.02529	0.00167	-0.06021	-0.03212
Conepatus	fucilli	AMNH	235512	F	Car	Can	0.06157	-0.01102	-0.03443	-0.03711
Conepatus	fucilli	AMNH	235513	M	Car	Can	0.07698	0.02528	-0.03561	-0.01270
Conepatus	leuconotus	AMNH	172187	M	Car	Can	0.06622	0.01809	-0.04681	-0.02930
Conepatus	leuconotus	AMNH	204289	F	Car	Can	0.05365	-0.02685	-0.04424	-0.01557
Conepatus	mesoleucus	AMNH	185357	M	Car	Can	0.08154	0.03269	-0.00328	-0.04617
Conepatus	mesoleucus	AMNH	2487	F	Car	Can	0.04002	0.01133	-0.03678	-0.01886
Conepatus	nicaraguae	AMNH	29281	M	Car	Can	0.08210	0.02264	-0.04023	-0.03159
Conepatus	nicaraguae	AMNH	29283	F	Car	Can	0.07742	0.01827	-0.02490	-0.02261
Conepatus	quitensis	AMNH	36463	F	Car	Can	0.09785	-0.00741	-0.01275	0.01107
Conepatus	quitensis	AMNH	36464	M	Car	Can	0.06014	0.01187	-0.04592	-0.02372
Conepatus	rex	FMNH	49732	F	Car	Can	0.03121	0.01246	-0.06846	-0.02419
Conepatus	rex	FMNH	49734	M	Car	Can	0.04809	0.00807	-0.05006	-0.03062
Conepatus	semistriatus	AMNH	172190	F	Car	Can	0.08079	-0.03393	-0.03164	-0.00645
Conepatus	semistriatus	AMNH	66722	M	Car	Can	0.17674	0.01459	-0.00872	-0.00742
Conepatus	sonoriensis	AMNH	26160	F	Car	Can	0.08643	0.00714	-0.06505	-0.04437
Conepatus	sonoriensis	AMNH	26166	M	Car	Can	0.08995	-0.00269	-0.06192	-0.03083

Cuon	alpinus	AMNH	100882	M	Car	Can	-0.00090	-0.00850	-0.01452	-0.00795
Cuon	alpinus	AMNH	102083	F	Car	Can	0.02055	0.00740	-0.00532	-0.02127
Eira	barbara	AMNH	98583	M	Car	Can	0.13323	-0.01960	0.03886	0.02287
Eira	barbara	AMNH	98584	F	Car	Can	0.09304	-0.03684	0.01723	0.05256
Enhydra	lutris	AMNH	146618	M	Car	Can	0.18225	0.02278	-0.05505	-0.04100
Enhydra	lutris	AMNH	215275	F	Car	Can	0.10240	0.06236	-0.05973	-0.01688
Galictis	cuja	AMNH	205832	F	Car	Can	0.06530	-0.07193	0.04910	0.02455
Galictis	cuja	AMNH	235992	M	Car	Can	0.09196	-0.04025	0.02298	0.02627
Galictis	vittata	AMNH	48094	F	Car	Can	0.03906	-0.08495	0.01447	0.04300
Galictis	vittata	AMNH	70339	M	Car	Can	0.06679	-0.09450	0.00859	0.05331
Gulo	gulo	AMNH	34506	F	Car	Can	0.10957	-0.01028	-0.08539	-0.01301
Gulo	gulo	AMNH	37432	M	Car	Can	0.11966	0.00613	-0.11945	0.00461
Helarctos	malayanus	AMNH	19155	M	Car	Can	0.05022	0.03000	-0.03097	0.03675
Helarctos	malayanus	AMNH	28254	F	Car	Can	0.03031	0.02548	-0.05597	0.01924
Hydrictis	maculicollis	AMNH	51825	F	Car	Can	0.03956	-0.09704	0.03368	0.03733
Hydrictis	maculicollis	AMNH	89808	M	Car	Can	0.03176	-0.09403	0.05414	0.03026
Hydrictis	maculicollis	NMNH	429136	F	Car	Can	0.00961	-0.09802	0.01312	0.05347
Ictonyx	libyca	AMNH	70554	M	Car	Can	0.04891	-0.06388	-0.00965	0.01562
Ictonyx	libyca	FMNH	107198	F	Car	Can	0.03861	-0.03622	0.01196	0.01441
Ictonyx	striatus	AMNH	168963	F	Car	Can	0.01627	-0.06074	0.00068	0.02526
Ictonyx	striatus	AMNH	168968	M	Car	Can	0.05136	-0.05105	-0.00450	0.00821
Lontra	canadensis	AMNH	207987	F	Car	Can	0.09347	-0.04451	0.00697	-0.00093
Lontra	canadensis	AMNH	35105	M	Car	Can	0.10156	-0.06438	0.01034	0.03066
Lontra	felina	NMNH	512791	F	Car	Can	0.01426	-0.08684	-0.02522	0.02582
Lontra	longicaudis	AMNH	133949	F	Car	Can	0.07051	-0.02509	0.01841	-0.03469
Lontra	longicaudis	AMNH	67099	M	Car	Can	0.09648	-0.05258	0.00744	0.02301
Lontra	longicaudis	NMNH	290886	M	Car	Can	0.03906	-0.09870	-0.01527	0.03189
Lontra	longicaudis	NMNH	336215	F	Car	Can	0.04986	-0.07730	-0.04096	0.04435
Lutra	lutra	AMNH	206592	M	Car	Can	0.07296	-0.05715	0.03672	0.01374
Lutra	lutra	AMNH	207729	F	Car	Can	0.11565	-0.01538	-0.00069	-0.02198
Lutra	sumatrana	NMNH	309014	F	Car	Can	0.01663	-0.11108	0.00490	0.02940
Lutra	sumatrana	NMNH	309015	M	Car	Can	0.01126	-0.10570	0.00936	0.05622
Lutrogale	perspicillata	NMNH	240483	M	Car	Can	0.01315	-0.11050	0.00617	0.04903
Lutrogale	perspicillata	NMNH	83252	F	Car	Can	0.01365	-0.12271	0.01702	0.05227
Lycalopex	culpaeus	AMNH	66737	M	Car	Can	-0.07069	-0.02197	-0.04334	-0.01682
Lycalopex	culpaeus	AMNH	67088	F	Car	Can	-0.07328	-0.02099	-0.03757	-0.02975
Lycalopex	griseus	AMNH	135081	M	Car	Can	-0.10204	-0.00031	-0.06883	-0.02783
Lycalopex	griseus	AMNH	135085	F	Car	Can	-0.09266	-0.02058	-0.04585	-0.00548
Lycalopex	gymnocercus	AMNH	205772	F	Car	Can	-0.05377	-0.01738	-0.05787	-0.04747
Lycalopex	gymnocercus	AMNH	205782	M	Car	Can	-0.08166	-0.01538	-0.06412	-0.05352

Lycalopex	sechurae	AMNH	46532	F	Car	Can	-0.07224	-0.01226	-0.03305	-0.02507
Lycalopex	sechurae	AMNH	46533	M	Car	Can	-0.07023	-0.01451	-0.03890	-0.03107
Lycalopex	vetulus	AMNH	100100	F	Car	Can	-0.06701	-0.00608	-0.03769	-0.03508
Lycalopex	vetulus	AMNH	133928	M	Car	Can	-0.05095	0.00699	-0.03703	-0.03417
Lycaon	pictus	AMNH	164162	M	Car	Can	0.00199	-0.00497	-0.03759	0.00170
Lycaon	pictus	AMNH	82088	F	Car	Can	-0.02597	-0.05520	-0.02390	-0.00130
Martes	americana	AMNH	184596	F	Car	Can	0.04200	-0.04291	-0.00458	0.01441
Martes	americana	AMNH	8224	M	Car	Can	0.00052	-0.06737	0.00335	0.01944
Martes	americana	NMNH	53360	F	Car	Can	0.00456	-0.05004	-0.03539	0.02762
Martes	americana	NMNH	57939	M	Car	Can	0.00116	-0.07427	-0.00098	0.04167
Martes	flavigula	AMNH	107135	F	Car	Can	0.06843	0.01965	-0.00237	-0.01601
Martes	flavigula	AMNH	163581	M	Car	Can	0.04790	-0.01101	0.00084	0.02756
Martes	foina	AMNH	6289	F	Car	Can	0.05114	-0.04912	-0.03310	0.02230
Martes	foina	AMNH	70236	M	Car	Can	0.03948	-0.05284	-0.03520	0.01944
Martes	martes	NMNH	188001	M	Car	Can	-0.00701	-0.07715	-0.01825	0.01812
Martes	martes	NMNH	188100	F	Car	Can	-0.00263	-0.07593	-0.03550	0.03693
Martes	melampus	NMNH	13832	M	Car	Can	0.00899	-0.06983	-0.01192	0.01666
Martes	pennanti	AMNH	150304	M	Car	Can	0.12061	-0.01952	-0.02107	0.01147
Martes	pennanti	AMNH	165691	F	Car	Can	0.03576	-0.04792	0.01179	0.01945
Martes	zibellina	NMNH	113968	U	Car	Can	0.00642	-0.10208	-0.00456	0.05097
Meles	anakuma	NMNH	23934	M	Car	Can	0.00898	-0.08866	0.02768	0.01378
Meles	meles	AMNH	88698	M	Car	Can	0.08507	-0.00919	0.00345	-0.02372
Meles	meles	AMNH	88700	F	Car	Can	0.04379	-0.01625	-0.00739	0.00016
Mellivora	capensis	AMNH	119622	M	Car	Can	0.11755	-0.01864	0.05853	0.04814
Mellivora	capensis	AMNH	81232	F	Car	Can	0.08406	0.02213	0.02845	-0.02564
Melogale	moschata	NMNH	294294	F	Car	Can	0.00836	0.03899	0.01029	-0.05285
Melogale	moschata	NMNH	358572	M	Car	Can	-0.02162	-0.00115	0.00294	-0.04624
Melogale	personata	NMNH	356597	F	Car	Can	-0.01230	-0.01686	0.01309	-0.02641
Melogale	personata	NMNH	356600	M	Car	Can	-0.00504	0.01716	0.02350	-0.03012
Melursus	ursinus	AMNH	54464	F	Car	Can	0.04152	0.00464	-0.00147	0.05892
Melursus	ursinus	AMNH	54467	M	Car	Can	0.02527	-0.01578	-0.00344	0.05187
Mephitis	macroura	NMNH	205889	M	Car	Can	0.02205	-0.05879	-0.04345	-0.01202
Mephitis	macroura	NMNH	46328	F	Car	Can	-0.00332	-0.04678	-0.06717	0.00459
Mephitis	mephitis	AMNH	139911	F	Car	Can	0.07418	0.00640	-0.00908	-0.05551
Mephitis	mephitis	AMNH	139913	M	Car	Can	0.07858	-0.04533	0.00725	-0.02943
Mephitis	mephitis	NMNH	225124	M	Car	Can	0.04936	-0.07148	0.01133	0.00254
Mephitis	mephitis	NMNH	37274	F	Car	Can	0.02620	-0.05867	-0.04833	-0.00593
Mustela	africana	AMNH	61813	F	Car	Can	0.11988	-0.03747	0.00245	0.00010
Mustela	altaica	FMNH	44349	M	Car	Can	0.06624	-0.04997	-0.01944	0.00758
Mustela	altaica	FMNH	49923	F	Car	Can	0.02146	-0.04568	-0.02287	0.00005

Mustela	erminea	AMNH	121426	M	Car	Can	0.05368	-0.02470	-0.00088	0.00470
Mustela	erminea	AMNH	19970	F	Car	Can	0.08031	-0.00283	0.00606	0.01235
Mustela	eversmanii	NMNH	172631	M	Car	Can	0.08799	-0.07764	0.02532	0.04090
Mustela	eversmanii	NMNH	188448	F	Car	Can	0.05774	-0.05250	-0.01070	0.01873
Mustela	frenata	AMNH	138377	M	Car	Can	0.10760	-0.04002	-0.03444	0.02543
Mustela	frenata	AMNH	138380	F	Car	Can	0.03898	-0.04659	-0.00664	0.01760
Mustela	itatsi	NMNH	140901	M	Car	Can	0.06576	-0.07221	-0.01119	0.03712
Mustela	itatsi	NMNH	140902	F	Car	Can	0.02369	-0.06606	-0.04378	0.06108
Mustela	kathiah	AMNH	163579	M	Car	Can	0.07281	-0.07706	-0.02922	0.03587
Mustela	kathiah	AMNH	56940	F	Car	Can	0.06984	-0.02938	-0.01412	0.02359
Mustela	lutreola	AMNH	106670	M	Car	Can	0.09221	-0.07015	0.01600	0.04980
Mustela	lutreola	AMNH	206590	F	Car	Can	0.04806	-0.08983	-0.02709	0.03640
Mustela	nigripes	AMNH	41994	M	Car	Can	0.09974	-0.09049	-0.01738	0.02336
Mustela	nigripes	NMNH	174655	M	Car	Can	0.07357	-0.04797	-0.00386	0.03458
Mustela	nigripes	NMNH	241014	F	Car	Can	0.06944	-0.07021	-0.01033	0.02487
Mustela	nivalis	AMNH	129277	F	Car	Can	0.02575	-0.05972	-0.02782	0.00809
Mustela	nivalis	AMNH	31383	M	Car	Can	0.00275	-0.06911	-0.04516	0.00075
Mustela	nudipes	AMNH	106065	M	Car	Can	0.07495	-0.05534	-0.02233	0.03722
Mustela	putorius	AMNH	18019	M	Car	Can	0.06611	-0.10233	0.01421	0.02279
Mustela	putorius	AMNH	243106	F	Car	Can	0.06507	-0.08085	0.02096	0.02308
Mustela	sibirica	AMNH	110467	M	Car	Can	0.07279	-0.06929	0.00821	0.05253
Mustela	sibirica	AMNH	43171	F	Car	Can	0.04647	-0.06968	-0.04162	0.02809
Mydaus	javanensis	NMNH	121497	F	Car	Can	-0.03954	0.04791	0.00593	-0.04477
Mydaus	javanensis	NMNH	34894	M	Car	Can	-0.02111	0.03305	0.00933	-0.05130
Mydaus	marchei	NMNH	478277	F	Car	Can	-0.03513	-0.00831	-0.00982	-0.01957
Mydaus	marchei	NMNH	478278	M	Car	Can	-0.04144	-0.01168	-0.00813	-0.00536
Nasua	narica	NMNH	88144	M	Car	Can	-0.07033	0.00880	-0.00200	-0.03347
Nasua	narica	NMNH	88146	F	Car	Can	-0.10025	-0.02411	-0.01850	-0.02554
Nasua	nasua	AMNH	136294	F	Car	Can	-0.08791	0.00037	0.00469	-0.06765
Nasua	nasua	AMNH	33899	M	Car	Can	-0.06769	0.01551	0.00341	-0.04115
Nasuella	olivacea	AMNH	33047	F	Car	Can	-0.09829	0.04943	0.02925	-0.06045
Nasuella	olivacea	AMNH	33049	M	Car	Can	-0.07791	0.03568	0.03091	-0.06065
Neovison	vison	AMNH	35720	F	Car	Can	0.07067	-0.07557	0.00799	0.03141
Neovison	vison	AMNH	40858	M	Car	Can	0.05673	-0.06645	-0.00217	0.03212
Nyctereutes	procyonoides	AMNH	59322	F	Car	Can	-0.00844	-0.00402	0.02061	-0.02122
Nyctereutes	procyonoides	AMNH	59323	M	Car	Can	-0.04154	0.00868	0.00533	-0.02273
Nyctereutes	procyonoides	NMNH	255332	F	Car	Can	-0.06712	-0.02465	-0.03046	-0.01883
Nyctereutes	procyonoides	NMNH	255373	M	Car	Can	-0.05285	-0.02205	-0.00950	-0.01785
Odobenus	rosmarus	AMNH	29902	F	Car	Can	-0.02091	-0.05002	-0.01238	0.12771
Odobenus	rosmarus	AMNH	73303	M	Car	Can	-0.00279	0.01518	-0.02365	0.10373

Otocyon	megalotis	AMNH	63993	M	Car	Can	-0.07378	0.01470	-0.00728	-0.02994
Otocyon	megalotis	AMNH	70030	F	Car	Can	-0.04134	0.04032	0.00679	-0.05650
Poecilogale	albinucha	AMNH	82442	M	Car	Can	0.11158	-0.03831	0.03352	0.04219
Poecilogale	albinucha	AMNH	86490	F	Car	Can	0.06641	-0.05635	0.04750	0.01602
Potos	flavus	AMNH	134033	M	Car	Can	0.16210	0.12911	-0.01372	0.03974
Potos	flavus	AMNH	165624	F	Car	Can	0.17826	0.12675	-0.07098	0.01270
Potos	flavus	AMNH	95838	F	Car	Can	0.16648	0.13247	-0.04080	0.03886
Potos	flavus	AMNH	96288	M	Car	Can	0.21424	0.17818	-0.02355	0.02910
Procyon	cancrivorus	AMNH	141990	M	Car	Can	0.01510	0.01545	-0.01776	-0.03313
Procyon	cancrivorus	AMNH	14856	F	Car	Can	0.06287	0.03123	-0.01958	-0.06407
Procyon	lotor	AMNH	271481	M	Car	Can	-0.02797	-0.02373	-0.01693	-0.06137
Procyon	lotor	AMNH	67888	F	Car	Can	0.03345	0.01405	-0.02739	-0.03773
Procyon	pygmaeus	NMNH	108509	M	Car	Can	-0.09205	-0.02599	-0.04012	-0.04173
Procyon	pygmaeus	NMNH	108512	F	Car	Can	-0.06314	-0.01329	-0.03665	-0.03837
Pteronura	brasiliensis	AMNH	74432	F	Car	Can	0.02769	-0.09999	0.05472	0.02968
Pteronura	brasiliensis	AMNH	78513	M	Car	Can	0.05776	-0.03960	0.04426	0.01886
Speothos	venaticus	AMNH	175306	M	Car	Can	0.07311	-0.00653	0.03243	0.00823
Speothos	venaticus	AMNH	76806	F	Car	Can	0.04087	0.00002	0.00591	-0.02036
Spilogale	gracilis	NMNH	188462	F	Car	Can	0.01704	-0.02591	-0.08419	-0.04134
Spilogale	gracilis	NMNH	75644	M	Car	Can	0.02221	-0.04439	-0.07352	0.01207
Spilogale	putorius	AMNH	169985	F	Car	Can	0.06030	-0.05839	-0.01716	-0.01381
Spilogale	putorius	AMNH	35206	M	Car	Can	0.02991	-0.05755	-0.02944	-0.02330
Spilogale	pygmaea	AMNH	175183	M	Car	Can	0.07264	-0.04356	-0.00207	-0.01941
Spilogale	pygmaea	NMNH	523998	F	Car	Can	0.01750	-0.04466	-0.03116	-0.00325
Taxidea	taxus	AMNH	216484	F	Car	Can	0.06486	-0.02289	0.05137	-0.00755
Taxidea	taxus	AMNH	5495	M	Car	Can	0.06953	-0.01578	0.02029	0.00903
Tremarctos	ornatus	AMNH	67732	U	Car	Can	-0.02542	-0.06253	-0.02294	0.04231
Tremarctos	ornatus	FMNH	20311	F	Car	Can	-0.07439	-0.05695	-0.03781	0.03213
Tremarctos	ornatus	FMNH	85499	M	Car	Can	-0.05527	-0.04962	-0.02675	0.02715
Urocyon	cinereoargenteus	AMNH	19208	F	Car	Can	-0.03714	0.02827	0.01039	-0.04812
Urocyon	cinereoargenteus	AMNH	243098	M	Car	Can	-0.05724	0.02254	-0.01526	-0.03167
Urocyon	littoralis	NMNH	307395	M	Car	Can	-0.10996	-0.03277	-0.04727	0.00169
Urocyon	littoralis	NMNH	307396	F	Car	Can	-0.10150	-0.02351	-0.03952	-0.00581
Ursus	americanus	AMNH	148916	M	Car	Can	-0.04050	-0.04528	0.03051	0.04475
Ursus	americanus	AMNH	5044	F	Car	Can	-0.02310	-0.00960	0.00741	0.02799
Ursus	arctos	AMNH	85407	M	Car	Can	0.01021	0.00311	-0.04018	0.04226
Ursus	arctos	AMNH	90793	F	Car	Can	0.00090	0.00530	-0.02819	0.04387
Ursus	maritimus	AMNH	212876	F	Car	Can	-0.01545	0.00307	-0.02945	0.03473
Ursus	maritimus	AMNH	32680	M	Car	Can	-0.02620	-0.00595	-0.04448	0.04245
Ursus	thibetanus	AMNH	80248	F	Car	Can	-0.01481	0.00131	-0.03240	0.00376

Ursus	thibetanus	AMNH	84389	M	Car	Can	-0.00387	-0.02820	-0.01509	0.04081
Vormela	peregusna	AMNH	60103	U	Car	Can	0.08800	-0.06650	0.00026	0.04111
Vormela	peregusna	NMNH	154996	F	Car	Can	0.02399	-0.08450	-0.00400	0.03056
Vormela	peregusna	NMNH	200322	M	Car	Can	0.05604	-0.04967	-0.01766	0.01419
Vulpes	bengalensis	AMNH	54517	M	Car	Can	-0.03656	-0.00430	-0.03266	-0.04964
Vulpes	bengalensis	AMNH	54526	F	Car	Can	-0.06486	-0.01037	-0.03226	-0.03504
Vulpes	chama	NMNH	296103	M	Car	Can	-0.11504	-0.01250	-0.06189	0.01035
Vulpes	chama	NMNH	384117	F	Car	Can	-0.12536	-0.02566	-0.07888	-0.00016
Vulpes	lagopus	AMNH	40974	F	Car	Can	-0.05207	0.00342	-0.08005	-0.03394
Vulpes	lagopus	AMNH	40981	M	Car	Can	-0.05008	-0.02023	-0.08176	-0.01667
Vulpes	macrotis	AMNH	131834	F	Car	Can	-0.10616	-0.02834	-0.05122	-0.03094
Vulpes	macrotis	AMNH	22696	M	Car	Can	-0.07242	-0.01703	-0.06987	-0.03693
Vulpes	rueppellii	NMNH	401316	F	Car	Can	-0.12855	-0.03734	-0.07502	-0.01208
Vulpes	rueppellii	NMNH	476037	M	Car	Can	-0.13270	-0.04946	-0.06311	-0.00431
Vulpes	velox	AMNH	19019	F	Car	Can	-0.09218	0.00162	-0.05821	-0.02936
Vulpes	velox	AMNH	80127	M	Car	Can	-0.04258	0.01743	-0.05643	-0.03888
Vulpes	vulpes	AMNH	100079	F	Car	Can	-0.01677	0.03202	-0.06161	-0.02986
Vulpes	vulpes	AMNH	10717	M	Car	Can	-0.02635	-0.00839	-0.04975	-0.04068
Vulpes	zerda	NMNH	322047	M	Car	Can	-0.11429	-0.02512	-0.07081	-0.02759
Vulpes	zerda	NMNH	322050	F	Car	Can	-0.12318	-0.03028	-0.07168	-0.02617
Acinonyx	jubatus	FMNH	29634	F	Car	Fel	0.03926	0.08227	0.00915	-0.03800
Acinonyx	jubatus	FMNH	29635	M	Car	Fel	0.05737	0.08900	-0.00166	-0.02820
Arctictis	binturong	AMNH	106613	M	Car	Fel	0.00427	0.01345	0.02402	-0.01868
Arctictis	binturong	AMNH	106768	F	Car	Fel	0.01577	0.00510	0.03564	-0.04491
Arctictis	binturong	NMNH	259101	F	Car	Fel	0.02846	0.03772	0.04465	-0.03751
Arctictis	binturong	NMNH	49642	M	Car	Fel	0.02590	0.02562	0.04846	-0.03517
Arctogalidia	trivirgata	AMNH	107127	F	Car	Fel	-0.01855	0.02271	0.01174	-0.01341
Arctogalidia	trivirgata	AMNH	107128	M	Car	Fel	0.00651	0.01422	-0.00881	0.00164
Atilax	paludinosus	AMNH	116455	M	Car	Fel	-0.00474	-0.07276	-0.00129	0.03414
Atilax	paludinosus	AMNH	42058	F	Car	Fel	0.02029	-0.07015	0.01797	0.02392
Bdeogale	crassicauda	NMNH	182281	F	Car	Fel	-0.07119	-0.03875	0.00886	0.02668
Bdeogale	crassicauda	NMNH	318111	M	Car	Fel	-0.00579	-0.04015	0.02784	0.01732
Bdeogale	jacksoni	AMNH	33334	M	Car	Fel	-0.04559	-0.06041	0.04076	0.02722
Bdeogale	jacksoni	AMNH	83226	F	Car	Fel	-0.04185	-0.04882	0.00391	0.02491
Bdeogale	nigripes	AMNH	51580	F	Car	Fel	-0.06987	-0.05677	0.01662	0.01588
Bdeogale	nigripes	AMNH	51581	M	Car	Fel	-0.02934	-0.07222	0.04399	0.04626
Caracal	caracal	FMNH	32945	M	Car	Fel	0.02475	0.07161	0.00388	-0.06746
Caracal	caracal	FMNH	43292	M	Car	Fel	0.01372	0.03729	-0.03878	-0.00622
Caracal	caracal	FMNH	95922	F	Car	Fel	0.01877	0.06202	0.01337	-0.04138
Catopuma	badia	NMNH	198073	U	Car	Fel	0.06402	0.06397	-0.00257	-0.02925

Catopuma	temminckii	NMNH	240323	M	Car	Fel	0.02028	0.00618	-0.03182	0.00219
Catopuma	temminckii	NMNH	895843	F	Car	Fel	0.02193	0.00644	0.00465	-0.00142
Civettictis	civetta	AMNH	241391	M	Car	Fel	-0.04804	-0.02959	-0.00092	-0.01505
Civettictis	civetta	AMNH	6355	F	Car	Fel	-0.02872	-0.03180	-0.00623	-0.00740
Crocuta	crocuta	NMNH	182113	M	Car	Fel	0.02181	-0.02983	-0.05477	0.01968
Crocuta	crocuta	NMNH	429176	F	Car	Fel	0.04489	-0.01678	-0.07023	0.00728
Crossarchus	alexandri	AMNH	51651	F	Car	Fel	-0.04583	-0.01355	0.02932	-0.02203
Crossarchus	alexandri	AMNH	51653	M	Car	Fel	-0.04055	-0.02580	0.03218	-0.01518
Crossarchus	alexandri	NMNH	241124	F	Car	Fel	-0.01032	-0.03023	0.04380	-0.01843
Crossarchus	alexandri	NMNH	537892	M	Car	Fel	-0.07921	-0.02763	0.03826	-0.02403
Crossarchus	obscurus	AMNH	241395	F	Car	Fel	-0.04296	-0.00018	0.05383	-0.02733
Crossarchus	obscurus	AMNH	89396	M	Car	Fel	-0.05206	-0.03699	0.02286	-0.00815
Crossarchus	platycephalus	AMNH	236493	F	Car	Fel	-0.06352	-0.04835	0.01744	-0.00807
Crossarchus	platycephalus	AMNH	241397	M	Car	Fel	-0.03594	-0.03871	0.02893	-0.00627
Cryptoprocta	ferox	AMNH	188213	M	Car	Fel	0.06258	0.02925	0.04848	-0.00450
Cryptoprocta	ferox	FMNH	161707	F	Car	Fel	0.04541	0.02106	0.05688	0.00902
Cynictis	penicillata	NMNH	368474	M	Car	Fel	-0.08945	-0.06782	0.00547	-0.00716
Cynictis	penicillata	NMNH	368475	F	Car	Fel	-0.08017	-0.04180	0.03579	-0.00568
Cynogale	bennettii	AMNH	103993	M	Car	Fel	-0.03175	0.00882	-0.01000	-0.03795
Cynogale	bennettii	NMNH	145588	F	Car	Fel	-0.07929	-0.01955	0.00009	-0.00370
Dologale	dybowskii	AMNH	118954	M	Car	Fel	-0.03711	-0.03587	0.05037	-0.01191
Dologale	dybowskii	AMNH	169938	F	Car	Fel	-0.02373	-0.04940	0.02761	0.02274
Dologale	dybowskii	AMNH	51018	M	Car	Fel	-0.03153	-0.04113	0.04960	0.03301
Eupleres	goudotii	FMNH	30492	M	Car	Fel	-0.16223	0.02338	-0.01994	-0.00472
Felis	catus	NMNH	173336	F	Car	Fel	0.02763	0.05492	-0.00052	-0.01699
Felis	catus	NMNH	173337	M	Car	Fel	0.03530	0.05018	0.01585	-0.03671
Felis	chaus	AMNH	163170	M	Car	Fel	0.05007	0.01572	0.02313	-0.00062
Felis	chaus	AMNH	163172	F	Car	Fel	0.06960	0.04313	0.02401	-0.02912
Felis	manul	AMNH	186432	F	Car	Fel	0.12251	-0.00195	-0.03398	-0.03732
Felis	manul	FMNH	135737	M	Car	Fel	0.07313	0.04907	0.00478	-0.02463
Felis	margarita	FMNH	127295	M	Car	Fel	0.09104	0.08085	0.00071	-0.04355
Felis	margarita	FMNH	159995	F	Car	Fel	0.06194	0.10285	-0.00784	-0.05488
Felis	nigripes	AMNH	146838	M	Car	Fel	0.07285	0.07786	-0.05395	-0.04487
Felis	silvestris	AMNH	35236	M	Car	Fel	0.05316	0.02649	0.02428	-0.00725
Felis	silvestris	AMNH	35340	F	Car	Fel	0.07239	0.02804	-0.00645	-0.01958
Fossa	fossana	AMNH	100454	M	Car	Fel	-0.07752	-0.02078	0.03286	-0.02191
Fossa	fossana	AMNH	188209	F	Car	Fel	-0.09505	-0.01687	0.04922	-0.04216
Galerella	pulverulenta	AMNH	169039	F	Car	Fel	-0.04183	-0.05394	0.02097	0.00926
Galerella	pulverulenta	NMNH	424625	F	Car	Fel	-0.06959	-0.06188	0.04722	-0.00043
Galerella	pulverulenta	NMNH	452468	M	Car	Fel	-0.05946	-0.04462	0.02254	-0.00728

Galerella	sanguinea	AMNH	179306	F	Car	Fel	-0.03408	-0.03458	0.03417	-0.00145
Galerella	sanguinea	AMNH	179307	M	Car	Fel	-0.05845	-0.04030	0.03879	0.00961
Galerella	sanguinea	NMNH	424623	M	Car	Fel	-0.06050	-0.04135	0.02608	0.02560
Galerella	sanguinea	NMNH	469878	F	Car	Fel	-0.05726	-0.07051	0.02896	0.03534
Galidia	elegans	AMNH	100465	F	Car	Fel	0.01221	-0.00578	0.02665	0.01474
Galidia	elegans	AMNH	100466	M	Car	Fel	0.04069	-0.00654	0.00257	0.02812
Galidia	elegans	FMNH	156665	M	Car	Fel	-0.00417	-0.01749	0.01750	0.00827
Galidia	elegans	FMNH	173110	F	Car	Fel	-0.00281	-0.00851	0.03448	-0.00352
Galidictis	fasciata	FMNH	156549	F	Car	Fel	0.04013	0.00857	0.00783	0.01334
Galidictis	fasciata	FMNH	156652	M	Car	Fel	0.08912	0.05859	0.02972	0.00983
Genetta	abyssinica	FMNH	27218	M	Car	Fel	-0.04600	0.00099	0.03268	-0.02867
Genetta	abyssinica	FMNH	80818	F	Car	Fel	-0.09398	0.01092	0.04476	-0.04748
Genetta	angolensis	AMNH	83740	F	Car	Fel	-0.03548	0.00496	0.07523	-0.04278
Genetta	angolensis	AMNH	83744	M	Car	Fel	-0.03294	0.00166	0.05904	-0.04475
Genetta	genetta	NMNH	253507	M	Car	Fel	-0.08675	-0.02041	0.01602	-0.01980
Genetta	genetta	NMNH	255714	F	Car	Fel	-0.08948	-0.01759	0.02540	-0.02556
Genetta	maculata	AMNH	169068	M	Car	Fel	-0.02579	-0.02548	0.05416	-0.03009
Genetta	maculata	AMNH	241388	F	Car	Fel	-0.01916	0.01644	0.03815	-0.03560
Genetta	servalina	AMNH	51566	F	Car	Fel	-0.08137	-0.02288	0.02789	-0.01832
Genetta	servalina	AMNH	51569	M	Car	Fel	-0.06435	-0.03201	0.02401	-0.02158
Genetta	thierryi	NMNH	450968	M	Car	Fel	-0.06979	-0.01697	0.03777	-0.01186
Genetta	thierryi	NMNH	450969	F	Car	Fel	-0.07808	-0.00984	0.02673	-0.01833
Genetta	tigrina	AMNH	169060	F	Car	Fel	-0.03772	-0.03307	0.03002	-0.01911
Genetta	victoriae	AMNH	51429	F	Car	Fel	-0.06326	-0.00609	0.03443	-0.03115
Genetta	victoriae	AMNH	51430	M	Car	Fel	0.00213	0.01714	0.06235	-0.04077
Helogale	hirtula	AMNH	179094	M	Car	Fel	0.02385	-0.02056	0.04758	0.00682
Helogale	hirtula	AMNH	179109	F	Car	Fel	-0.03000	-0.05796	0.03839	0.01041
Helogale	parvula	AMNH	55868	M	Car	Fel	0.00560	-0.03989	0.03594	0.00630
Helogale	parvula	AMNH	83823	F	Car	Fel	-0.02147	-0.04783	0.06215	-0.02207
Hemigalus	derbyanus	AMNH	102450	M	Car	Fel	-0.09620	-0.01027	0.02061	-0.03609
Hemigalus	derbyanus	AMNH	32635	F	Car	Fel	-0.10725	-0.01790	0.01209	-0.02516
Hemigalus	derbyanus	NMNH	121647	F	Car	Fel	-0.11516	-0.02377	-0.00461	-0.02224
Hemigalus	derbyanus	NMNH	121648	M	Car	Fel	-0.10976	-0.01440	0.00909	-0.01265
Herpestes	brachyurus	AMNH	103988	M	Car	Fel	-0.02094	-0.04762	0.01862	0.01957
Herpestes	brachyurus	FMNH	88604	F	Car	Fel	-0.03778	-0.05019	0.02654	0.04221
Herpestes	edwardsi	AMNH	163178	M	Car	Fel	-0.01599	-0.03149	0.03073	0.00976
Herpestes	edwardsi	AMNH	70232	F	Car	Fel	-0.00243	-0.02082	0.02257	-0.00083
Herpestes	fuscus	AMNH	240856	M	Car	Fel	-0.00533	-0.02823	0.04949	0.02909
Herpestes	fuscus	FMNH	95035	F	Car	Fel	-0.03354	-0.03595	0.02096	0.02502
Herpestes	ichneumon	AMNH	82778	F	Car	Fel	-0.03105	-0.05374	0.10286	0.00659

Herpestes	ichneumon	AMNH	82779	M	Car	Fel	-0.05354	-0.08989	0.07963	0.01955
Herpestes	javanicus	AMNH	239630	F	Car	Fel	-0.02085	-0.03629	0.01527	0.01594
Herpestes	javanicus	AMNH	239631	M	Car	Fel	-0.04029	-0.05401	0.02788	0.01537
Herpestes	javanicus	FMNH	75804	F	Car	Fel	-0.05307	-0.05664	0.03598	0.00267
Herpestes	javanicus	FMNH	75805	M	Car	Fel	-0.05869	-0.05201	0.00821	0.01336
Herpestes	naso	AMNH	51621	M	Car	Fel	0.00721	-0.06542	0.04939	0.03922
Herpestes	naso	AMNH	51624	F	Car	Fel	-0.02388	-0.08099	0.04704	0.04839
Herpestes	semitorquatus	AMNH	103746	M	Car	Fel	-0.01077	-0.03404	0.02601	0.02608
Herpestes	semitorquatus	AMNH	108803	F	Car	Fel	0.01037	-0.03245	0.03434	0.01011
Herpestes	urva	AMNH	43130	M	Car	Fel	-0.02198	-0.05229	0.00573	0.02411
Herpestes	urva	AMNH	59324	F	Car	Fel	-0.04594	-0.04860	-0.00572	0.02547
Herpestes	vitticollis	AMNH	163180	M	Car	Fel	0.00925	-0.04008	0.02880	0.01860
Herpestes	vitticollis	AMNH	163182	F	Car	Fel	-0.01878	-0.03837	0.00703	0.00224
Hyaena	brunnea	AMNH	83588	F	Car	Fel	0.07333	0.01597	-0.05046	-0.03473
Hyaena	brunnea	AMNH	83590	M	Car	Fel	0.07861	0.00239	-0.05180	-0.03888
Hyaena	hyaena	AMNH	179144	F	Car	Fel	-0.00546	-0.03621	-0.01738	-0.03202
Hyaena	hyaena	FMNH	15999	M	Car	Fel	-0.01997	-0.00960	-0.02783	-0.01935
Ichneumia	albicauda	AMNH	113792	F	Car	Fel	-0.05498	-0.05853	0.06509	0.01236
Ichneumia	albicauda	AMNH	33315	M	Car	Fel	-0.05990	-0.04739	0.02595	-0.00177
Leopardus	colocolo	AMNH	133977	M	Car	Fel	0.08257	0.06903	0.02467	-0.04969
Leopardus	colocolo	AMNH	76150	M	Car	Fel	0.13913	0.05185	0.00524	-0.05310
Leopardus	geoffroyi	AMNH	39004	M	Car	Fel	0.09603	0.06108	0.01197	-0.03837
Leopardus	geoffroyi	AMNH	41551	F	Car	Fel	0.06232	0.03140	0.00871	-0.03917
Leopardus	guigna	AMNH	33283	M	Car	Fel	0.05291	0.02222	0.07744	-0.01651
Leopardus	guigna	AMNH	93323	F	Car	Fel	0.09020	0.04951	0.04265	-0.03070
Leopardus	pardalis	AMNH	24827	F	Car	Fel	0.09365	0.01659	0.02676	0.00891
Leopardus	pardalis	AMNH	25007	M	Car	Fel	0.10963	0.00637	0.02498	-0.03325
Leopardus	tigrinus	AMNH	181498	M	Car	Fel	0.07649	0.06478	0.01592	-0.01950
Leopardus	tigrinus	AMNH	80396	F	Car	Fel	0.06834	0.08722	0.05208	-0.04729
Leopardus	wiedii	AMNH	130109	F	Car	Fel	0.03479	0.00829	0.01478	-0.01876
Leopardus	wiedii	AMNH	70325	M	Car	Fel	0.03344	0.02781	0.03096	-0.06086
Leptailurus	serval	AMNH	239583	F	Car	Fel	0.07369	0.06107	-0.02204	-0.03250
Leptailurus	serval	AMNH	55041	M	Car	Fel	0.09895	0.06445	0.04907	-0.04391
Liberiictis	kuhni	NMNH	481997	M	Car	Fel	-0.07613	0.00405	0.00948	-0.02806
Liberiictis	kuhni	NMNH	481998	F	Car	Fel	-0.07324	0.00532	-0.00311	-0.02709
Lynx	canadensis	AMNH	2850	M	Car	Fel	0.09464	0.03910	0.02505	-0.03413
Lynx	canadensis	AMNH	2851	M	Car	Fel	0.08595	0.03020	0.01151	-0.02003
Lynx	lynx	NMNH	198468	F	Car	Fel	0.03447	0.04077	0.00867	-0.01856
Lynx	pardinus	AMNH	169492	M	Car	Fel	0.07233	0.03735	0.02821	-0.03671
Lynx	pardinus	NMNH	152619	M	Car	Fel	0.04701	0.03414	0.02926	-0.02596

Lynx	rufus	AMNH	16463	M	Car	Fel	0.08358	0.05335	-0.00047	-0.01833
Lynx	rufus	AMNH	60564	F	Car	Fel	0.08428	0.08420	0.06083	-0.02680
Mungos	mungo	AMNH	161138	F	Car	Fel	-0.03634	-0.01995	0.02166	-0.03304
Mungos	mungo	AMNH	185177	M	Car	Fel	-0.02118	-0.01887	0.03373	-0.00541
Mungotictis	decemlineata	FMNH	176128	M	Car	Fel	-0.00051	-0.00531	0.02815	-0.00352
Mungotictis	decemlineata	FMNH	184087	F	Car	Fel	-0.00843	-0.00368	0.02595	-0.02834
Nandinia	binotata	AMNH	236490	F	Car	Fel	0.01728	0.00893	0.02867	0.00346
Nandinia	binotata	AMNH	36012	M	Car	Fel	0.06404	0.01216	0.05848	-0.01313
Neofelis	nebulosa	AMNH	35273	F	Car	Fel	0.02689	0.03712	-0.00263	0.00552
Neofelis	nebulosa	AMNH	35808	M	Car	Fel	0.11554	0.03245	0.00187	-0.01340
Paguma	larvata	AMNH	103989	F	Car	Fel	-0.01135	0.00263	0.03550	-0.02013
Paguma	larvata	AMNH	163604	M	Car	Fel	0.01279	0.02585	0.06255	-0.02399
Panthera	leo	AMNH	52073	F	Car	Fel	0.12537	0.02542	-0.02209	0.01797
Panthera	leo	AMNH	52082	M	Car	Fel	0.14082	0.02346	-0.02447	0.01623
Panthera	onca	AMNH	35360	F	Car	Fel	0.11113	0.03337	-0.05860	0.00258
Panthera	onca	AMNH	35529	M	Car	Fel	0.10885	0.03942	-0.01190	-0.00080
Panthera	onca	AMNH	98679	F	Car	Fel	0.08143	0.01170	0.00686	-0.00210
Panthera	pardus	AMNH	35408	F	Car	Fel	0.09540	0.02589	-0.03027	0.00097
Panthera	pardus	AMNH	35522	M	Car	Fel	0.10598	0.03469	-0.00309	0.02639
Panthera	tigris	AMNH	35444	M	Car	Fel	0.11294	0.02744	-0.01835	0.00045
Panthera	tigris	AMNH	35756	F	Car	Fel	0.11862	0.01597	-0.02479	-0.01503
Paracynictis	selousi	NMNH	368483	F	Car	Fel	-0.09664	-0.03936	0.01295	-0.02783
Paracynictis	selousi	NMNH	368484	M	Car	Fel	-0.07734	-0.01734	0.01112	-0.00196
Paradoxurus	hermaphroditus	AMNH	102038	F	Car	Fel	-0.02699	-0.01341	0.05726	-0.01589
Paradoxurus	hermaphroditus	AMNH	103341	F	Car	Fel	0.00126	0.00624	0.02840	-0.00998
Paradoxurus	hermaphroditus	AMNH	103342	M	Car	Fel	-0.01333	0.02768	0.06172	-0.02041
Paradoxurus	hermaphroditus	AMNH	163599	M	Car	Fel	-0.01158	0.00891	0.00803	-0.01587
Paradoxurus	zeylonensis	NMNH	277230	M	Car	Fel	-0.01655	0.01523	0.00399	-0.01429
Pardofelis	marmorata	AMNH	102844	M	Car	Fel	0.03484	-0.02095	0.04586	0.01243
Pardofelis	marmorata	AMNH	35399	F	Car	Fel	0.00793	-0.01719	0.09732	-0.03266
Pardofelis	marmorata	FMNH	60020	F	Car	Fel	0.03571	0.02739	-0.00315	-0.04627
Poiana	richardsonii	AMNH	114209	F	Car	Fel	-0.09435	-0.02535	0.02738	-0.01698
Poiana	richardsonii	AMNH	51439	M	Car	Fel	-0.08262	-0.01045	0.01617	-0.06547
Prionailurus	bengalensis	AMNH	87352	F	Car	Fel	0.08437	0.03768	0.06023	-0.05158
Prionailurus	bengalensis	AMNH	87355	M	Car	Fel	0.08192	0.05687	0.04199	-0.04113
Prionailurus	planiceps	AMNH	35398	F	Car	Fel	0.08123	-0.00161	0.07941	-0.03632
Prionailurus	planiceps	FMNH	127432	M	Car	Fel	0.01437	0.00737	0.06306	-0.01567
Prionailurus	rubiginosus	FMNH	95037	M	Car	Fel	0.05319	0.07507	0.03291	-0.03621
Prionailurus	rubiginosus	FMNH	95137	F	Car	Fel	0.02887	0.02088	0.04661	-0.00467
Prionailurus	viverrinus	AMNH	11093	F	Car	Fel	0.10696	0.02326	0.07276	-0.02070

Prionailurus	viverrinus	AMNH	70128	M	Car	Fel	0.07959	-0.00313	0.04732	0.00396
Prionodon	linsang	NMNH	303036	M	Car	Fel	-0.08410	-0.00681	0.04111	-0.01569
Prionodon	linsang	NMNH	395048	F	Car	Fel	-0.10562	-0.00478	-0.01006	-0.00134
Prionodon	pardicolor	NMNH	308234	M	Car	Fel	-0.09664	-0.03375	-0.01907	-0.01515
Profelis	aurata	FMNH	121528	F	Car	Fel	0.05009	0.00310	-0.02423	-0.01209
Proteles	cristata	AMNH	169089	F	Car	Fel	-0.00088	0.06264	0.02795	-0.05794
Proteles	cristata	AMNH	81044	M	Car	Fel	0.02833	0.04685	0.02068	-0.04635
Puma	concolor	AMNH	1339	F	Car	Fel	0.12609	0.06406	0.02394	-0.01076
Puma	concolor	AMNH	1340	M	Car	Fel	0.09215	0.01352	0.00957	0.00812
Puma	yagouaroundi	AMNH	147577	F	Car	Fel	0.06843	0.01886	0.03921	-0.02014
Puma	yagouaroundi	AMNH	178705	M	Car	Fel	0.10484	0.03667	0.06170	-0.03493
Puma	yagouaroundi	NMNH	35645	M	Car	Fel	0.03527	0.01658	0.06770	-0.00079
Puma	yagouaroundi	NMNH	44600	F	Car	Fel	0.03526	0.02359	0.04209	-0.01600
Rhynchogale	melleri	NMNH	367378	M	Car	Fel	-0.08709	-0.00887	0.04207	-0.02911
Salanoia	concolor	FMNH	33946	U	Car	Fel	-0.01316	-0.02162	0.02332	-0.01751
Suricata	suricatta	AMNH	83645	F	Car	Fel	-0.01926	-0.03189	0.02368	0.02000
Suricata	suricatta	AMNH	83646	M	Car	Fel	0.00252	-0.02936	0.02183	0.02058
Uncia	uncia	NMNH	176048	F	Car	Fel	0.05492	0.01486	0.00109	0.00462
Uncia	uncia	NMNH	589696	M	Car	Fel	-0.03468	0.07324	-0.02105	-0.01923
Viverra	megaspila	AMNH	31287	M	Car	Fel	-0.05773	-0.01139	0.00367	-0.01683
Viverra	megaspila	NMNH	308232	M	Car	Fel	-0.06796	-0.02655	0.00325	0.00061
Viverra	megaspila	NMNH	308233	F	Car	Fel	-0.08665	-0.03687	0.01982	-0.02102
Viverra	tangalunga	AMNH	152883	M	Car	Fel	-0.05959	-0.01314	0.03216	-0.02693
Viverra	tangalunga	AMNH	207581	F	Car	Fel	-0.05231	-0.03262	0.04246	-0.02157
Viverra	zibetha	AMNH	87366	F	Car	Fel	-0.09740	-0.04104	-0.02707	-0.00039
Viverra	zibetha	AMNH	87367	M	Car	Fel	-0.07498	-0.04438	0.02079	-0.01386
Viverricula	indica	AMNH	59946	F	Car	Fel	-0.08179	-0.06149	0.03500	-0.00619
Viverricula	indica	AMNH	59952	M	Car	Fel	-0.05989	-0.04192	0.06919	-0.01722
Antechinomys	laniger	AMNH	196833	F	Das	Das	-0.06249	0.15259	0.02140	0.04255
Antechinus	flavipes	AMNH	196699	M	Das	Das	-0.07566	0.12757	-0.01019	0.02523
Antechinus	flavipes	AMNH	196703	F	Das	Das	-0.08450	0.13174	-0.02641	0.01170
Antechinus	godmani	AMNH	183380	M	Das	Das	-0.08227	0.07996	0.04080	0.04617
Antechinus	godmani	AMNH	183382	F	Das	Das	-0.12017	0.08322	0.00120	0.02558
Antechinus	leo	AMNH	154253	M	Das	Das	-0.04714	0.09733	0.04541	0.06142
Antechinus	leo	AMNH	154254	F	Das	Das	-0.05716	0.10944	0.04093	0.04292
Antechinus	stuartii	AMNH	160404	F	Das	Das	-0.06977	0.11614	0.03079	0.03494
Antechinus	stuartii	AMNH	160405	M	Das	Das	-0.05615	0.10573	0.02501	0.03427
Antechinus	swainsonii	AMNH	220073	M	Das	Das	-0.08282	0.10082	0.01623	0.04444
Antechinus	swainsonii	AMNH	65720	F	Das	Das	-0.11756	0.07334	-0.00693	0.07134
Dasycercus	cristicauda	AMNH	15009	F	Das	Das	0.04348	0.09802	-0.00371	0.13054

Dasyuroides	byrnei	AMNH	257603	M	Das	Das	0.05576	0.13059	0.00116	0.09961
Dasyurus	albopunctatus	AMNH	109420	F	Das	Das	-0.04874	0.05623	-0.01359	0.03972
Dasyurus	albopunctatus	AMNH	109421	M	Das	Das	-0.01800	0.15811	-0.04253	0.04696
Dasyurus	geoffroii	AMNH	196837	M	Das	Das	0.03954	0.16091	0.01145	0.01786
Dasyurus	geoffroii	FMNH	35329	F	Das	Das	-0.08047	0.05203	0.00806	0.06036
Dasyurus	hallucatus	AMNH	154525	F	Das	Das	-0.08298	0.06135	0.01813	0.04834
Dasyurus	hallucatus	AMNH	154531	M	Das	Das	-0.02681	0.07580	0.05019	0.04938
Dasyurus	maculatus	AMNH	183379	M	Das	Das	-0.03210	0.04763	0.02368	0.06669
Dasyurus	viverrinus	AMNH	35688	F	Das	Das	-0.02693	0.11491	0.04240	0.07653
Dasyurus	viverrinus	AMNH	65690	M	Das	Das	-0.08645	0.05770	0.03342	0.06928
Murexechinus	melanurus	AMNH	109819	M	Das	Das	-0.07154	0.07876	0.01205	0.04740
Murexechinus	melanurus	AMNH	109828	F	Das	Das	-0.07540	0.10057	0.01323	0.03154
Murexechinus	melanurus	FMNH	128351	M	Das	Das	-0.10770	0.04519	-0.01095	0.06852
Murexia	longicaudata	AMNH	194711	F	Das	Das	-0.09438	0.09316	0.00790	0.04210
Murexia	longicaudata	AMNH	194712	M	Das	Das	-0.11536	0.06536	-0.00264	0.01565
Myoictis	melas	AMNH	101976	F	Das	Das	-0.05740	0.08386	0.01410	-0.00966
Myoictis	melas	AMNH	152003	M	Das	Das	-0.06339	0.08999	-0.00163	0.01739
Myrmecobius	fasciatus	AMNH	155330	M	Das	Das	-0.12624	0.09499	-0.04729	0.00308
Neophascogale	lorentzi	AMNH	152022	F	Das	Das	-0.06594	0.10457	0.00056	0.02169
Neophascogale	lorentzi	AMNH	152024	M	Das	Das	-0.07650	0.11704	-0.01238	0.01980
Paramurexia	rothschildi	AMNH	108106	M	Das	Das	-0.10027	0.08482	0.01478	0.01382
Phascogale	calura	AMNH	196687	F	Das	Das	-0.04476	0.15830	0.01020	0.05332
Phascogale	calura	FMNH	36052	M	Das	Das	-0.05801	0.13688	-0.01311	0.03227
Phascolosorex	doriae	AMNH	151991	F	Das	Das	-0.09397	0.07145	0.02923	0.03890
Phascolosorex	doriae	AMNH	151992	M	Das	Das	-0.09886	0.06930	0.00520	0.04369
Phascolosorex	dorsalis	AMNH	109781	F	Das	Das	-0.10278	0.07102	0.00944	0.04570
Phascolosorex	dorsalis	AMNH	109784	M	Das	Das	-0.12325	0.04880	-0.02463	0.04663
Phascomurexia	naso	AMNH	109809	F	Das	Das	-0.10862	0.05957	0.01142	0.06345
Phascomurexia	naso	AMNH	109814	M	Das	Das	-0.12030	0.06569	0.00247	0.04230
Phascomurexia	naso	AMNH	190876	M	Das	Das	-0.11130	0.05566	0.01813	0.03740
Phascomurexia	naso	AMNH	190877	F	Das	Das	-0.13031	0.05289	0.00414	0.04117
Pseudantechinus	macdonnellensis	AMNH	162569	F	Das	Das	-0.07418	0.12671	0.03744	0.07142
Pseudantechinus	macdonnellensis	AMNH	196692	M	Das	Das	-0.04761	0.12368	0.03681	0.08055
Pseudantechinus	ningbing	FMNH	119799	M	Das	Das	-0.05839	0.12667	0.03668	0.08350
Sarcophilus	harrisii	AMNH	65670	M	Das	Das	0.14268	0.12697	-0.06705	0.11094
Sarcophilus	harrisii	AMNH	65673	F	Das	Das	0.09570	0.14647	-0.12384	0.13591
Sminthopsis	butleri	AMNH	196804	F	Das	Das	-0.06894	0.13704	0.02671	0.03344
Sminthopsis	crassicaudata	FMNH	104788	F	Das	Das	-0.09151	0.12225	0.02432	0.03413
Sminthopsis	gilberti	FMNH	129557	M	Das	Das	-0.08893	0.09739	-0.00422	0.02929
Sminthopsis	griseoventer	FMNH	129559	F	Das	Das	-0.09393	0.11301	0.02216	0.02929

Sminthopsis	macroura	AMNH	108934	M	Das	Das	-0.06210	0.09736	0.01937	0.04530
Sminthopsis	macroura	AMNH	196832	F	Das	Das	-0.07482	0.10991	0.01709	0.05414
Sminthopsis	virginiae	AMNH	105827	M	Das	Das	-0.06645	0.10706	0.01737	0.04212
Sminthopsis	virginiae	AMNH	105828	F	Das	Das	-0.07888	0.10837	0.00303	0.01970
Thylacinus	cynocephalus	AMNH	144316	M	Das	Das	0.09877	0.20372	-0.07923	0.09728

Table S4.1: Catalogue, gender, clade assignments, and PC scores for the Carnivora and Dasyuromorphia

Carnivora

V1	V2	V3	V4	V5	V6	V7	V8	V9	V10	V11	V12
1	-0.2992492	0.63870535	-0.2862051	-0.4979219	-0.1281616	0.00024823	0.10083374	-0.0231893	0.24477162	0.26969917	-0.5311919
-0.2992492	1	-0.1188855	-0.4145428	-0.0611179	0.2484462	0.26140408	0.16821205	0.0711545	-0.2455706	-0.3943912	-0.2005415
0.63870535	-0.1188855	1	-0.4035578	-0.4877397	-0.1402253	0.06503904	0.28443427	-0.1586003	0.16268321	0.17204525	-0.485315
-0.2862051	-0.4145428	-0.4035578	1	0.50994056	-0.198697	-0.4098315	-0.3746283	-0.216524	-0.0467277	-0.0015011	0.41288137
-0.4979219	-0.0611179	-0.4877397	0.50994056	1	0.11329222	-0.1750422	-0.2782171	-0.0963139	-0.4553826	-0.4260025	0.4282811
-0.1281616	0.2484462	-0.1402253	-0.198697	0.11329222	1	0.51255025	-0.0164437	-0.1094904	-0.5809983	-0.5033122	-0.0695275
0.00024823	0.26140408	0.06503904	-0.4098315	-0.1750422	0.51255025	1	0.35212634	0.08708873	-0.4377832	-0.4888521	-0.180153
0.10083374	0.16821205	0.28443427	-0.3746283	-0.2782171	-0.0164437	0.35212634	1	-0.0114068	-0.1509582	-0.2548228	-0.2142811
-0.0231893	0.0711545	-0.1586003	-0.216524	-0.0963139	-0.1094904	0.08708873	-0.0114068	1	-0.0202555	-0.2093818	-0.164665
0.24477162	-0.2455706	0.16268321	-0.0467277	-0.4553826	-0.5809983	-0.4377832	-0.1509582	-0.0202555	1	0.75098541	-0.2722171
0.26969917	-0.3943912	0.17204525	-0.0015011	-0.4260025	-0.5033122	-0.4888521	-0.2548228	-0.2093818	0.75098541	1	-0.197385
-0.5311919	-0.2005415	-0.485315	0.41288137	0.4282811	-0.0695275	-0.180153	-0.2142811	-0.164665	-0.2722171	-0.197385	1

Caniformia

V1	V2	V3	V4	V5	V6	V7	V8	V9	V10	V11	V12
1	-0.2424308	0.62813722	-0.2174384	-0.5054734	-0.1432131	0.04660494	0.16362619	-0.0200064	0.2025615	0.14492507	-0.4892051
-0.2424308	1	-0.1020373	-0.4597649	-0.0796055	0.25937528	0.2812002	0.12906737	0.13240311	-0.2110468	-0.3845462	-0.2975151
0.62813722	-0.1020373	1	-0.3662119	-0.5359738	-0.0816793	0.12270603	0.34954784	-0.1314189	0.14798554	0.06090248	-0.4837692
-0.2174384	-0.4597649	-0.3662119	1	0.51986931	-0.1690101	-0.470542	-0.4300737	-0.2949603	-0.0105749	0.11089659	0.33257197
-0.5054734	-0.0796055	-0.5359738	0.51986931	1	0.13872509	-0.2616683	-0.3510579	-0.1183623	-0.4040005	-0.3552384	0.41575303
-0.1432131	0.25937528	-0.0816793	-0.1690101	0.13872509	1	0.44601043	-0.0100103	-0.2279623	-0.6210715	-0.5222749	0.01050512
0.04660494	0.2812002	0.12270603	-0.470542	-0.2616683	0.44601043	1	0.4009936	0.08378067	-0.384193	-0.4836763	-0.2058721
0.16362619	0.12906737	0.34954784	-0.4300737	-0.3510579	-0.0100103	0.4009936	1	0.01887326	-0.1336097	-0.274322	-0.2769302
-0.0200064	0.13240311	-0.1314189	-0.2949603	-0.1183623	-0.2279623	0.08378067	0.01887326	1	0.05265395	-0.2003177	-0.189321
0.2025615	-0.2110468	0.14798554	-0.0105749	-0.4040005	-0.6210715	-0.384193	-0.1336097	0.05265395	1	0.69545651	-0.2772597
0.14492507	-0.3845462	0.06090248	0.11089659	-0.3552384	-0.5222749	-0.4836763	-0.274322	-0.2003177	0.69545651	1	-0.0558296
-0.4892051	-0.2975151	-0.4837692	0.33257197	0.41575303	0.01050512	-0.2058721	-0.2769302	-0.189321	-0.2772597	-0.0558296	1

Feliformia

V1	V2	V3	V4	V5	V6	V7	V8	V9	V10	V11	V12
1	-0.3485954	0.65705845	-0.3503736	-0.4630433	-0.280031	-0.1078026	0.04366202	-0.0406053	0.29912895	0.38727538	-0.5660732
-0.3485954	1	-0.1336391	-0.3961912	-0.0719085	0.37564988	0.26678375	0.22132731	-0.0203946	-0.2844351	-0.3948768	-0.1612962
0.65705845	-0.1336391	1	-0.4738108	-0.4011564	-0.3015674	-0.0289182	0.20442037	-0.1998027	0.16603857	0.29200477	-0.5371785
-0.3503736	-0.3961912	-0.4738108	1	0.50418558	-0.0855886	-0.2595558	-0.3237143	-0.0843552	-0.143116	-0.1434517	0.46602694
-0.4630433	-0.0719085	-0.4011564	0.50418558	1	0.20144217	-0.0251752	-0.2158398	-0.1115492	-0.5270365	-0.4924488	0.435678
-0.280031	0.37564988	-0.3015674	-0.0855886	0.20144217	1	0.57576752	0.04195798	0.06662752	-0.6262775	-0.7180244	0.157533
-0.1078026	0.26678375	-0.0289182	-0.2595558	-0.0251752	0.57576752	1	0.29422649	0.14967864	-0.5157071	-0.5636001	-0.0468852
0.04366202	0.22132731	0.20442037	-0.3237143	-0.2158398	0.04195798	0.29422649	1	-0.1489993	-0.1564398	-0.1774628	-0.2097132
-0.0406053	-0.0203946	-0.1998027	-0.0843552	-0.1115492	0.06662752	0.14967864	-0.1489993	1	-0.0396463	-0.164305	-0.0953556
0.29912895	-0.2844351	0.16603857	-0.143116	-0.5270365	-0.6262775	-0.5157071	-0.1564398	-0.0396463	1	0.8170782	-0.3505168
0.38727538	-0.3948768	0.29200477	-0.1434517	-0.4924488	-0.7180244	-0.5636001	-0.1774628	-0.164305	0.8170782	1	-0.3551882
-0.5660732	-0.1612962	-0.5371785	0.46602694	0.435678	0.157533	-0.0468852	-0.2097132	-0.0953556	-0.3505168	-0.3551882	1

Dasyuromorphia

V1	V2	V3	V4	V5	V6	V7	V8	V9	V10	V11	V12
1	-0.2390387	0.73950053	-0.4234103	-0.5817207	-0.0610261	-0.280018	0.2742501	0.34815173	0.20393246	0.05430807	-0.5014079
-0.2390387	1	-0.2697289	-0.3009201	-0.1786838	0.02216136	0.29524953	0.08184344	0.04943511	-0.1594155	-0.2525818	-0.124949
0.73950053	-0.2697289	1	-0.3019245	-0.3899424	-0.3769307	-0.3040188	0.44501883	0.30961329	0.23102053	0.07072995	-0.4429252
-0.4234103	-0.3009201	-0.3019245	1	0.43549045	-0.2489683	-0.1409371	-0.2326391	-0.6041336	-0.0062529	0.21707887	0.36106823
-0.5817207	-0.1786838	-0.3899424	0.43549045	1	0.15491556	0.31371031	-0.2373094	-0.2893505	-0.4775267	-0.3816422	0.46868366
-0.0610261	0.02216136	-0.3769307	-0.2489683	0.15491556	1	0.40993826	-0.5382481	0.0570743	-0.4544631	-0.3735727	0.02518129
-0.280018	0.29524953	-0.3040188	-0.1409371	0.31371031	0.40993826	1	-0.1658387	-0.0232405	-0.6297471	-0.6796214	0.2277408
0.2742501	0.08184344	0.44501883	-0.2326391	-0.2373094	-0.5382481	-0.1658387	1	0.38034962	0.05786751	-0.1869183	-0.1729371
0.34815173	0.04943511	0.30961329	-0.6041336	-0.2893505	0.0570743	-0.0232405	0.38034962	1	0.03700094	-0.3541951	-0.3287815
0.20393246	-0.1594155	0.23102053	-0.0062529	-0.4775267	-0.4544631	-0.6297471	0.05786751	0.03700094	1	0.75500043	-0.535766
0.05430807	-0.2525818	0.07072995	0.21707887	-0.3816422	-0.3735727	-0.6796214	-0.1869183	-0.3541951	0.75500043	1	-0.2876485
-0.5014079	-0.124949	-0.4429252	0.36106823	0.46868366	0.02518129	0.2277408	-0.1729371	-0.3287815	-0.535766	-0.2876485	1

Table S4.2: Vector congruence correlation coefficient matrices for all taxa groupings

Landmarks	Model 1	Model 2	Model 3	Model 4	Model 5	Model 6	Model 7	Model 8
Anterior edge of dentary	1	1	1	1	1	1	1	1
Posterior edge of canine	1	1	1	1	1	1	1	1
Ventral base of dentary suture	1	1	1	1	1	1	1	1
Ventral base of the ramus	1	1	1	4	1	4	1	5
Dorsal base of the ramus	1	1	1	4	1	4	1	5
Posterior edge of angular	1	2	2	2	2	2	2	2
Concave point between angular and condyloid	1	2	2	2	2	2	2	2
Distal edge of condyloid	1	2	3	3	2	2	3	3
Proximal edge of condyloid	1	2	3	3	2	2	3	3
Concave point between condyloid and coronoid	1	2	2	2	3	3	4	4
Dorsal edge of coronoid	1	2	2	2	3	3	4	4
Anterior border of the masseteric fosa	NA	NA	NA	NA	NA	NA	NA	NA

Table S4.3: Landmark partitions for each modularity hypothesis

BIBLIOGRAPHY

Adams, D. C. 2014: Quantifying and comparing phylogenetic evolutionary rates for shape and other high-dimensional phenotypic data. Systematic biology 63:166–177.

Adams, D. C., and E. Otárola-Castillo. 2013: Geomorph: an R Package for the Collection and Analysis of Geometric Morphometric Shape Data. Methods in Ecology and Evolution 4:393–399.

Adams, D. C., and R. N. Felice. 2014: Assessing trait covariation and morphological integration on phylogenies using evolutionary covariance matrices. PloS one 9:e94335.

Albertson, R. C., J. T. Streelman, T. D. Kocher, and P. C. Yelick. 2005: Integration and evolution of the cichlid mandible: the molecular basis of alternate feeding strategies. Proceedings of the National Academy of Sciences of the United States of America 102:16287–16292.

Anderson, P. S. L. 2009: The effects of trapping and blade angle of notched dentitions on fracture of biological tissues. The Journal of experimental biology 212:3627–3632.

Anderson, P. S. L., and M. LaBarbera. 2008: Functional consequences of tooth design: effects of blade shape on energetics of cutting. The Journal of experimental biology 211:3619–3626.

Anderson, P. S. L., P. G. Gill, and E. J. Rayfield. 2011: Modeling the effects of cingula structure on strain patterns and potential fracture in tooth enamel. Journal of morphology 272:50–65.

Anderson, P. S. L., S. Renaud, and E. J. Rayfield. 2014: Adaptive plasticity in the mouse mandible. BMC evolutionary biology 14:85.

Anthwal, N., and A. S. Tucker. 2012: Molecular biology of the mammalian dentary: insights into how complex skeletal elements can be shaped during development and evolution. Pp.207–229 *in* Clone to Bone: The Synergy of Morphological and Molecular Tools in Palaeobiology. Cambridge University Press, Cambridge, UK.

Anthwal, N., Y. Chai, and A. S. Tucker. 2008: The role of transforming growth factor-beta signalling in the patterning of the proximal processes of the murine dentary. Developmental Dynamics 237:1604–1613.

Anthwal, N., H. Peters, and A. S. Tucker. 2015: Species-specific modifications of mandible shape reveal independent mechanisms for growth and initiation of the coronoid. EvoDevo 6:35.

Appelqvist, I. A. M. 2013: In-mouth measurement of food quality. Pp.255–283 *in* D. Kilcast, ed. Instrumental Assessment of Food Sensory Quality: A Practical Guide. Woodhead Publishing Limited, Oxford, UK.

Atchley, W. R., and B. K. Hall. 1991: A model for development and evolution of complex morphological structures. Biological reviews of the Cambridge Philosophical Society 66:101–157.

Averianov, A., and A. Lopatin. 2008: "Protocone" in a pretribosphenic and upper dentition of tinodontid "symmetrodontans."Journal of Vertebrate Paleontology 28:548–552.

Begg, C. M., K. S. Begg, J. T. Du Toit, and M. G. L. Mills. 2003: Sexual and seasonal variation in the diet and foraging behaviour of a sexually dimorphic carnivore, the honey badger (Mellivora capensis). Journal of Zoology 260:301–316.

Bennett, C. V., and A. Goswami. 2013: Statistical support for the hypothesis of developmental constraint in marsupial skull evolution. BMC biology 11:52.

Benton, M. J. 2005: Vertebrate Palaeontology. John Wiley & Sons, New York, NY, 472 p.

Berthaume, M. a. 2016: Food mechanical properties and dietary ecology. American Journal of Physical Anthropology 159:S79–104.

Blows, M. W. 2007: A tale of two matrices: multivariate approaches in evolutionary biology. Journal of evolutionary biology 20:1–8.

Bluhm, B. A., and R. Gradinger. 2008: Regional Variability in Food Availability for Arctic Marine Mammals. Ecological Applications 18:77–96.

Botero, C. a, R. Dor, C. M. McCain, and R. J. Safran. 2013: Environmental harshness is positively correlated with intraspecific divergence in mammals and birds. Molecular ecology 23:259–268.

Britanova, O., M. Depew, and M. Schwark. 2006: Satb2 haploinsufficiency phenocopies 2q32-q33 deletions, whereas loss suggests a fundamental role in the coordination of jaw development. The American Journal of Human Genetics 79:668–678.

Bubadué, J. de M., N. Cáceres, R. Dos Santos Carvalho, and C. Meloro. 2016: Ecogeographical Variation in Skull Shape of South-American Canids: Abiotic or Biotic Processes? Evolutionary biology 43:145–159.

Cáceres, N., C. Meloro, F. Carotenuto, F. Passaro, J. Sponchiado, G. L. Melo, and P. Raia. 2014: Ecogeographical variation in skull shape of capuchin monkeys. Journal of Biogeography 41:501–512.

Canepuccia, A. D., M. M. Martinez, and A. I. Vassallo. 2007: Selection of waterbirds by Geoffroy's cat: Effects of prey abundance, size, and distance. Mammalian Biology - Zeitschrift für Säugetierkunde 72:163–173.

Clark, C. T., and K. K. Smith. 1993: Cranial Osteogenesis in Monodelphis dornestica (Didelphidae) and Macropus eugenii (Macropodidae). Journal of Morphology 215:119–149.

Clarke, A., and H.-O. Pörtner. 2010: Temperature, metabolic power and the evolution of endothermy. Biological reviews of the Cambridge Philosophical Society 85:703–727.

Claverie, T., and S. N. Patek. 2013: Modularity and rates of evolutionary change in a power-amplified prey capture system. Evolution; international journal of organic evolution 67:3191–3207.

Cooper, N., and A. Purvis. 2010: Body size evolution in mammals: complexity in tempo and mode. The American naturalist 175:727–738.

Cooper, N., R. P. Freckleton, and W. Jetz. 2011: Phylogenetic conservatism of environmental niches in mammals. Proceedings. Biological sciences / The Royal Society 278:2384–2391.

Cooper, W. J., C. B. Carter, A. J. Conith, A. N. Rice, and M. W. Westneat. 2016: The evolution of jaw protrusion mechanics has been tightly coupled to bentho-pelagic divergence in damselfishes (Pomacentridae). The Journal of Experimental Biology:10.1242/jeb.143115.

Crompton, A. W., and F. A. Jenkins. 1968: Molar occlusion in Late Triassic mammals. Biological Reviews 43:427–458.

Crompton, A. W., and K. Hiiemäe. 1969: Functional occlusion in tribosphenic molars. Nature 222:678–679.

Crompton, A. W., and A. Sita-Lumsden. 1970: Functional significance of the therian molar pattern. Nature 227:197–199.

Crompton, A. W., A. J. Thexton, P. Parker, and K. Hiiemae. 1977: The activity of the jaw and hyoid musculature in the Virginia opossum, Didelphis virginiana. Pp.287–305 *in* B. Stonehouse and D. Gilmore, eds. The Biology of Marsupials. Macmillan, London, UK.

Davis, B. M. 2011: Evolution of the Tribosphenic Molar Pattern in Early Mammals, with Comments on the "Dual-Origin" Hypothesis. Journal of Mammalian Evolution 18:227–244.

Davis, J. L., S. E. Santana, E. R. Dumont, and I. R. Grosse. 2010: Predicting bite force in mammals: two-dimensional versus three-dimensional lever models. The Journal of experimental biology 213:1844–1851.

Depew, M. J., T. Lufkin, and J. L. R. Rubenstein. 2002: Specification of Jaw Subdivisions by Dlx Genes. Science 298:381–385.

Derryberry, E. P., S. Claramunt, G. Derryberry, R. T. Chesser, J. Cracraft, A. Aleixo, J. Pérez-Emán, J. V Remsen, and R. T. Brumfield. 2011: Lineage diversification and

morphological evolution in a large-scale continental radiation: the neotropical ovenbirds and woodcreepers (aves: Furnariidae). Evolution; international journal of organic evolution 65:2973–2986.

Diniz-Filho, J. A. F., M. Á. Rodríguez, L. M. Bini, M. Á. Olalla-Tarraga, M. Cardillo, J. C. Nabout, J. Hortal, and B. A. Hawkins. 2009: Climate history, human impacts and global body size of Carnivora (Mammalia: Eutheria) at multiple evolutionary scales. Journal of Biogeography 36:2222–2236.

Dowd, J. L. B., and E. M. Gese. 2012: Seasonal Variation of Coyote Diet in Northwestern Wyoming : Implications for Dietary Overlap with Canada Lynx ? Seasonal Variation of Coyote Diet in Northwestern Wyoming : Implications for Dietary Overlap with Canada Lynx ? Northwest Scientific Association 86:289–299.

Drake, A. G., and C. P. Klingenberg. 2010: Large-scale diversification of skull shape in domestic dogs: disparity and modularity. The American naturalist 175:289–301.

Dumont, E. R., L. M. Davalos, A. Goldberg, S. E. Santana, K. Rex, and C. C. Voigt. 2012: Morphological innovation, diversification and invasion of a new adaptive zone. Proceedings of the Royal Society B: Biological Sciences 279:1797–1805.

Dumont, E. R., K. Samadevam, I. Grosse, O. M. Warsi, B. Baird, and L. M. Davalos. 2014: Selection for mechanical advantage underlies multiple cranial optima in new world leaf-nosed bats. Evolution; international journal of organic evolution 68:1436–1449.

Echarri, S., and F. J. Prevosti. 2014: Differences in mandibular disparity between extant and extinct species of metatherian and placental carnivore clades. Lethaia.

Evans, A. R., and G. D. Sanson. 1998: The effect of tooth shape on the breakdown of insects. Journal of Zoology 246:391–400.

Evans, A. R., and G. D. Sanson. 2005: Correspondence between tooth shape and dietary biomechanical properties in insectivorous microchiropterans. Evolutionary Ecology Research 7:453–478.

——— 2006: Spatial and functional modeling of carnivore and insectivore molariform teeth. Journal of morphology 267:649–662.

Evans, A. R., G. P. Wilson, M. Fortelius, and J. Jernvall. 2007: High-level similarity of dentitions in carnivorans and rodents. Nature 445:78–81.

Fakhouri, S., S. B. Hutchens, and A. J. Crosby. 2015: Puncture mechanics of soft solids. Soft matter 11:4723–4730.

Fine, P. V. a. 2015: Ecological and Evolutionary Drivers of Geographic Variation in Species Diversity. Annual Review of Ecology, Evolution, and Systematics 46:369–392.

Fraser, D., C. Hassall, R. Gorelick, and N. Rybczynski. 2014: Mean annual precipitation explains spatiotemporal patterns of Cenozoic mammal beta diversity and latitudinal diversity gradients in North America. PloS one 9:e106499.

Freeman, P., and C. Lemen. 2006: Puncturing ability of idealized canine teeth: edged and non-edged shanks. Journal of Zoology 269:51–56.

Fritz, S. a, O. R. P. Bininda-Emonds, and A. Purvis. 2009: Geographical variation in predictors of mammalian extinction risk: big is bad, but only in the tropics. Ecology letters 12:538–549.

Gao, C.-L., G. P. Wilson, Z.-X. Luo, A. M. Maga, Q. Meng, and X. Wang. 2010: A new mammal skull from the Lower Cretaceous of China with implications for the evolution of obtuse-angled molars and “amphilestid” eutriconodonts. Proceedings of the Royal Society B: Biological Sciences 277:237–246.

Gill, P. G., M. a. Purnell, N. Crumpton, K. R. Brown, N. J. Gostling, M. Stampanoni, and E. J. Rayfield. 2014: Dietary specializations and diversity in feeding ecology of the earliest stem mammals. Nature 512:303–305.

Gomes Rodrigues, H., R. Šumbera, and L. Hautier. 2015: Life in Burrows Channelled the Morphological Evolution of the Skull in Rodents: the Case of African Mole-Rats (Bathyergidae, Rodentia). Journal of Mammalian Evolution 23:175–189.

Gorgadze, G. 2013: Seasonal Diet of the Otter (Lutra lutra) On the Alazani River (Georgia). Hystrix, the Italian Journal of … 24:157–160.

Goswami, A. 2006a: Cranial modularity shifts during mammalian evolution. The American naturalist 168:270–280.

——— 2006b: Morphological integration in the carnivoran skull. Evolution; international journal of organic evolution 60:169–183.

Goswami, A., and P. D. Polly. 2010: The influence of modularity on cranial morphological disparity in Carnivora and Primates (Mammalia). PLOS ONE 5:e9517.

Goswami, A., and J. A. Finarelli. 2016: EMMLi: A maximum likelihood approach to the analysis of modularity. Evolution 70:1622–1637.

Goswami, A., N. Milne, and S. Wroe. 2011: Biting through constraints: cranial morphology, disparity and convergence across living and fossil carnivorous mammals. Proceedings of the Royal Society B: Biological Sciences 278:1831–1839.

Goswami, A., J. B. Smaers, C. Soligo, and P. D. Polly. 2014: The macroevolutionary consequences of phenotypic integration : from development to deep time. Philosophical Transactions of the Royal Society B: Biological Sciences 369:20130254.

Goswami, A., W. J. Binder, J. Meachen, and F. R. O'Keefe. 2015: The fossil record of phenotypic integration and modularity: A deep-time perspective on developmental and evolutionary dynamics. Proceedings of the National Academy of Sciences of the United States of America 112:4891–4896.

Goszczynski, J. 1999: Food composition of weasels (Mustela nivalis) in Poland. Mammalia 63:431–436.

Gould, S. J., and N. Eldredge. 1977: Punctuated Equilibria: The Tempo and Mode of Evolution Reconsidered. Paleobiology 3:115–151.

Grossnickle, D. M., and P. D. Polly. 2013: Mammal disparity decreases during the Cretaceous angiosperm radiation. Proceedings of the Royal Society B: Biological Sciences 280:20132110.

Hallgrímsson, B., D. E. Lieberman, N. M. Young, T. Parsons, and S. Wat. 2007: Evolution of covariance in the mammalian skull. Novartis Foundation Symposium 284:164–185; discussion 185–190.

Hallgrímsson, B., H. Jamniczky, N. M. Young, C. Rolian, T. E. Parsons, J. C. Boughner, and R. S. Marcucio. 2009: Deciphering the Palimpsest: Studying the Relationship Between Morphological Integration and Phenotypic Covariation. Evolutionary Biology 36:355–376.

Harjunmaa, E., K. Seidel, T. Häkkinen, E. Renvoisé, I. J. Corfe, A. Kallonen, Z.-Q. Zhang, A. R. Evans, M. L. Mikkola, I. Salazar-Ciudad, O. D. Klein, and J. Jernvall. 2014: Replaying evolutionary transitions from the dental fossil record. Nature 512:44–48.

Harmon, L. J., J. T. Weir, C. D. Brock, R. E. Glor, and W. Challenger. 2008: GEIGER: investigating evolutionary radiations. Bioinformatics (Oxford, England) 24:129–131.

Herbst, M., and M. G. L. Mills. 2010: The feeding habits of the Southern African wildcat, a facultative trophic specialist, in the southern Kalahari (Kgalagadi Transfrontier Park, South Africa/Botswana). Journal of Zoology 280:403–413.

Holliday, J. a., and S. J. Steppan. 2004: Evolution of hypercarnivory: the effect of specialization on morphological and taxonomic diversity. Paleobiology 30:108–128.

Hu, Y., K. Parsons, and R. C. Albertson. 2014: Evolvability of the Cichlid Jaw: New Tools Provide Insights into the Genetic Basis of Phenotypic Integration. Evolutionary Biology 41:145–153.

Hu, Y., L. Ghigliotti, M. Vacchi, E. Pisano, H. W. Detrich, and R. C. Albertson. 2016: Evolution in an extreme environment: developmental biases and phenotypic integration in the adaptive radiation of antarctic notothenioids. BMC evolutionary biology 16:142.

Hua, X., and J. J. Wiens. 2013: How does climate influence speciation? The American Naturalist 182:1–12.

Huttenlocker, A. K., C. a. Sidor, and R. M. H. Smith. 2011: A new specimen of Promoschorhynchus (Therapsida: Therocephalia: Akidnognathidae) from the Lower Triassic of South Africa and its implications for theriodont survivorship across the Permo-Triassic boundary. Journal of Vertebrate Paleontology 31:405–421.

Iriarte, J. A., W. L. Franklin, W. E. Johnson, and K. H. Redford. 1990: Biogeographic variation of food habits and body size of the America puma. Oecologia 85:185–190.

Jácomo, A. T. de A., L. Silveira, and J. A. F. Diniz-Filho. 2004: Niche separation between the maned wolf (Chrysocyon brachyurus), the crab-eating fox (Dusicyon thous) and the hoary fox (Dusicyon vetulus) in central Brazil. Journal of Zoology 262:99–106.

Jones, K. E., J. Bielby, M. Cardillo, S. A. Fritz, J. O'Dell, C. D. L. Orme, K. Safi, W. Sechrest, E. H. Boakes, C. Carbone, C. Connolly, M. J. Cutts, J. K. Foster, R. Grenyer, M. Habib, C. A. Plaster, S. A. Price, E. A. Rigby, J. Rist, A. Teacher, O. R. P. Bininda-Emonds, J. L. Gittleman, G. M. Mace, and A. Purvis. 2009: PanTHERIA: a species-level database of life history, ecology, and geography of extant and recently extinct mammals. Ecology 90:2648–2648.

Kashtan, N., E. Noor, and U. Alon. 2007: Varying environments can speed up evolution. Proceedings of the National Academy of Sciences of the United States of America 104:13711–13716.

Kashtan, N., A. E. Mayo, T. Kalisky, and U. Alon. 2009: An Analytically Solvable Model for Rapid Evolution of Modular Structure. PLoS Computational Biology 5:e1000355.

Kelly, E. M., and K. E. Sears. 2011: Limb specialization in living marsupial and eutherian mammals: constraints on mammalian limb evolution. Journal of Mammalogy 92:1038–1049.

Kielan-Jaworowska, Z., R. L. Cifelli, and Z.-X. Luo. 2004: Mammals from the Age of Dinosaurs: Origins, Evolution, and Structure. Columbia University Press, New York, NY, 700 p.

Klingenberg, C. P. 1998: Heterochrony and allometry: the analysis of evolutionary change in ontogeny. Biological Reviews of the Cambridge Philosophical Society 73:79–123.

——— 2008: Morphological Integration and Developmental Modularity. Annual Review of Ecology, Evolution, and Systematics 39:115–132.

——— 2009: Morphometric integration and modularity in configurations of landmarks: tools for evaluating a priori hypotheses. Evolution & Development 11:405–421.

——— 2010: Evolution and development of shape: integrating quantitative approaches. Nature reviews. Genetics 11:623–635.

——— 2014: Studying morphological integration and modularity at multiple levels: concepts and analysis. Philosophical transactions of the Royal Society of London. Series B, Biological sciences 369:20130249.

Klingenberg, C. P., K. Mebus, and J.-C. Auffray. 2003: Developmental integration in a complex morphological structure: how distinct are the modules in the mouse mandible? Evolution & development 5:522–531.

Kolbe, J., L. Revell, B. Szekely, E. D. Brodie III, and J. B. Losos. 2011: Convergent evolution of phenotypic integration and its alignment with morphological diversification in Caribbean Anolis ecomorphs. Evolution; international journal of organic evolution 65:3608–3624.

Lanszki, J., S. Körmendi, C. Hancz, and A. Zalewski. 1999: Feeding habits and trophic niche overlap in a Carnivora community of Hungary. Acta Theriologica 44:429–442.

Luo, Z. X., R. L. Cifelli, and Z. Kielan-Jaworowska. 2001: Dual origin of tribosphenic mammals. Nature 409:53–57.

Luo, Z.-X. 2007: Transformation and diversification in early mammal evolution. Nature 450:1011–1019.

Luo, Z.-X., Z. K. Jaworowska, and R. L. Cifelli. 2002: In quest for a phylogeny of Mesozoic mammals. Acta Palaeontologica Polonica 47:1–78.

Luo, Z.-X., Q. Ji, and C.-X. Yuan. 2007a: Convergent dental adaptations in pseudo-tribosphenic and tribosphenic mammals. Nature 450:93–97.

Luo, Z.-X., P. Chen, G. Li, and M. Chen. 2007b: A new eutriconodont mammal and evolutionary development in early mammals. Nature 446:288–293.

Maier, W. 1990: Phylogeny and ontogeny of mammalian middle ear structures. Netherlands Journal of Zoology 40:55–75.

Mannion, P. D., P. Upchurch, R. B. J. Benson, and A. Goswami. 2014: The latitudinal biodiversity gradient through deep time. Trends in ecology & evolution 29:42–50.

Marroig, G., and J. Cheverud. 2001: A comparison of phenotypic variation and covariation patterns and the role of phylogeny, ecology, and ontogeny during cranial evolution of new world monkeys. Evolution; international journal of organic evolution 55:2576–2600.

Martinoli, A., D. G. Preatoni, B. Chiarenzi, L. a. Wauters, and G. Tosi. 2001: Diet of stoats (Mustela erminea) in an Alpine habitat: The importance of fruit consumption in summer. Acta Oecologica 22:45–53.

Meloro, C., and P. O'Higgins. 2011: Ecological Adaptations of Mandibular Form in Fissiped Carnivora. Journal of Mammalian Evolution 18:185–200.

Meloro, C., P. Raia, and P. Piras. 2008: The shape of the mandibular corpus in large fissiped carnivores: allometry, function and phylogeny. Zoological Journal of the Linnean Society 154:832–845.

Meloro, C., P. Raia, F. Carotenuto, and S. N. Cobb. 2011: Phylogenetic signal, function and integration in the subunits of the carnivoran mandible. Evolutionary Biology 38:465–475.

Meng, J., Y. Wang, and C. Li. 2011: Transitional mammalian middle ear from a new Cretaceous Jehol eutriconodont. Nature 472:181–185.

Meng, Q.-J., Q. Ji, Y.-G. Zhang, D. Liu, D. M. Grossnickle, and Z.-X. Luo. 2015: An arboreal docodont from the Jurassic and mammaliaform ecological. Science 347:764–768.

Meredith, R. W., J. E. Janečka, J. Gatesy, O. a Ryder, C. a Fisher, E. C. Teeling, A. Goodbla, E. Eizirik, T. L. L. Simão, T. Stadler, D. L. Rabosky, R. L. Honeycutt, J. J. Flynn, C. M. Ingram, C. Steiner, T. L. Williams, T. J. Robinson, A. Burk-Herrick, M. Westerman, N. a Ayoub, M. S. Springer, and W. J. Murphy. 2011: Impacts of the Cretaceous Terrestrial Revolution and KPg extinction on mammal diversification. Science 334:521–524.

Merritt, J. F., M. Lima, and F. Bozinovic. 2001: Seasonal Regulation in Fluctuating Small Mammal Populations: Feedback Structure and Climate. Oikos 94:505–514.

Milakovic, B., and K. L. Parker. 2011: Using stable isotopes to define diets of wolves in northern British Columbia, Canada. Journal of Mammalogy 92:295–304.

Mills, J. R. E. 1971: The dentition of Morganucodon. Pp.29–63 *in* Early Mammals. .

Monteiro, L. R., and M. R. Nogueira. 2010: Adaptive radiations, ecological specialization, and the evolutionary integration of complex morphological structures. Evolution; international journal of organic evolution 64:724–744.

Nogueira, M. R., A. L. Peracchi, and L. R. Monteiro. 2009: Morphological correlates of bite force and diet in the skull and mandible of phyllostomid bats. Functional Ecology 23:715–723.

Nyakatura, K., and O. R. Bininda-Emonds. 2012: Updating the evolutionary history of Carnivora (Mammalia): a new species-level supertree complete with divergence time estimates. BMC Biology 10:12.

Oka, K., S. Oka, T. Sasaki, Y. Ito, P. Bringas, K. Nonaka, and Y. Chai. 2007: The role of TGF-beta signaling in regulating chondrogenesis and osteogenesis during mandibular development. Developmental biology 303:391–404.

Oka, K., S. Oka, R. Hosokawa, P. Bringas, H. C. Brockhoff, K. Nonaka, and Y. Chai. 2008: TGF-beta mediated Dlx5 signaling plays a crucial role in osteo-chondroprogenitor cell lineage determination during mandible development. Developmental biology 321:303–309.

Osborn, H. F. 1907: Evolution of Mammalian Molar Teeth. Macmillan, New York, NY, 250 p.

Paradis, E. 2012: Analysis of Phylogenetics and Evolution with R. *in* R. Gentleman, K. Kornik, and G. Parmigiani, eds. Springer, New York, NY, 386 p.

Paradis, E., J. Claude, and K. Strimmer. 2004: APE: Analyses of Phylogenetics and Evolution in R language. Bioinformatics 20:289–290.

Parrington, F. R. 1978: A Further Account of the Triassic Mammals. Philosophical Transactions of the Royal Society B: Biological Sciences 282:177–204.

Pianka, E. R. . 1966: Latitudinal Gradients in Species Diversity: A Review of Concepts. The American naturalist 100:33–46.

Pigliucci, M. 2008: Is evolvability evolvable? Nature reviews. Genetics 9:75–82.

Prevosti, F. J., G. F. Turazzini, M. D. Ercoli, and E. Hingst-Zaher. 2012: Mandible shape in marsupial and placental carnivorous mammals: a morphological

comparative study using geometric morphometrics. Zoological Journal of the Linnean Society 164:836–855.

Price, S. A., R. Holzman, T. J. Near, and P. C. Wainwright. 2011: Coral reefs promote the evolution of morphological diversity and ecological novelty in labrid fishes. Ecology letters 14:462–469.

Price, S. A., S. S. B. Hopkins, K. K. Smith, and V. L. Roth. 2012: Tempo of trophic evolution and its impact on mammalian diversification. Proceedings of the National Academy of Sciences 109:7008–7012.

R Core Team. 2014: R: A Language and Environment for Statistical Computing. .

Rabosky, D. L., F. Santini, J. Eastman, S. a Smith, B. Sidlauskas, J. Chang, and M. E. Alfaro. 2013: Rates of speciation and morphological evolution are correlated across the largest vertebrate radiation. Nature communications 4:1958.

Ramaesh, T., and J. B. L. Bard. 2003: The growth and morphogenesis of the early mouse mandible: a quantitative analysis. Journal of Anatomy 203:213–222.

Renaud, S. 1999: Size and shape variability in relation to species differences and climatic gradients in the African rodent Oenomys. Journal of Biogeography 26:857–865.

Renaud, S., J. Michaux, D. N. Schmidt, J.-P. Aguilar, P. Mein, and J.-C. Auffray. 2005: Morphological evolution, ecological diversification and climate change in rodents. Proceedings of the Royal Society B: Biological Sciences 272:609–617.

Richman, J., and P. J. Mitchell. 1996: Craniofacial development: Knockout mice take one on the chin. Current Biology 6:364–367.

Ricklefs, R. E. 2004: Cladogenesis and morphological diversification in passerine birds. Nature 430:338–341.

Rodrigues, H. G., S. Renaud, C. Charles, Y. Le Poul, F. Solé, J.-P. Aguilar, J. Michaux, P. Tafforeau, D. Headon, J. Jernvall, and L. Viriot. 2013: Roles of dental

development and adaptation in rodent evolution. Nature communications 4:2504.

Rohlf, F. J. 1998: On applications of geometric morphometrics to studies of ontogeny and phylogeny. Systematic biology 47:147–167.

——— 2004: *TPS Software*. Downloaded from http://www.life.bio.sunysb.edu/morph/ .

Rolland, J., F. L. Condamine, F. Jiguet, and H. Morlon. 2014: Faster Speciation and Reduced Extinction in the Tropics Contribute to the Mammalian Latitudinal Diversity Gradient. PLoS Biology 12:e1001775.

Rose, K. D. 2006: The Beginning of the Age of Mammals. Johns Hopkins University Press, Baltimore, MD, 448 p.

Rot-Nikcevic, I., K. J. Downing, B. K. Hall, and B. Kablar. 2007: Development of the mouse mandibles and clavicles in the absence of skeletal myogenesis. Histology and Histopathology 22:51–60.

Roth, J. D., J. D. Marshall, D. L. Murray, D. M. Nickerson, and T. D. Steury. 2007: Geographical gradients in diet affect population dynamics of Canada lynx. Ecology 88:2736–2743.

Rougier, G. W., J. R. Wible, R. M. D. Beck, and S. Apesteguía. 2012: The Miocene mammal Necrolestes demonstrates the survival of a Mesozoic nontherian lineage into the late Cenozoic of South America. Proceedings of the National Academy of Sciences of the United States of America 109:20053–20058.

Le Rouzic, A., J. M. Álvarez-Castro, and T. F. Hansen. 2013: The Evolution of Canalization and Evolvability in Stable and Fluctuating Environments. Evolutionary Biology 40:317–340.

Sanchez-villagra, M. R., and K. K. Smith. 1997: Diversity and Evolution of the Marsupial Mandibular Angular Process. Journal of Mammalian Evolution 4:119–144.

Sánchez-Villagra, M. R., S. Gemballa, S. Nummela, K. K. Smith, and W. Maier. 2002: Ontogenetic and phylogenetic transformations of the ear ossicles in marsupial mammals. Journal of morphology 251:219–238.

Sanger, T. J., D. L. Mahler, A. Abzhanov, and J. B. Losos. 2012: Roles for modularity and constraint in the evolution of cranial diversity among Anolis lizards. Evolution 66:1525–1542.

Sanson, G. 2016: Cutting food in terrestrial carnivores and herbivores. Interface Focus 6.

Santana, S. E., E. R. Dumont, and J. L. Davis. 2010: Mechanics of bite force production and its relationship to diet in bats. Functional Ecology 24:776–784.

Santana, S. E., I. R. Grosse, and E. R. Dumont. 2012: Loading behavior, dietary hardness and the evolution of skull form in bats. Evolution 66:2587–2598.

Schemske, D. W., G. G. Mittelbach, H. V. Cornell, J. M. Sobel, and K. Roy. 2009: Is There a Latitudinal Gradient in the Importance of Biotic Interactions? Annual Review of Ecology, Evolution, and Systematics 40:245–269.

Schluter, D. 2000: The ecology of adaptive radiations. Oxford University Press, Oxford, UK, 296 p.

Schneider, C. a, W. S. Rasband, and K. W. Eliceiri. 2012: NIH Image to ImageJ: 25 years of image analysis. Nature Methods 9:671–675.

Scognamillo, D., I. E. Maxit, M. Sunquist, and J. Polisar. 2003: Coexistence of jaguar (Panthera onca) and puma (Puma concolor) in a mosaic landscape in the Venezuelan llanos. Journal of Zoology 259:269–279.

Sidlauskas, B. 2008: Continuous and arrested morphological diversification in sister clades of characiform fishes: a phylomorphospace approach. Evolution; international journal of organic evolution 62:3135–3156.

Slater, G. J. 2013: Phylogenetic evidence for a shift in the mode of mammalian body size evolution at the Cretaceous-Palaeogene boundary. Methods in Ecology and Evolution 4:734–744.

Smith, A. J., N. Nelson-Maney, K. J. Parsons, W. James Cooper, and R. Craig Albertson. 2015: Body Shape Evolution in Sunfishes: Divergent Paths to Accelerated Rates of Speciation in the Centrarchidae. Evolutionary Biology 42:283–295.

Smith, K. K. 1994: Development of Craniofacial Musculature in Monodelphis domestica (Marsupialia, Dideiphidae). Journal of Morphology 222:149–173.

——— 2001: Early development of the neural plate, neural crest and facial region of marsupials. Journal of Anatomy 199:121–131.

——— 2006: Craniofacial development in marsupial mammals: developmental origins of evolutionary change. Developmental Dynamics 235:1181–1193.

Strait, S. G. 1993: Molar morphology and food texture among small-bodied insectivorous mammals. Journal of Mammalogy 74:391–402.

Symonds, M. R. E., and S. P. Blomberg. 2014: A primer on phylogenetic generalised least squares (PGLS). Pp.105–130 *in* L. Z. Garamszegi, ed. Modern Phylogenetic Comparative Methods and Their Application in Evolutionary Biology: Concepts and Practice. Springer, Berlin.

Thinley, P., J. F. Kamler, S. W. Wang, K. Lham, U. Stenkewitz, and D. W. Macdonald. 2011: Seasonal diet of dholes (Cuon alpinus) in northwestern Bhutan. Mammalian Biology 76:518–520.

Van Valkenburgh, B. 2007: Déjà vu: the evolution of feeding morphologies in the Carnivora. Integrative and Comparative Biology 47:147–163.

Vincent, J. F. V, and U. G. K. Wegst. 2004: Design and mechanical properties of insect cuticle. Arthropod structure & development 33:187–199.

Wagner, G. P., M. Pavlicev, and J. M. Cheverud. 2007: The road to modularity. Nature reviews. Genetics 8:921–931.

Weir, J. T., and D. Schluter. 2007: The latitudinal gradient in recent speciation and extinction rates of birds and mammals. Science 315:1574–1576.

Wright, B. W., K. a Wright, J. Chalk, M. P. Verderane, D. Fragaszy, E. Visalberghi, P. Izar, E. B. Ottoni, P. Constantino, and C. Vinyard. 2009: Fallback foraging as a way of life: using dietary toughness to compare the fallback signal among capuchins and implications for interpreting morphological variation. American journal of physical anthropology 140:687–699.

Wroe, S., C. McHenry, and J. Thomason. 2005: Bite club: comparative bite force in big biting mammals and the prediction of predatory behaviour in fossil taxa. Proceedings of the Royal Society B: Biological Sciences 272:619–625.

Yoder, J. B., E. Clancey, S. Des Roches, J. M. Eastman, L. Gentry, W. Godsoe, T. J. Hagey, D. Jochimsen, B. P. Oswald, J. Robertson, B. a J. Sarver, J. J. Schenk, S. F. Spear, and L. J. Harmon. 2010: Ecological opportunity and the origin of adaptive radiations. Journal of evolutionary biology 23:1581–1596.

Young, N. M., and B. Hallgrímsson. 2005: Serial homology and the evolution of mammalian limb covariation structure. Evolution 59:2691–2704.

Zelditch, M. L., D. L. Swiderski, and H. D. Sheets. 2012: Geometric Morphometrics for Biologists: A Primer. Academic Press, Waltham, MA, 488 p.

Zelditch, M. L., A. R. Wood, R. M. Bonett, and D. L. Swiderski. 2008: Modularity of the rodent mandible: Integrating bones, muscles, and teeth. Evolution and Development 10:756–768.

Zhou, Y., W. Chen, Y. Kaneko, C. Newman, Z. Liao, X. Zhu, C. D. Buesching, Z. Xie, and D. W. Macdonald. 2014: Seasonal dietary shifts and food resource exploitation by the hog badger (Arctonyx collaris) in a Chinese subtropical forest. European Journal of Wildlife Research 61:125–133.